ISAS - INTERNATIONAL SCHOOL FOR ADVANCED STUDIES

THESIS FOR THE TITLE OF "MAGISTER PHILOSOPHIAE"

TOWARD SELF-CONSISTENT MASSIVE STARS MODELS AND EVOLUTION: THE LINE DRIVEN WIND

Section: Astrophysics

Supervisor: Prof. Cesare Chiosi

Candidate: Claudio Veltroni

Academic Year: 1986/87

SISSA - SCUOLA INTERNAZIONALE SUPERIORE DI STUDI AVANZATI

Strada Costiera 11, TRIESTE

TOWARD SELF-CONSISTENT MASSIVE STARS MODELS AND EVOLUTION: THE LINE DRIVEN WIND

1. INTRODUCTION: THE HR DIAGRAM OF LUMINOUS STARS 1

2. MASS LOSS: OBSERVATION AND THEORY 15

2.1 Diagnostics of mass loss 15

2.2 Methods to determine mass loss rate 17

2.3 Mass loss rate parametrizations 20

2.4 Mass loss theories 22

2.5 The fluctuation theory of Andriesse 24

3. THE LINE DRIVEN WIND 27

3.1 The line acceleration 27

3.2 The force multiplier 29

3.3 The finite disk correction 41

3.4 The equation of motion of CAK and M-CAK winds: discussion of the solutions 42

3.5 The critical point of M-CAK wind 47

3.6 The integration strategy 49

4. THE BEHAVIOUR OF THE MODEL IN THE HR DIAGRAM 51

REFERENCES 72

1. INTRODUCTION: THE HR DIAGRAM OF LUMINOUS STARS

The composite HR diagram for luminous stars in our galaxy and in the LMC by Humphreys & McElroy (1984) are shown in figure 1 and 2, respectively. Note, first of all, the upper luminosity limit of OBA stars, which approximately goes from (M_{BOL},logT) = (-11,4.5) to (-9,4.0). The reality of this limit has been somewhat questioned. It seems that among the most luminous stars in each spectral type the least luminous are those at T≈10000°K. This corresponds roughly to zero bolometric correction, that is to the best observable stars in visual wavelenghts. More luminous stars are observed both at higher and lower temperatures. It has been suggested that the bolometric corrections are not well calculated and this is true at least for the hottest and coolest stars.

This envelope has been tentatively explained through the location of main sequence stars and/or core helium burning stars. Figure 3 from Bressan et al. (1981) show the main sequence band for constant mass evolutionary models and in presence of mass loss and/or overshooting. As it is seen in figure 4, the best agreement is obtainable in the case of mass loss and overshooting. Surely no agreement is obtainable with constant mass models as is evidenced in figure 5 from Chiosi (1981), expecially because of the theoretical location of core helium burning models. This location is drastically changed if mass loss is taken into account, as it is visible in figure 6, from Chiosi (1981). The modification seems to go in the direction to explain the observed HR diagram, but it is still insufficient. In fact

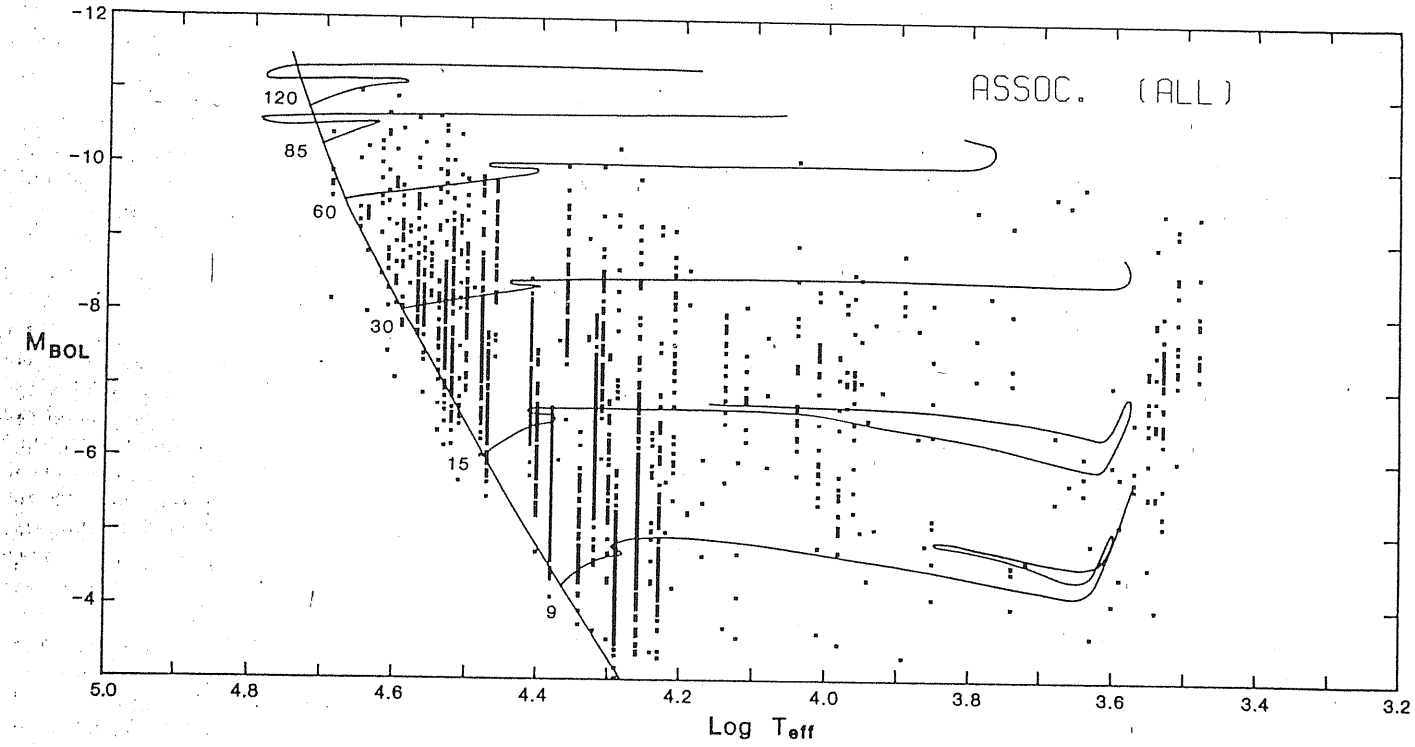

FIGURE 1. The composite HR diagram of our galaxy (Humphreys & McElroy, 1984).

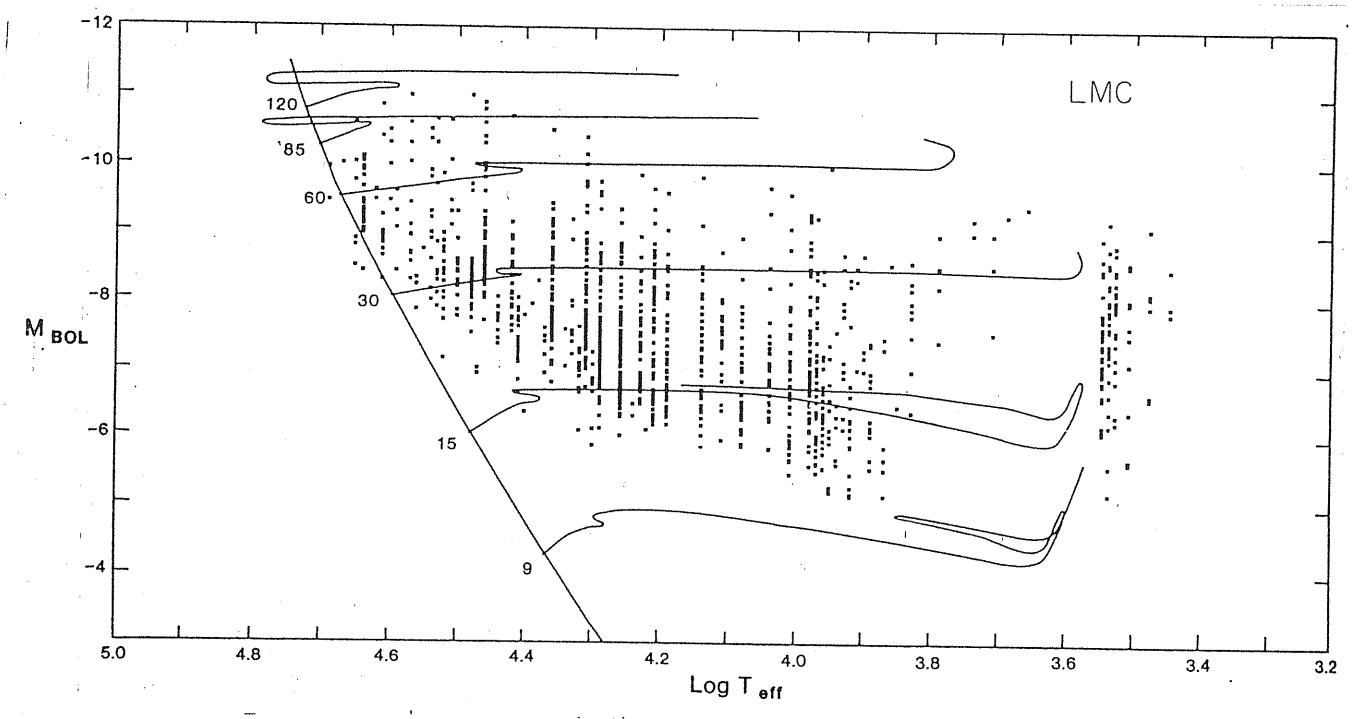

FIGURE 2. The HR diagram of LMC (Humphreys & McElroy, 1984).

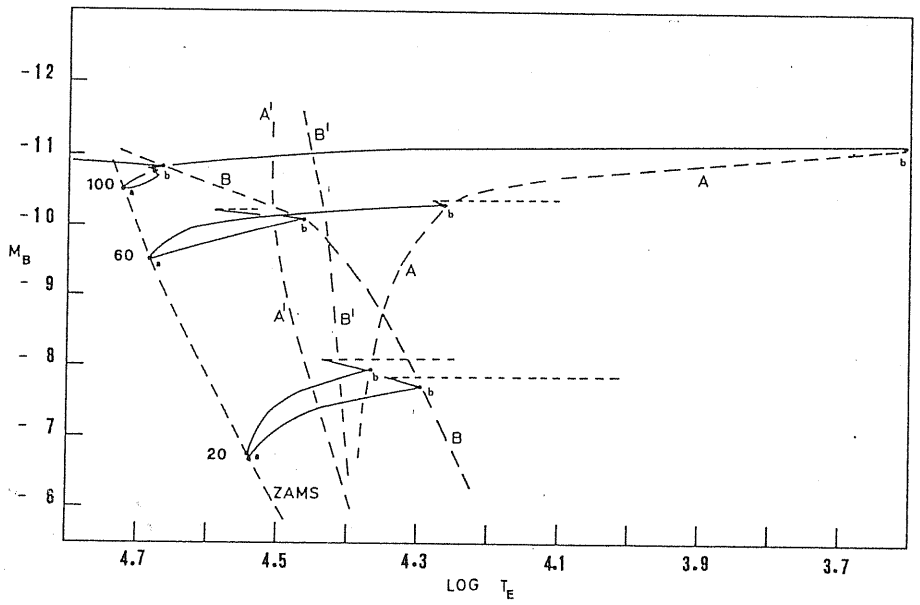

FIGURE 3. The ZAMS and the coolest edge of the core H-burning band (Bressan et al., 1981) for:
A: constant mass and overshooting;
A': " " " standard convection and semiconvection;
B: mass loss and overshooting;
B': " " " standard convection and semiconvection.

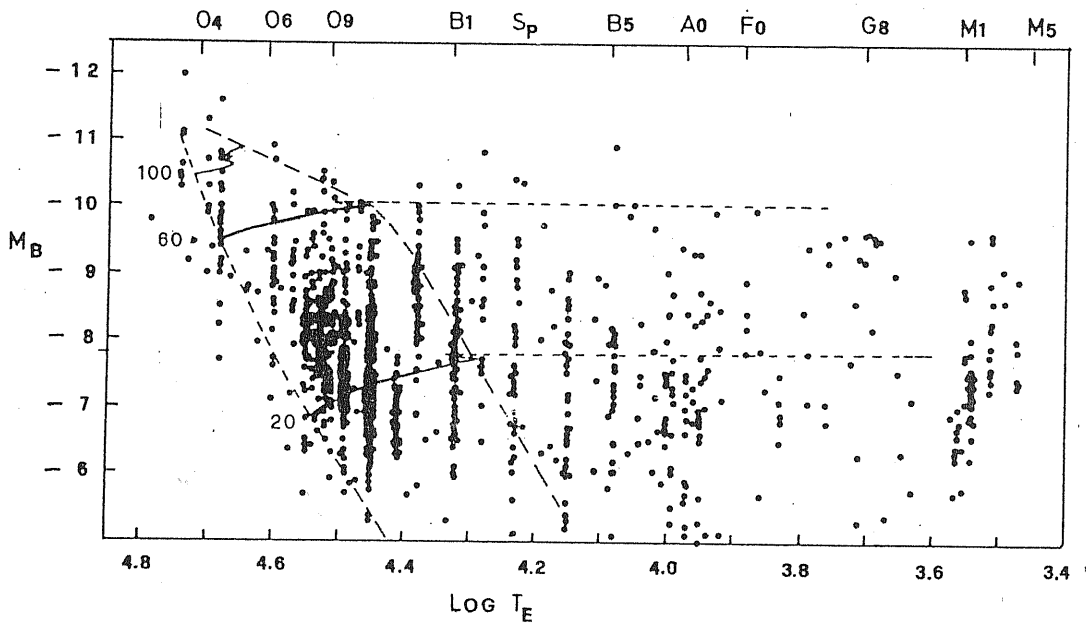

FIGURE 4. The main sequence band in presence of mass loss and overshooting and the observational HR diagram (Bressan et al., 1981).

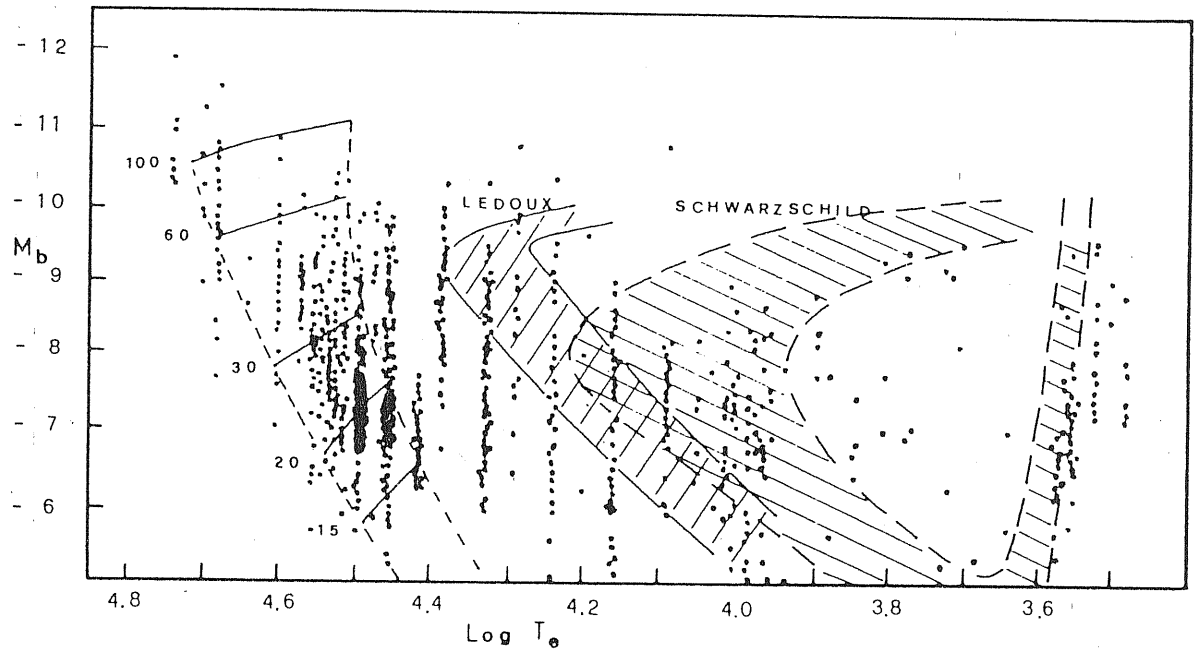

FIGURE 5. The main sequence band and core He-burning band for constant mass evolution and the observational HR diagram (Chiosi, 1981).

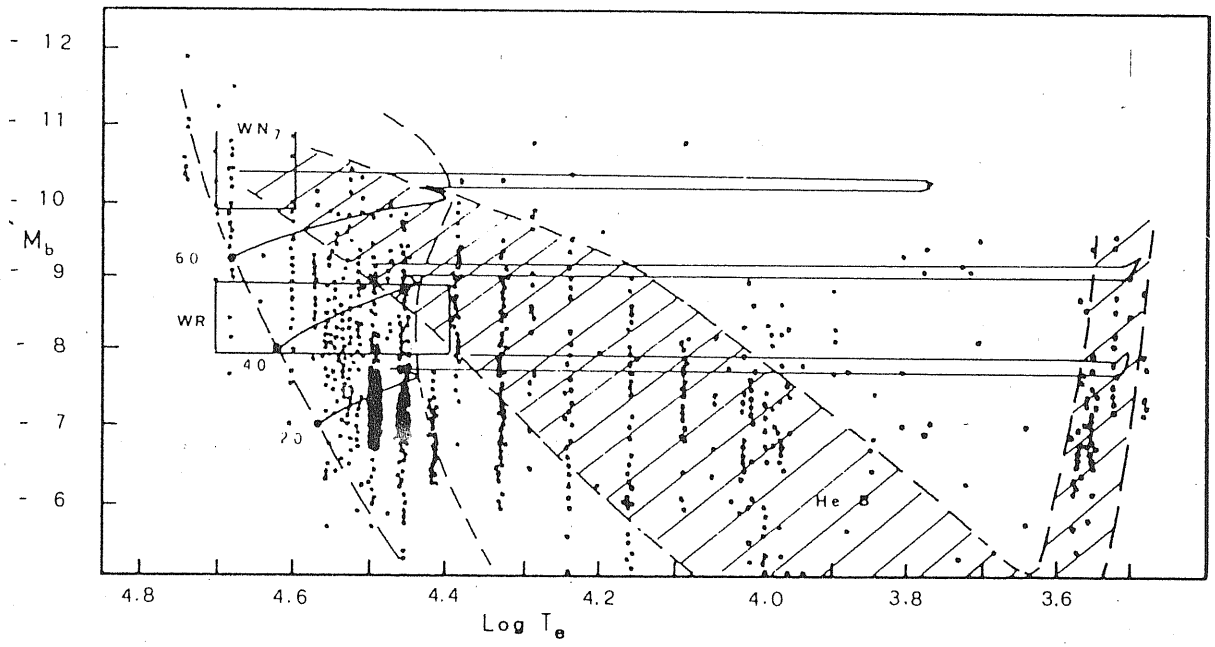

FIGURE 6. The same as fig. 5, but taking into account the mass loss (Chiosi, 1981).

Nasi (1986) has computed synthetic HR diagrams in different scenarios: neither evolution with mass loss nor with mass loss and overshooting are able to reproduce the observed HR diagram. It is necessary to introduce an extra-ingredient. Nasi (1986) showed that it could be a moderate increase of standard radiative opacities in the region of CNO ionization (figure 7). This solution was proposed by Bertelli et al. (1984) to explain the stellar counts on the HR diagram: the ratio between the core helium burning lifetime t_{He} and core hydrogen burning lifetime t_H is an estimate of the ratio between the stars outside and inside the main sequence band. If the theoretical ratios t_{He}/t_H are right than the main sequence band has to be wider than theoretically expected. Bertelli et al. (1984) found that the discrepancy is reduced if we consider mass loss and overshooting, but nethertheless the main sequence has to extend to logT=4.00 for $-9<M_{BOL}<-7$, and it seems to be removed if we introduce the CNO opacity bump. This hypotesis, however, has grown in the controversy between Los Alamos and Carson's opacities, which concluded with the confirmation of the usual opacities (Carson et al, 1984).

De Loore et al. (1982) suggested another possible cause: the development of massive and, therefore, optically thick winds which re-define the stellar photosphere. But it seems to apply only to the stars located near the observed limit, such as the Luminous Blue Variables, LBV (Hubble-Sandage Variables, HSV, S Doradus type stars,...) whose mass loss rates change according to the temperature and visual luminosity (whereas L_{BOL} is constant).

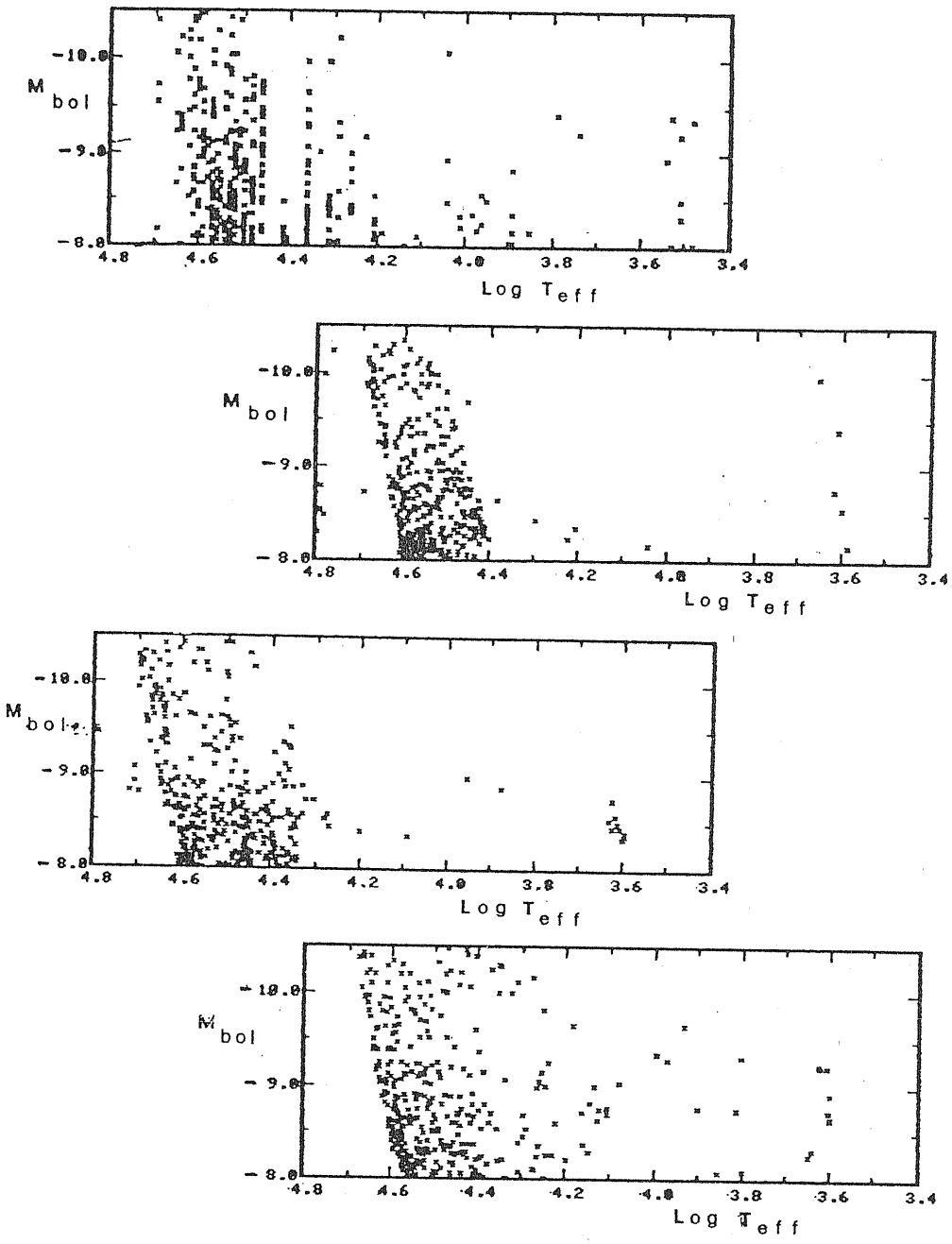

FIGURE 7. From top to bottom:

a) the HR diagram of The Galaxy (Humphreys & McElroy, 1984);
b) synthetic HR diagram for models with mass loss;
c) as b) plus overshooting;
d) as c) plus modified CNO opacities (Nasi, 1986).

Several authors have tried to explain the location of these unusual stars, substantiating the physical reality of the observed envelope since the two coincide (figure 8).

De Jager (1980a, 1984) observed that the Hayashy limit (the locus of fully convective stars) at high luminosity is no longer a vertical line, but turns to higher temperatures. Even the hottest stars develope convective envelopes (figure 9) which may be considered as reservoirs of turbulent energy whose dissipation powers the wind.

Appenzeller (1986) observed that for a constant luminosity $L=4\pi R^2\sigma T^4$ the gravitational acceleration is expected to vary approximately according to $g \propto R^{-2} \propto T^4$. The effective acceleration can be written as

$$g_{eff} = g - g_R - \ldots = g \left(1 - g_R/g - \ldots \right)$$

If g_R also varies as T^4 or more rapidly, it is easy to see that the wind is stable against a temperature or mass loss rate fluctuation. Instead, if g_R varies less rapidly, the wind is unstable. In this case, infact, a temperature decrease produces a decrease of g_{eff} and therefore the mass loss rate may grow, increasing the optical thickness of the wind and decreasing the T_{eff} and thus the fluctuation grows. Appenzeller noted that this condition arises at temperatures approximately corresponding to the LBV (figure 10).

P Cygni type stars, the supergiant stars with the highest mass loss rates, have approximately the same location of LBV. Lamers (1986) suggested that their high mass loss rates are due to the development at $T \leqslant 25000°K$ of many efficient absorbing metal lines in the Balmer continuum, resulting, as long as the

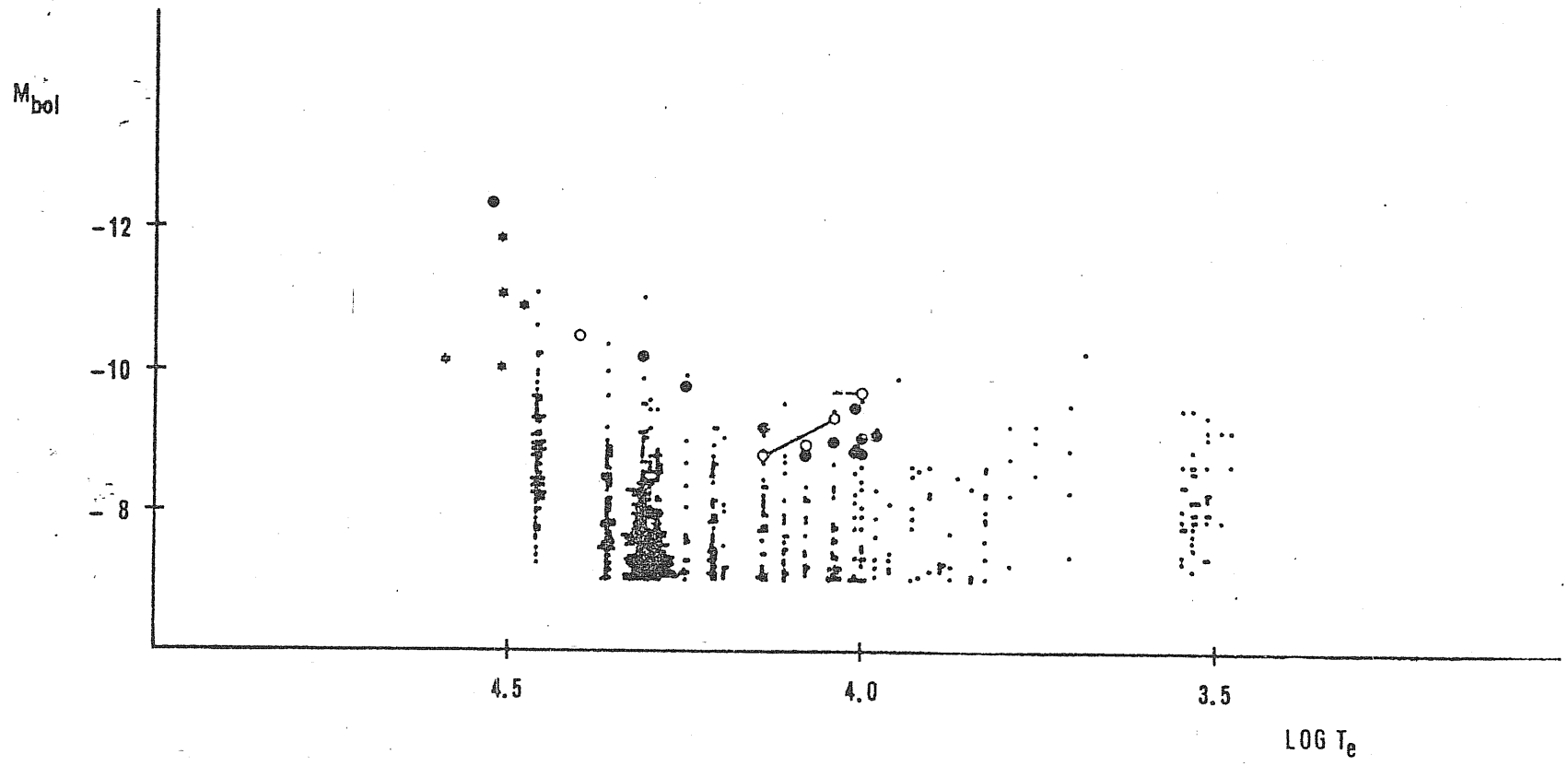

FIGURE 8. The HR diagram of LMC and the location of HSV (open circles), OBA(PC) (filled circles) and Of stars (stars) (Veltroni, 1984).

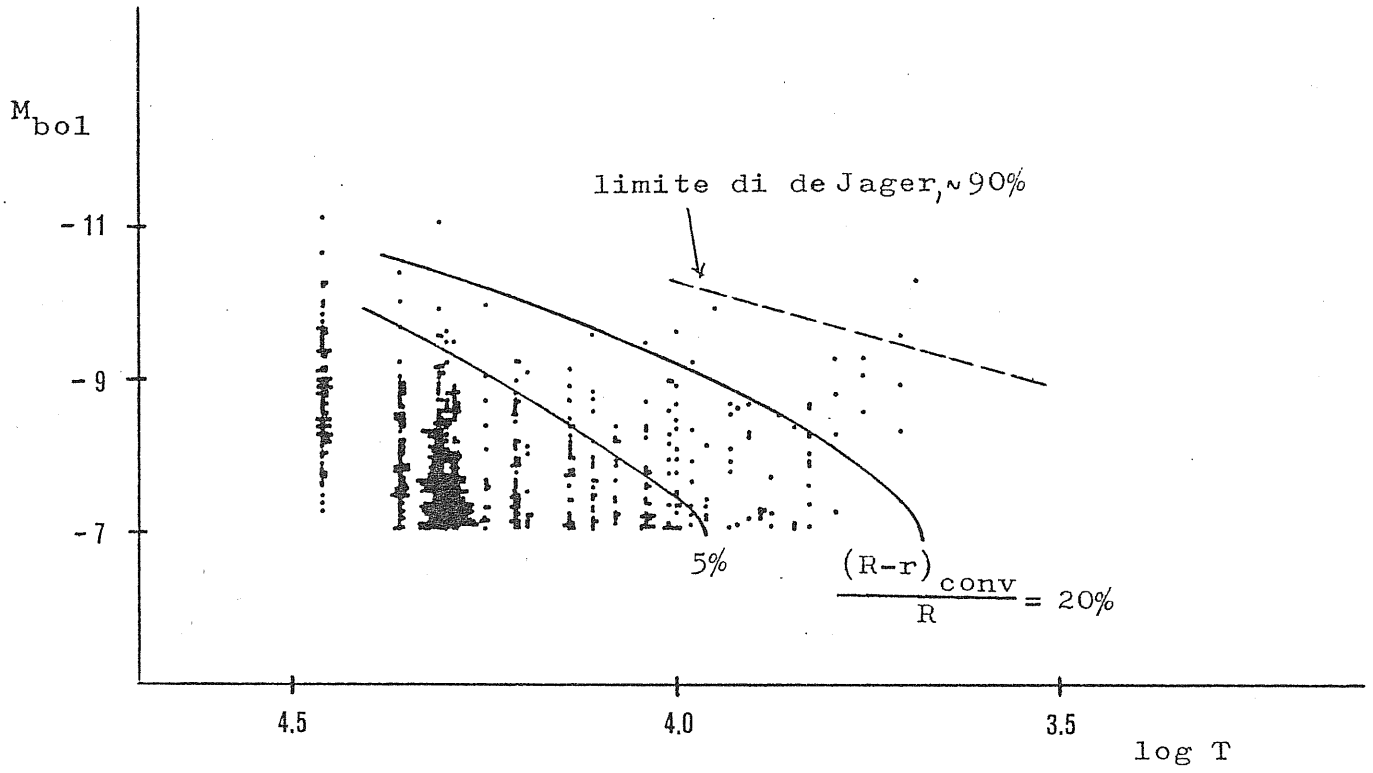

FIGURE 9. Extension of superficial convective regions of core H-burning models (Maeder, 1980) and de Jager limit (de Jager, 1980) onto the LMC hr diagram.

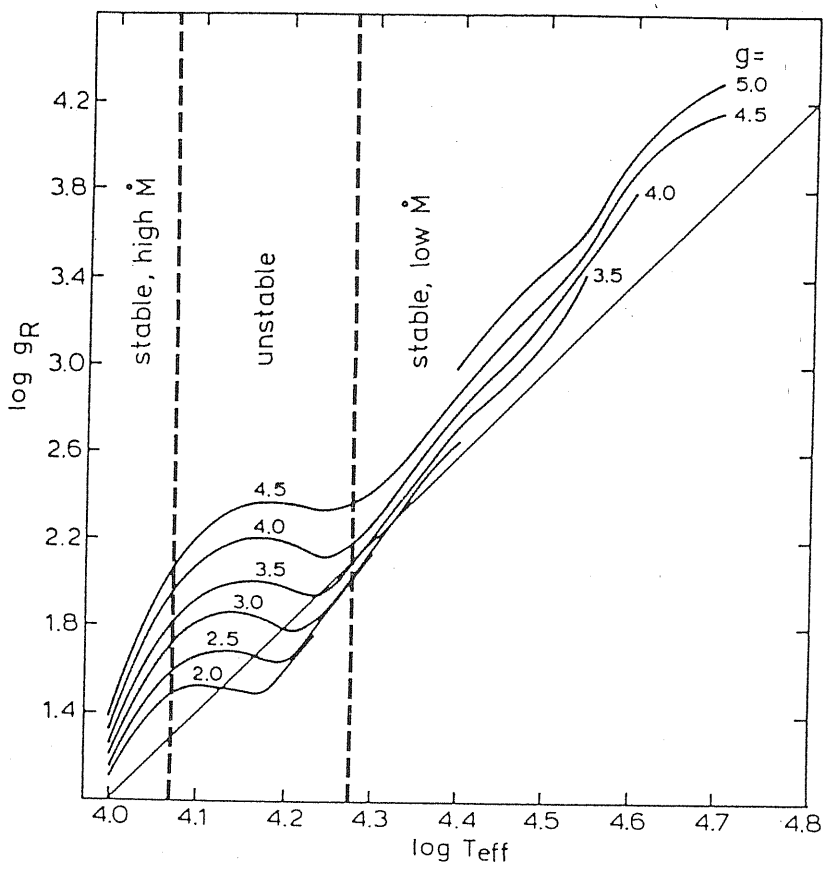

Figure 10. The radiative acceleration g_R (at a Rosseland optical depth of 10^{-4}) as a function of the effective temperature T_{eff} for different values of the gravitational acceleration g (Kurucz and Schild 1976). The solid straight line indicates the relation $g_R \sim T_{eff}^4$.

temperature decreases, in an increase in the mass loss rate and a decrease of the wind velocity, since in efficient winds

$$Mv_{\infty} = L/c$$

and L is constant in these stars that are crossing the HR diagram.

In any case, all these hypoteses support the idea that the observed envelope is the locus of the reddest points of evolutionary tracks because of mass loss. The surface temperature evolution, infact, is regulated by some criteria:

a) the mirror criterium: when a burning shell is present, a contraction of the core is accompanied by an expansion of the envelope (and viceversa) and this is precisely what is happening in stars that are crossing the HR diagram at constant luminosity, after central hydrogen exhaustion;

b) the ratio $M_{He-core}/M_{tot}$ of the mass of helium core to the total mass favours redward evolution up to some critical value and blueward evolution afterwards;

c) the surface composition: an increase of the superficial helium fraction Y tends to shift the star to the left of the HR diagram toward the helium sequence.

A high mass loss rate, therefore, favours a blueward evolution since, peeling away the hydrogen envelope, it increases the ratio $M_{He-core}/M_{tot}$ and the superficial Y.

Another problem in the top of HR diagram is the paucity of O stars. These are the hottest stars, apart the WR stars, and therefore are not easy to detect and classify because of their high bolometric correction. For the same reason, the methods to determine their effective temperature are probably unadequate

(Stasinska & Tylenda, 1986). So, it is not definitely clear if O stars are really few or if they have been lost because of selection effects or unadequate detection techniques. However, some explanations have been proposed. These massive stars are so short lived that when they emerge from their parental cloud they could be already evolved away from the ZAMS (Appenzeller, 1980). The high mass loss rates of these stars also contribute to move them away from the ZAMS directly toward the WR phase. But the simulation of this fact in evolutionary models depends critically on the mass loss rate parametrization adopted. It has been suggested, too, that the theoretical ZAMS may be too blue. This would imply either an overestimate of T_{eff} due to neglecting atmospheric effects caused by gas outflow or an underestimate of the opacity in the outer layers.

It is seen that the HR diagram of luminous stars puts a lot of problems to stellar evolution theory. But the problems are not only on the observational side: there are evident unconsistencies in the theoretical approach.

For example, usual stellar models adopt a thin plane parallel hydrostatic grey atmosphere; on the contrary, atmospheres of supergiant stars are evidently extended, non hydrostatic and non grey.

The observed mass loss rates, moreover, require supersonic photospheric velocities, while envelopes of stars are usually assumed hydrostatic.

Finally, the subphotospheric hydrostatic structure of models out of the main sequence band exhibits, in some T_{eff} range a

strange density inversion, that is there is a shell in which the density decreases inward.

When evolutionary models are taken into account, it has been claimed by Prantzos et al. (1986) that the mass loss rate parametrization of Lamers (1981) is unconsistent because it has been derived using evolutionary tracks (in order to estimate the stellar mass) with a different mass loss parametrization. So, now, we doubt on the consistency of the other parametrizations, too. See also chapter 2.3. Furthermore, there is often an unconsistency between the evolutionary phase to which a mass loss rate is attributed and the type of star from which the rates are derived, since stars in different evolutionary phases crowd the same locus in the HR diagram. Finally, when cure is spent to assure this consistency, the unpleasant sensation is that of an "ad hoc" evolution, since many different mass loss parametrizations for different stellar phases are needed (Doom et al., 1986) and we renounce to understand the physical connection between, possibly apparent, different mass loss phases.

This scenario enforces the need of new self consistent evolutionary models in which:

- the atmosphere is not hydrostatic and thin, but exhibits a wind and therefore is extended;

- the mass loss rate is not parametrized, but is an 'eigenvalue' of the structure itself;

- the subphotospheric structure, in case, is treated non-hydrostatically.

This project is expected to improve the agreement between stellar evolution theory and observation and to develope a better

tool for galaxy evolution theory, since massive stars dominate in the luminosity, produce most of helium and heavier elements and affect deeply the dynamics of the gas through stellar winds, ionization an supernovae.

The present study regards the individuation of the best trusted wind model among those proposed in literature, able to fix univocally the mass loss rate once stellar parameters are specified, and the study of his behaviour on the HR diagram.

The second step, the development of a subphotospheric non-hydrostatic structure, is presently in progress, since the analysis of photospheric conditions has confirmed his necessity.

The next chapter reviews the methods to determine the mass loss rates, the current mass loss parametrizations and, briefly, mass loss theories. Some more word is spent about the fluctuation theory of Andriesse.

In chapter 3 the radiative wind theory of Castor, Abbott & Klein (1975) is described in detail together with its recent improvements, some new implementations and his numerical solution.

In chapter 4 the behaviour of the model in HR diagram is discussed and some considerations on work in progress are made as a word of conclusion.

2. MASS LOSS: OBSERVATION AND THEORY

2.1 DIAGNOSTICS OF MASS LOSS

There are several usual indicators of winds around stars, the most evident being the observation of emission lines, eventually with P Cygni profiles. The violet edge of the absorption component or the half-width of the emission line give v_∞. An infrared excess reveals the presence of warm dust envelopes originated by the winds or, alternatively, a free-free emission by electrons in the winds. This free-free excess has been detected in the IR region of the spectrum (1-20μm) and in the radio region (e.g. at 6 cm). Probably all stars loose mass, notwithstanding the presence or absence of this wind indicators, which depict huge mass loss rates. The solar wind, for example, is not observable at normal interstellar distances, but it is present indeed, though the mass loss rate is so low ($\simeq 1.4 \cdot 10^{-14}$ M_s/yr) that it has no consequence on the stellar evolution nor on the interstellar medium and galaxy evolution. Theoretical considerations of various type lead to the conclusion that stars must have winds: consistent models for spherical, non-expanding, finite mass atmospheres cannot be derived (De Jager, 1980b; see also chapter 3.1). A study of the LMC supergiants contained in the catalog of Rousseau et al. (1978) has shown a dependence of the color excess on luminosity, which can be understood with the presence of circumstellar envelopes produced by the stars themselves, whose mass loss grows, precisely, with luminosity, increasing, correspondingly, the mass and the optical thickness of the envelopes (fig. 11 from Veltroni, 1984).

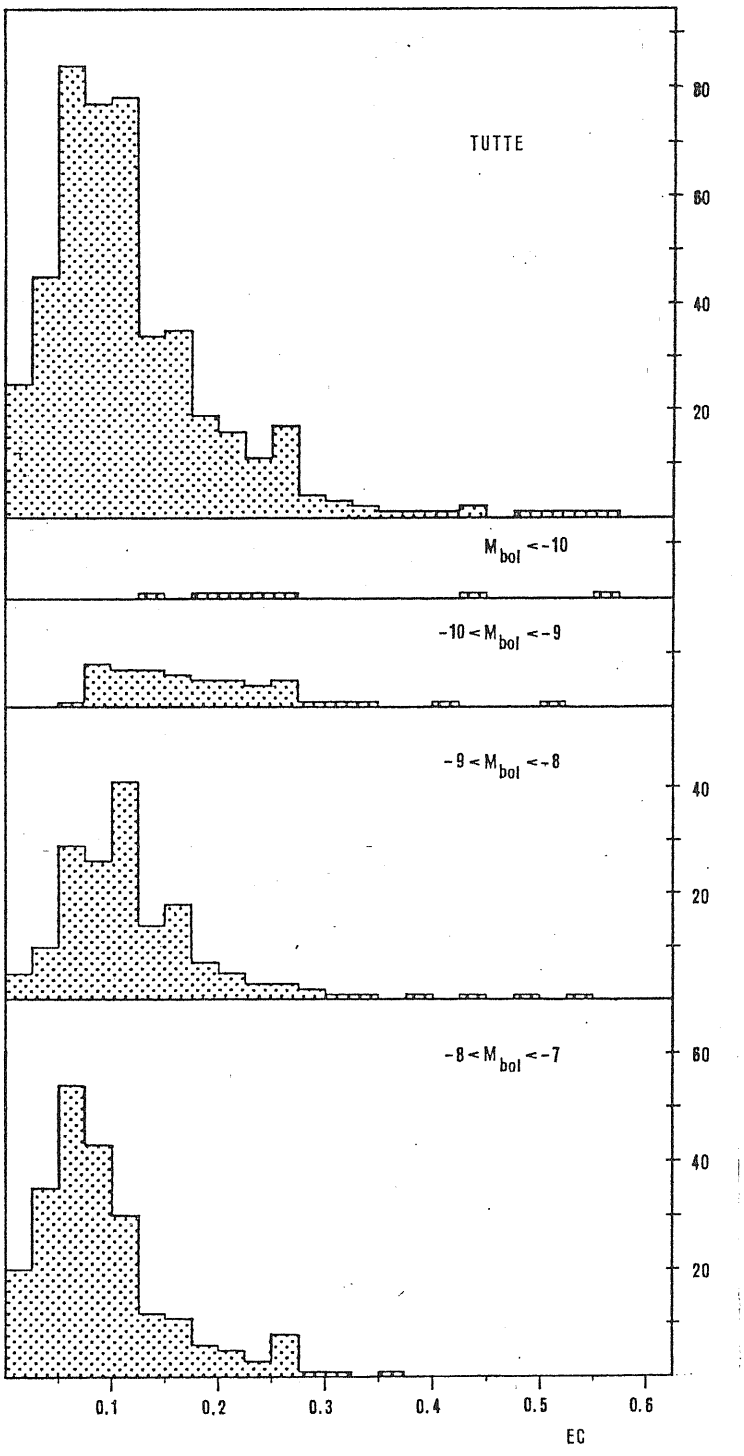

FIGURE 11. The color excess EC=(B-V)-$(B-V)_o$ in the LMC. The mean values in each magnitude interval are, respectively, from bottom to top: 0.09, 0.12, 0.17, 0.30; (Veltroni, 1984).

2.2 METHODS TO DETERMINE MASS LOSS RATE

1) UV method

Figure 12 show an idealized P Cygni profile, unsaturated (i.e. some radiation escapes at all wavelenghts) and with a sharp violet edge which unequivocally defines a terminal velocity.

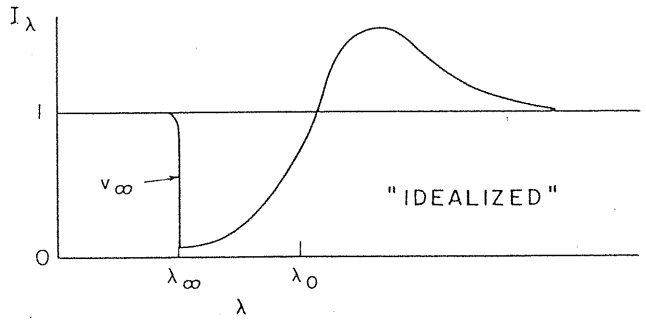

FIGURE 12.

Under the usual assumption of a Sobolev approximation (wind velocity large compared to the sound velocity) a radial optical depth for scattering may be written

$$(1) \qquad \tau = \frac{\pi e^2}{m_e c} f_i \lambda_0 n_i (dv/dr)^{-1}$$

(see chapter 3.1) where f_i is the oscillator strenght, λ_0 the rest wavelenght of the transition, n_i the number density of the absorbers, dv/dr the radial velocity gradient. We can derive τ from the intensity profile (e.g. through $\tau=-\ln(I/I_0)$) as a function of $v=(1-\lambda/\lambda_0)/c$. If we have P Cygni profiles of the same element in different excitation or ionization states, we have

$$(2) \qquad \frac{n_i}{n_j} = F(v) = \frac{\lambda_{0_j} f_j \tau_i(v)}{\lambda_{0_i} f_i \tau_j(v)}$$

Using Boltzmann and Saha equations we can determine T(v) and $P_e(v)$. Assuming the chemical composition or after having

derived it, we can obtain $\rho(v)$, $n_i(v)$ and consequently dv/dr as a function of v and, finally, through an integration, v(r) and $\rho(r)$. So, we have

(3) $\dot{M} = 4 \pi r^2 v(r) \rho(r)$

which should be constant over r for stationary accelerated winds. A common uncertainty is introduced by the fact that the commonly observed lines are not in the predominant ionization stages and large corrections to the total element abundance must be made.

2) optical method

Klein and Castor (1978) derived the mass loss rate from the core of hydrogen and helium optical emission lines. They found that H_α equivalent width scales as the square of the mass loss rate. The largest uncertainties are the adoption of a scaled v(r) relation and the contribution of the absorption part.

Olson and Ebbets (1980) developed an analysis of emission line wings, which are optically thin, obtaining the mass loss rate and v(r). The method is probably very accurate but applies only to stars with the highest mass loss rates.

3) radio method (cm)

Free-free emission of electrons in the fields of protons is present in ionized hydrogen winds at $T \geqslant 10^4$ °K. The emission coefficient in IR and radio regions is $\varepsilon \propto \nu^{-2}$. Assuming a density $n=n_0 r^{-\beta}$ Panagia & Felli (1975) and Wright & Barlow (1975) found that the radio spectral index is

(4) $\alpha = (4\beta-6)/(2\beta-1)$

For $\beta=2$ (i.e., $v=v_\infty$), $\alpha=2/3$. If $T \propto r^{-m}$, we have (Hartmann & Cassinelli, 1977)

(5) $\alpha = (4\beta-m-6)/(2\beta-1.5m-1)$

Barlow (1979) found that the expanding gas will start to cool when the adiabatic cooling rate is comparable to the radiative one and this happens only beyond

(6) $$r_c = 4.3 \cdot 10^{22} \dot{M}_{(Ms/yr)} v^{-2}_{(Km/s)} \quad (Km)$$

In the hypotesis $v=v_\infty$ and T=const. Panagia & Felli (1975) and Wright & Barlow (1975) derived

(7) $$\dot{M} = \frac{0.095\ \mu\ v_\infty\ S_\nu^{3/4}\ d^{3/2}}{Z\ \gamma^{1/2}\ g^{1/2}\ \nu^{1/2}} \quad M_s/yr$$

with

γ = number of electrons per ion;

g = the gaunt factor = $(3^{1/2}/\pi)\{\ln[(2KT)^{3/2}/(\pi Ze^2 \nu m_e^{1/2})]-1.44\}$;

Z = average (rms) charge of the ions;

(the weak dependence of g on ν tends to flatten α from 2/3 to 0.6)

d = distance from the Earth (Kpc);

ν = the frequence (Hz);

v_∞ = terminal velocity (Km/s);

S_ν = the observed flux (Jy).

4) IR method ($\approx$20 μm)

The method is the same as in the radio case, but in IR region of the spectrum the free-free emission is added to the possibly present thermal emission of dust shells and, contrary to the radio case, the photospheric contribution cannot be neglected. Moreover, the IR free-free emission comes from a region of the stellar wind where $v<v_\infty$.

2.3 MASS LOSS RATE PARAMETRIZATIONS

I will not refer here to the mass loss rates predicted by some mass loss theory, which I will consider in the next paragraph. Here I refer to the empirical and semi-empirical relations (in the sense that the choice of the parameters is driven not only by observational evidence, but also rests on some theoretical considerations more or less well-grounded) that numerous authors have derived correlating through a best fit various stellar parameters and mass loss rates. In the first case, the mass loss rate is expressed as a function of luminosity alone (this is a wide group) or luminosity and radius (or, equivalently, temperature): these are the best known parameters of stars. In the second case, a dependence on stellar mass M, the effective gravity g, the ratio $L/L_E=\Gamma$, the terminal velocity (in very efficient radiative winds, $L/c=\dot{M}v_\infty$), the acustic luminosity, etc., is introduced. The major part of these stellar quantities, however, are poorly known.

Mass loss rate parametrizations have been derived for different stellar groups, tipically: for O-Of-B stars, for red supergiants, for WR stars. Only two authors (Waldron, 1984; de Jager et al., 1985) have derived a relation which holds all across the HR diagram.

Table 1 lists current mass loss rate parametrizations. The differences from one another are quite evident in each stellar group: look, for example, at the difference in constants and coefficients when the same parameter dependence is assumed. The most recent determinations should be the better ones.

TABLE 1 (modified from Chiosi & Maeder, 1986)

O-Of-B stars:	
$\log\dot{M}=1.10\log L+\text{const.}$	Barlow & Cohen (1977)
$\log\dot{M}=1.56\log L-14.10$	Abbott et al. (1981)
$\log\dot{M}=1.50\log L-14.00$	de Loore (1984)
$\log\dot{M}=1.73\log L-15.80$	Garmany et al. (1981)
$\log\dot{M}=1.62\log L-14.97$	Garmany & Conti (1984)
$\log\dot{M}=0.72\log L+2.5\log(R/(1-\Gamma)/M)-9.59$	Chiosi (1981b)
$\log\dot{M}=-1.75\log L+\log(R/(1-\Gamma)/M)$	Chiosi & Olson (1983, in Garmany & Conti, 1984)
$\log\dot{M}=1.4\log L+0.06\log R-0.99\log M-15.3$	Lamers (1981)
$\log\dot{M}=\log L+0.8\log R+0.6\log M-13.36$	Garmany & Conti (1984)
$\log\dot{M}=1.3\log L+1.2\log(v_\infty/v_{esc})$	" " " "
$\log\dot{M}=\log(L/v_\infty)-10.63$	Wilson & Dopita (1985)
Red Supergiants:	
$\log\dot{M}=\log\eta+\log(L/g/R)$	Reimers (1975)
$\log\dot{M}=\log\eta_{FR}+\log(L_a/g/R)$	Fusi-Pecci & Renzini (1975)
$\log\dot{M}=\log\varepsilon+\log(L_a/v_{esc}/v_s)$	Chiosi et al. (1978)
$\log\dot{M}=1.3\log L+\text{const.}$	Maeder (1981a,b); Bertelli et al. (1984)
WR stars:	
$0.8\cdot10^{-5}\leqslant\dot{M}\leqslant8\cdot10^{-5}$	Abbott et al. (1986)
$\langle\dot{M}\rangle=2\cdot10^{-5}$	
$\dot{M}\approx7\cdot10^{-8}(M/M_s)^{2.3}$	
$\dot{M}\approx7\cdot10^{-14}(L/L_s)^{1.6}$	
All across the HR diagram:	
$\log\dot{M}=1.07\log L+1.77\log R-14.3$	Waldron (1984)
$\log\dot{M}=-a_1-a_2x-a_3x^2-a_4x^3-a_5y-a_6y^2-a_7y^3-a_8xy-a_9x^2y-a_{10}xy^2$	
$x=\log T-4$ $y=\log L-5$ $a_1=6.3168$	de Jager et al. (1985)
$a_2=0.1104$ $a_3=-0.4311$ $a_4=3.579$	
$a_5=-1.571$ $a_6=-0.0109$ $a_7=-0.2175$	
$a_{10}=0.8381$ $a_9=-1.2487$ $a_{10}=1.5822$	

$\dot{M}$ is in solar masses per year; L, M, R are in solar units; v_{th}, thermal velocity; v_∞, terminal velocity; v_{esc}, escape velocity; L_a, acustic luminosity.

Nethertheless, it seems desirable a re-analysis of the stellar samples used by the different authors. The discrepancies could be due to the use of poor stellar samples, in which case a bias is introduced through the unexpressible, but present, dependence on other stellar parameters, such as the mass, or to imprecise mass loss rate determinations.

2.4 MASS LOSS THEORIES

There are fundamentally three different supposed driving mechanisms for winds:

- gas pressure;
- radiation pressure;
- waves.

In the fist case, we deal with an high temperature (of the order of 10^5-10^6 °K) corona such as the solar one, therefore this case is referred to as "solar type wind" or "Parker wind" since he first proposed and developed the model (Parker, 1958) for an isothermal, steady-state, radial flow. In his solution the transonic point is at

$$(8) \qquad r_c/R_s = (8\cdot 10^6/T)\ (M/M_s)$$

Assuming a density stratification as in the hydrostatic equilibrium case

$$(9) \qquad \rho(r) = \rho_0\ e^{-r/d}\ ;\ d = \frac{KT}{\mu Hg}$$

it is found $r_c=4R_s$, $M\approx 10^{-14}M_s$/yr for the sun ($T_{corona}\approx 2\cdot 10^6$°K).

In the second case we have momentum transfer from the radiation to the matter through:

a) dust grains absorption;

b) electron scattering;

c) line scattering.

a) In this case, after grain condensation and growth, we have first momentum transfer from the radiation field to the grains, and then momentum transfer to the gas by grain-gas and then gas-gas collisions. This process seems to be efficient only in late type giants and supergiants.

b) Turolla et al. (1986) have developed an electron scattering wind model, modifying a preceding model envisaged for jets, assuming radiative transport. This kind of wind makes sense for very hot stars in which electron scattering is the main source of opacity. This wind has a critical point located at the adiabatic or isothermal sonic point in the optical thin or thick case, respectively. Moreover, in the optically thick case, it has a subcritical point located at the adiabatic sonic point. However it is not clear if this point is still present once convective transport is included and if the choice of a photospheric temperature and luminosity is able to fix univocally the mass loss rate.

c) This case is the best investigated and I extensively review it in the next chapter.

The last case refers to momentum transfer from turbulence waves, shock waves or hydromagnetic waves. These , though interesting - since there are indications they may play an important role in certain stellar phases - are much less developed than the preceding ones and need some "ad hoc" assumptions.

2.5 THE FLUCTUATION THEORY OF ANDRIESSE

This theory (Andriesse, 1981) moves from the observation that the mass flows from the stars appear to be variable, often in an erratic way. Then it is of fundamental importance the concept of thermodynamic fluctuation. Thermodynamic fluctuations are the fluctuations of a quantity X such that the relaxation time for the establishment of partial equilibrium for a given value X is much less than the relaxation time required to reach the equilibrium value of X itself (Landau-Lifshitz, 1969). There are two tipical relaxation times:

(10) $$\tau_D \simeq (R^3/GM)^{1/2} \propto \langle\rho\rangle^{-1/2}$$

is the dynamical time scale, an estimate of the free fall time or the propagation time of a pressure wave throughout the star.

(11) $$\tau_T \simeq \frac{|\Omega|}{L} \approx \frac{GM^2}{RL}$$

is the thermal time scale, the Kelvin-Helmoltz time, an estimate of the HR diagram crossing time.

If $\tau_D \ll \tau_T$, the stellar atmosphere can reach a partial equilibrium different from thermodynamic equilibrium. If the mass loss rate is not fixed by some eigenvalue condition as in the CAK wind model, than we must apply the theory of thermodynamic fluctuations: X is the mass loss rate or the adimensional quantity

(12) $$\dot{\lambda} = \frac{GM\dot{M}/R}{L}$$

that is the ratio of mechanical to luminous power.

We set in the case that a mass flow is present not regarding to the physical cause, which could reside in the atmosphere, but

we assume that the fluctuations onset under the photosphere, where momentum equation is

$$\dot{u} + \nu u + \frac{1}{\rho}\frac{dp}{dr} + \frac{GM}{r^2} = 0 \qquad (13)$$

with a friction term.

$$\nu = \xi v_{th}/l = \xi v_{th} n\sigma = \xi v_{th}(\rho/\mu H)\sigma \qquad (14)$$

where $v_{th}=[KT/(\mu H)]^{1/2}$ is the thermal velocity, l is the mean free path and σ the atomic collision cross section. Since

$$\dot{M} = 4\pi r^2 \rho u \qquad (15)$$

we have

$$\dot{M} = 4\pi r^2 \dot{\rho} u + 4\pi r^2 \rho \dot{u} \qquad (16)$$

and

$$\dot{M} + \nu \dot{M} - 4\pi r^2(\dot{\rho}u - \rho g_{eff}) \qquad (17)$$

Andriesse assumes $\nu=1/\tau_T$, $\rho=\rho/\tau_D$, and so the momentum equation becomes

$$\dot{M} = - \dot{M}/\tau_T + 4\pi r^2 \rho(u/\tau_D - g_{eff}) \qquad (18)$$

or

$$\dot{\lambda} = - \lambda/\tau_T + 4\pi r GM\rho(u/\tau_D - g_{eff})/L \qquad (19)$$

where

$$\dot{\lambda} = \frac{GM\dot{M}}{RL} \qquad (20)$$

This equation may be formally written as

$$\dot{\lambda} = - \lambda/\tau_T + A(t) \qquad (21)$$

which has the formal solution

$$\lambda = \lambda_o e^{-t/\tau_T} + \int_o^t A(t-y) e^{-y/\tau_T} dy \qquad (22)$$

In absence of the stochastic term A(t), the mass loss rate decreases to zero in thermal timescale. In presence of A(t) the decrease is stopped at a value corresponding to

(23) $$\int_0^t A(t-y)e^{-y/\tau_T}dy$$

A(t) is of stochastic nature with a positive definite mean value. Integrating, Andriesse finds

(24) $$\langle\lambda\rangle = (\tau_D\tau_T)^{1/2}\ \langle A\rangle$$

Then he assumes equipartition of kinetic mechanical power and thermal power in the atmosphere

(25) $$L = \Omega/\tau_T = K/\tau_D$$

where K is the total kinetic energy of the atmosphere. Since stochastic force perturbs the gravitational energy, one expects

(26) $$K/\tau_D \propto \langle A\rangle\Omega$$

and therefore

(27) $$\langle A\rangle = \chi/\tau_T\ ;\ \langle\lambda\rangle = \chi(\tau_D/\tau_T)^{1/2}\ ;\ \chi \approx 1$$

Substituting

(28) $$\langle\dot{M}\rangle = 2.114\cdot10^{-14}(L/L_s)^{3/2}(R/R_s)^{9/4}(M/M_s)^{-9/4}\ M_s/yr$$

or

(29) $$\log\langle\dot{M}\rangle = 3.250+2.625\log(L/L_s)-4.5\log T-2.25\log(M/M_s)$$

3. THE LINE DRIVEN WIND

3.1 THE LINE ACCELERATION

The total cross-section of an atom is

$$(30) \qquad \int_{\text{all lines}} \alpha_\nu d\nu = \frac{\pi e^2}{m_e c} n \quad (cm^2)$$

(we are using Gauss units: $1C = 10c$ u.e.s. $\simeq 3 \cdot 10^9$ u.e.s.) where n is the number of electrons which are able to perform some transition. For a single line

$$(31) \qquad \int \alpha_\nu d\nu = \frac{\pi e^2}{m_e c} f_i$$

where f_i is the oscillator strenght of the line, with $\sum_i f_i = n$. So, the impulse transferred from the radiation to unit mass in the line is

$$(32) \qquad g_i = \frac{\pi e^2}{m_e c} f_i \frac{X}{Am_H} \frac{F_\nu}{c}$$

where A is the atomic number of the element, X the fraction of total mass in the element, being able to absorbe effectively in line i. Since the flux is attenuated progressively in the line, the mean acceleration is

$$(33) \qquad \begin{aligned} \langle g_i \rangle &= \frac{\pi e^2}{m_e c} f_i \frac{X}{Am_H} \frac{1}{\tau_\ell} \int_0^{\tau_\ell} \frac{F_\nu}{c} e^{-\tau} d\tau \\ &= \frac{\pi e^2}{m_e c} f_i \frac{X}{Am_H} \frac{F_\nu}{c} \frac{1-e^{-\tau_\ell}}{\tau_\ell} \\ &\approx \frac{\pi e^2}{m_e c} f_i \frac{X}{Am_H} \frac{F_\nu}{c} \min(1, 1/\tau_\ell) \end{aligned}$$

in the approximation of Castor, Abbott & Klein (CAK, 1975), with

$$(34) \qquad \tau_\ell = \frac{1}{\Delta\nu_D} \frac{\pi e^2}{m_e c} f_i \frac{X}{Am_H} \int \rho \, dr$$

where $\Delta\nu_D = \nu_0 v_{th}/c$ is the Doppler width of the line. If τ_ℓ is large

$$(35) \qquad \langle g_i \rangle = (F_\nu/c)\cdot(\Delta\nu/\int\rho dr)$$

that is the total impulse absorbed in the line divided the column mass of the absorbers. If τ_ℓ is small

$$(36) \qquad \langle g_i \rangle = \frac{\pi e^2}{m_e c} f_i \frac{X}{Am_H} \frac{F_\nu}{c}$$

Let us compare it to the total electron scattering impulse

$$(37) \qquad g_{es} = \sigma_0 \frac{1}{\mu_e m_H} \frac{F}{c} = \sigma_e \frac{F}{c}$$

($\sigma_e \approx 0.4$ cm^2 gr^{-1}). Assuming $\sum f_i = A/2$, being $F/F_\nu \approx 2.5KT/h$, we have

$$(38) \qquad \frac{\langle g \rangle}{g_{es}} \approx 0.4\cdot 10^8 \left(\frac{10^4}{T}\right) X$$

X is of the order of 10^{-4}, so the ratio $\langle g \rangle/g_{es}$ is of the order of 10^3. Since the ratio

$$(39) \qquad \frac{g_{es}}{g_{grav}} = \frac{\sigma_e L}{4\pi cGM} \simeq 3\cdot 10^{-5} \frac{L/L_s}{M/M_s}$$

is of the order of 10^{-1} in supergiant stars, hydrostatic equilibrium in the outermost layers is not possible and an outflow of material must inevitably occur.

Once the gas in the uppermost layer begins to move outward, its spectral lines will be Doppler shifted away from their rest wavelenghts and will therefore begin to intercept the intense photospheric flux in the adiacent continuum, which enhances the momentum input to the material, hence increases its outward acceleration. The underlying layers must expand to fill the rarefaction left by the outward motion of the upper layers. Furthermore, also the absorption lines in the lower layers begin

to desaturate because of the Doppler shift. In this case, infact, the optical thickness of the line at $\nu = \nu_0 \cdot (1+v/c)$ is

$$(40) \qquad \tau_\ell = \frac{1}{\Delta\nu} \frac{\pi e^2}{m_e c} f_i \frac{X}{A m_H} \frac{\rho v_{th}}{dv/dr|_v}$$

much smaller than in the static case, because the column mass is smaller. Hence, the lower layers also begin to experience a radiative force that exceeds gravity.

3.2 THE FORCE MULTIPLIER

The ratio g_{lines}/g_{es} is the force multiplier M. Castor, Abbott and Klein (1975) evaluated M for the lines of the CIII spectrum assuming LTE, blackbody continuum, abundance of 10^{-3} (total of C, N and O), at T=30000, 40000, 50000 as a function of electron scattering optical depth t. They found $M=kt^{-\alpha}$ with:

TABLE 2

T	k	α
30000	0.0076	0.742
40000	0.0026	0.737
50000	0.0021	0.811

Abbott (1982) used Kurucz (1979) models instead of a blackbody continuum and calculated the line acceleration using a tabulation of atomic lines complete for the elements from H to Zn, up to the sixth stage of ionization. He tabulated the force multiplier at $t=-1,-2,\ldots-7$ for 8 temperatures between 6000 and 50000 °K and 3 different densities (tab. 3).

TABLE 3 (Abbott, 1982)

THE CALCULATED LINE ACCELERATION LOG (Force Multiplier)

T_{eff} (K)	log g	δ	N_e/W (cm^{-3})	t 10^{-7}	10^{-6}	10^{-5}	10^{-4}	10^{-3}	10^{-2}	10^{-1}	k	α	σ
6000	0.5	0.16	6.8(+6)	1.478	1.236	0.750	0.316	−0.196	−0.729	−1.291	0.018	0.502	0.055
			6.8(+8)	1.480	1.240	0.761	0.344	−0.129	−0.590	−1.113	0.029	0.465	0.037
			6.8(+11)	2.008	1.911	1.733	1.351	0.854	0.342	−0.263	0.272	0.444	0.123
8000	1.0	0.02	1.7(+6)	2.322	2.045	1.676	1.214	0.687	0.106	−0.553	0.110	0.521	0.079
			1.7(+9)	2.409	2.166	1.778	1.262	0.715	0.127	−0.529	0.105	0.542	0.079
			1.7(+12)	2.581	2.305	1.815	1.294	0.746	0.165	−0.477	0.108	0.555	0.024
10,000	1.5	0.05	3.2(+6)	2.593	2.307	1.961	1.588	1.093	0.482	−0.198	0.288	0.499	0.113
			3.2(+9)	3.000	2.667	2.256	1.818	1.283	0.663	−0.037	0.362	0.538	0.099
			3.2(+12)	3.041	2.690	2.272	1.840	1.301	0.677	−0.026	0.370	0.540	0.102
15,000	2.0	0.12	1.3(+7)	2.525	2.249	1.866	1.296	0.774	0.310	−0.245	0.189	0.505	0.013
			1.3(+10)	2.904	2.468	1.959	1.450	0.922	0.446	−0.096	0.253	0.511	0.020
			1.3(+13)	3.351	2.956	2.555	2.159	1.641	1.034	0.356	0.945	0.517	0.092
20,000	2.5	0.089	3.0(+7)	2.888	2.556	1.965	1.333	0.711	0.266	−0.213	0.140	0.559	0.068
			3.0(+10)	2.976	2.664	2.242	1.702	1.227	0.734	0.124	0.477	0.506	0.035
			3.0(+13)	3.335	2.898	2.406	1.890	1.385	0.873	0.261	0.617	0.523	0.031
30,000	3.5	0.12	1.0(+8)	2.952	2.432	1.857	1.269	0.655	0.109	−0.426	0.093	0.576	0.022
			1.0(+11)	3.289	2.918	2.243	1.523	0.957	0.443	−0.150	0.156	0.609	0.057
			1.0(+14)	3.356	3.032	2.493	1.902	1.379	0.881	0.291	0.571	0.545	0.018
40,000	4.0	0.12	1.8(+8)	3.003	2.737	2.180	1.474	0.770	0.067	−0.639	0.051	0.684	0.041
			1.8(+11)	3.155	2.823	2.292	1.710	1.076	0.452	−0.188	0.174	0.606	0.034
			1.8(+14)	3.355	3.102	2.610	2.026	1.485	0.913	0.228	0.533	0.571	0.046
50,000	4.5	0.092	3.1(+8)	2.970	2.679	2.202	1.590	0.922	0.231	−0.486	0.089	0.640	0.071
			3.1(+11)	3.028	2.785	2.339	1.743	1.106	0.456	−0.199	0.178	0.606	0.062
			3.1(+14)	3.318	3.074	2.635	2.062	1.449	0.845	0.197	0.472	0.582	0.056

The force multiplier decreases with t, increases with density and is roughly constant over the temperature range 50000 to 10000 °K being smaller by a factor ≃3 at T≃8000 and a factor ≃6 at T≃6000. However, at these temperatures, it is evident observationally that molecules are absorbing a large amount of radiation, but molecular lines are not included yet in the calculated line acceleration. In Abbott calculations, at T>20000°K the acceleration is mostly provided by C, N, O lines (but also Ne through Ca), in Balmer and Lyman (T>30000°K) continuum; at 20000>T>8000 the acceleration is dominated by iron group lines (Cr, Mn, Fe, Ni) in Balmer continuum. At T≃6000, Ca, Ti and H are important. Assuming

(41) $M = k\, t^{-\alpha}\, (N_{11}/W)^{\delta}$

where $N_{11}=N_e/10^{11}$ and $W=0.5\{1-[1-(R_*/R)^2]^{1/2}\}$ is the dilution factor, Abbott fitted his data with:

TABLE 4

T	k	α	δ
50000 to 10000	0.28	0.56	0.09

(M is accurate within a factor of 3).

Pauldrach et al. (1986) used the data of Abbott (1982) to derive the constants k, α, δ by the following iterative procedure: with a first guess of k, α, δ they resolved the wind for the individual star and determined the relevant domain in the (t, N_e/W) plane. Then the final values of k, α, δ were fitted to reproduce the tabulated force multiplier values just in this relevant domain. They obtained:

TABLE 5

T	k	α	δ
20000	0.32	0.565	0.02
30000	0.17	0.59	0.09
40000	0.124	0.64	0.07
50000	0.124	0.64	0.07

Their procedure is interesting and should be used to obtain accurate wind models. But the k, α, δ so obtained are inevitably model dependent. In order to have both accuracy and generality, I have performed a least squares fit of Abbott's data with the expression

(42) $\log M = \log k - \alpha \log t + \delta \log(N_{11}/W)$

for all densities and optical depths but separately for each temperature, obtaining

TABLE 6

T	k	α	δ	$\sigma_{\log M}$
6000	0.146	0.433	0.190	0.207
8000	0.150	0.500	0.022	0.128
10000	0.494	0.490	0.047	0.155
15000	0.524	0.489	0.126	0.129
20000	0.429	0.510	0.084	0.090
30000	0.222	0.561	0.107	0.084
40000	0.205	0.578	0.098	0.148
50000	0.240	0.561	0.083	0.154

For intermediate temperatures, I used spline interpolation, as illustrated in fig. 13;a,b,c.

In fig. 14;a-h the Abbott's data (tab. 3) are rapresented together with (42) according to the parameters of the preceding table and densities tabulated by Abbott.

Abbott's data are for a solar composition: metallicity enters in the acceleration (33) explicitly, through X, and implicitly, through τ_ℓ, see (34). So the complete expression of the force multiplier is

(43) $$M(t) = k\, t^{-\alpha}\, (N_{11}/W)^{\delta}\, (Z/Z_s)^{1-\alpha}$$

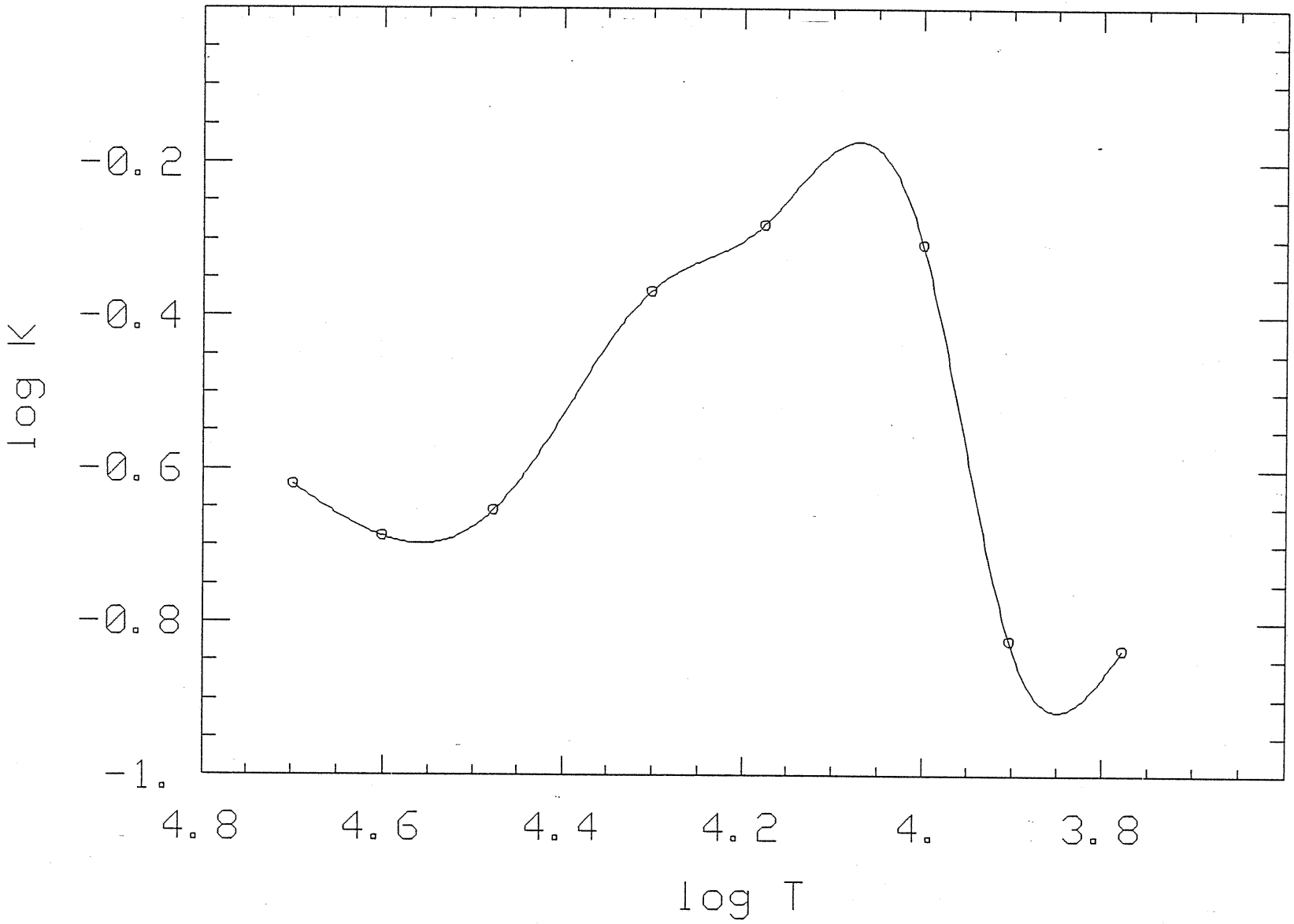

FIGURE 13a. logk as in table 6 and spline interpolation.

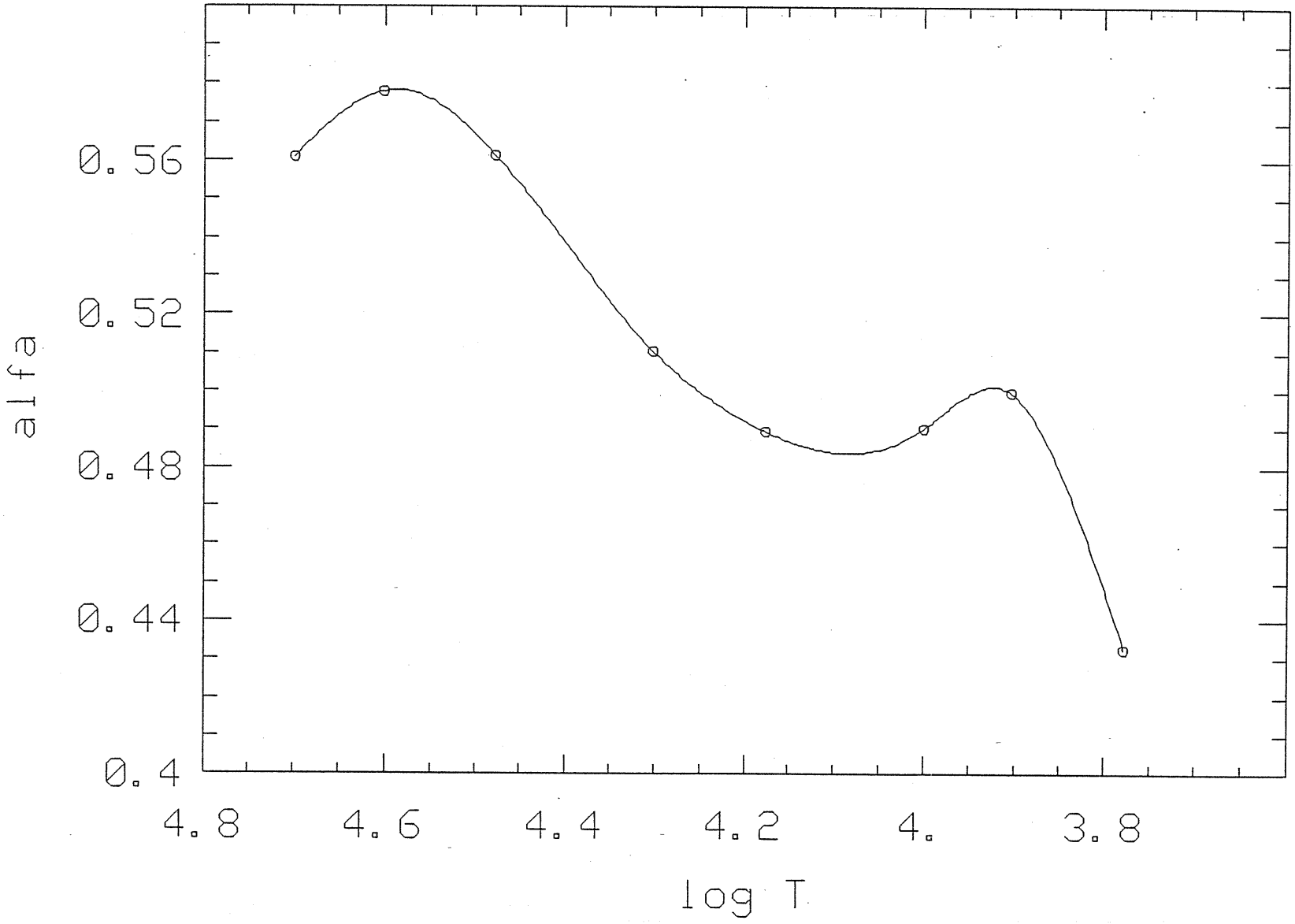

FIGURE 13b. α as in table 6 and spline interpolation.

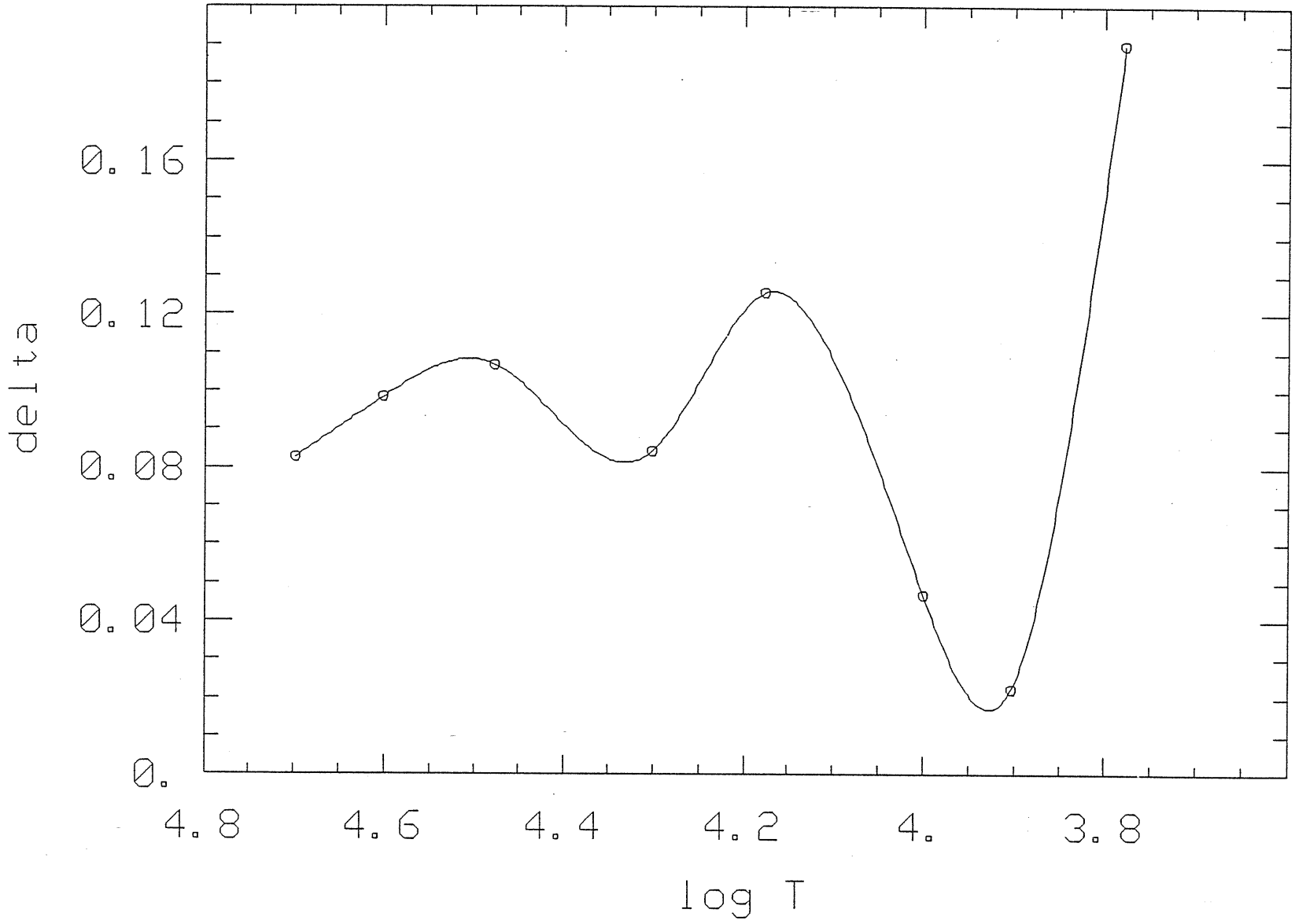

FIGURE 13c. δ as in table 6 and spline interpolation.

FIGURE 14a.

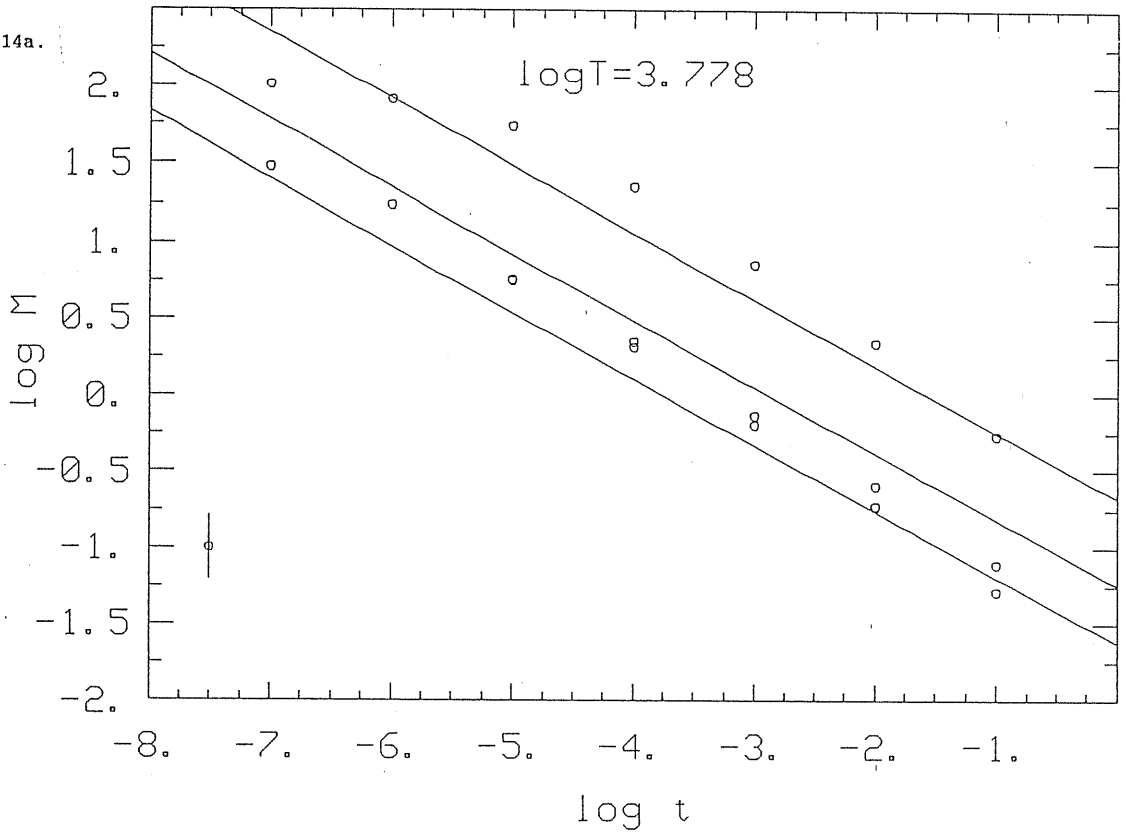

FIGURE 14b.

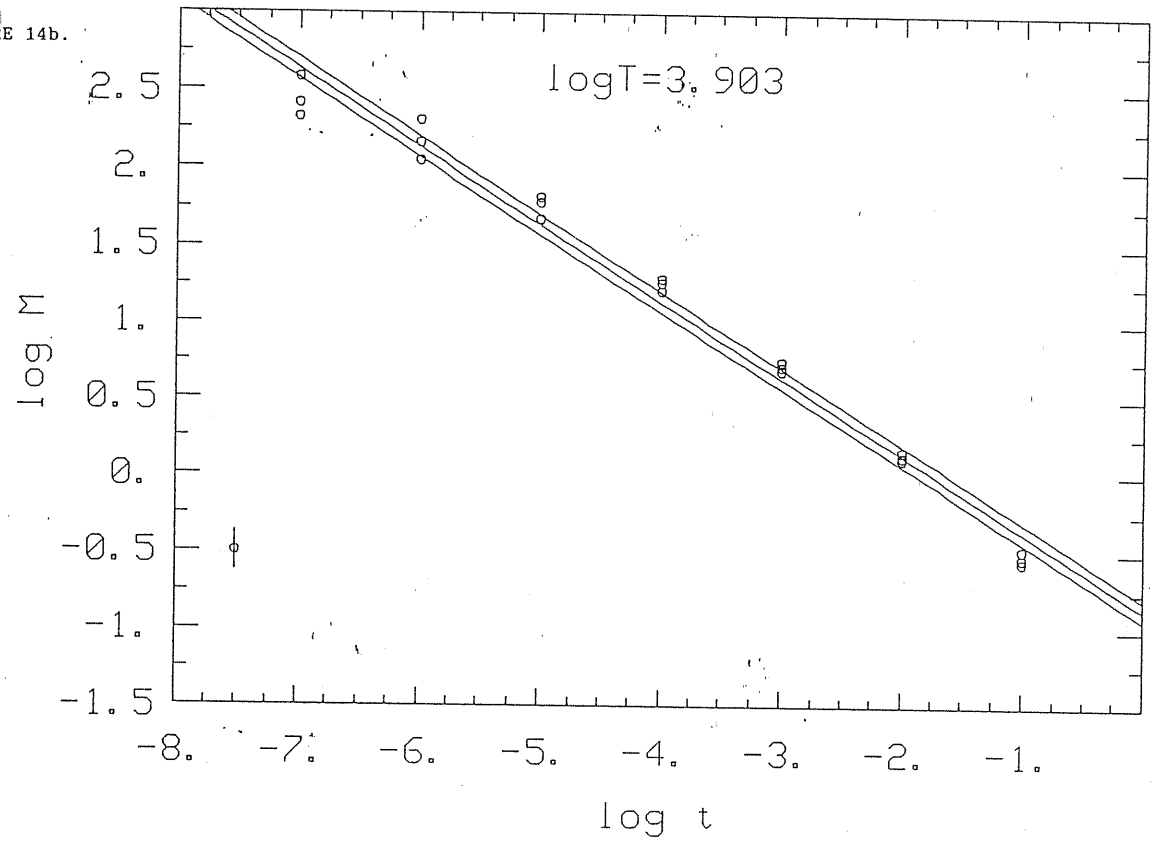

FIGURE 14c.

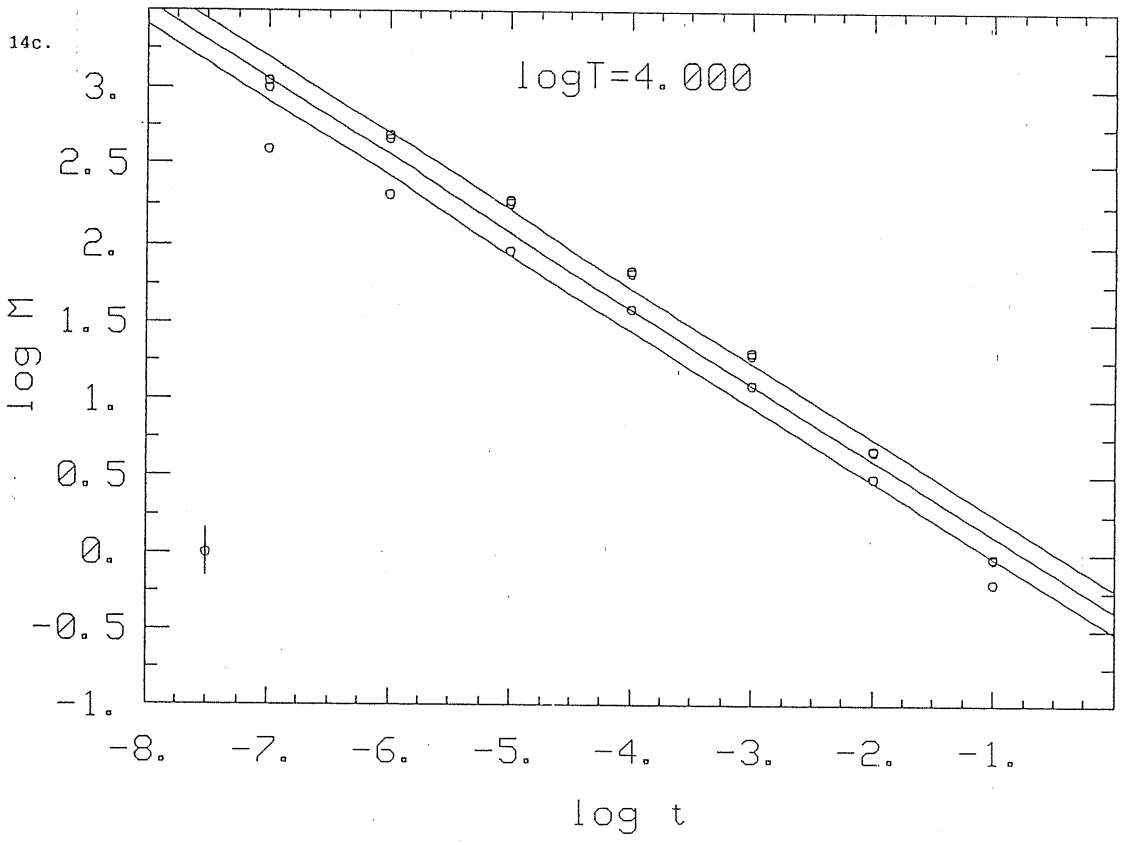

FIGURE 14d.

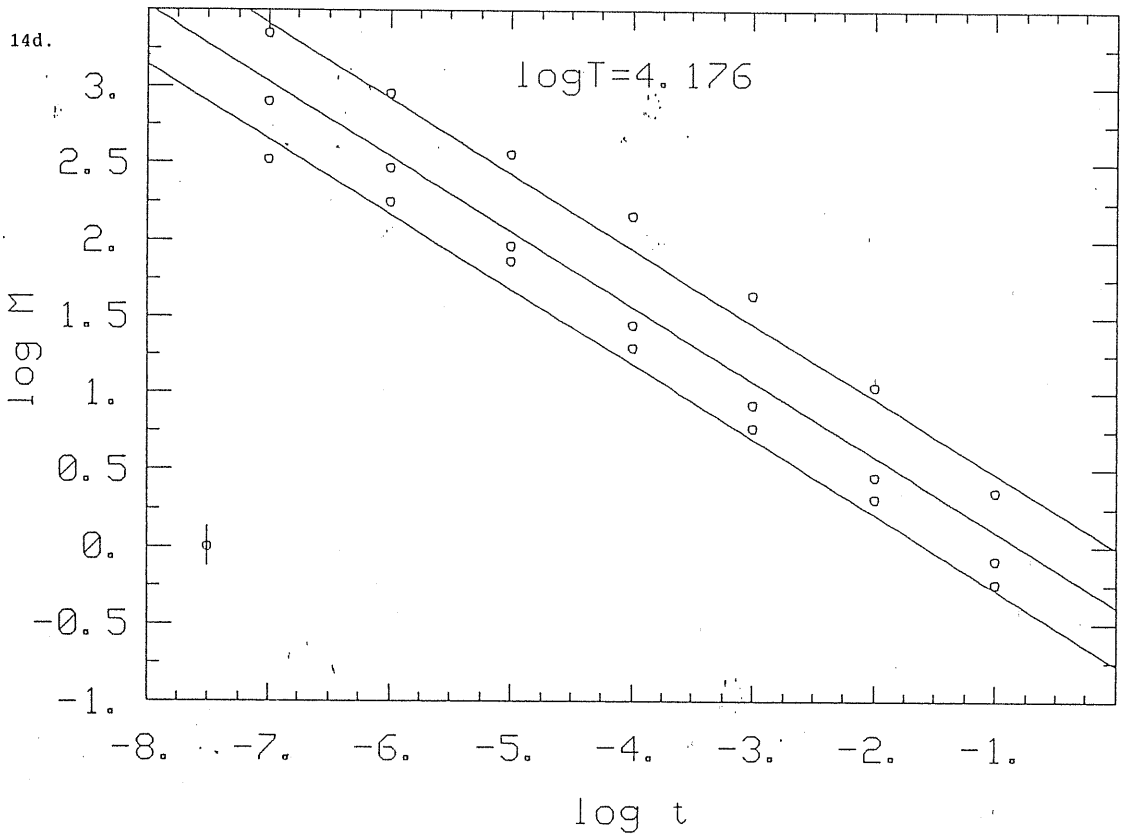

FIGURE 14e.

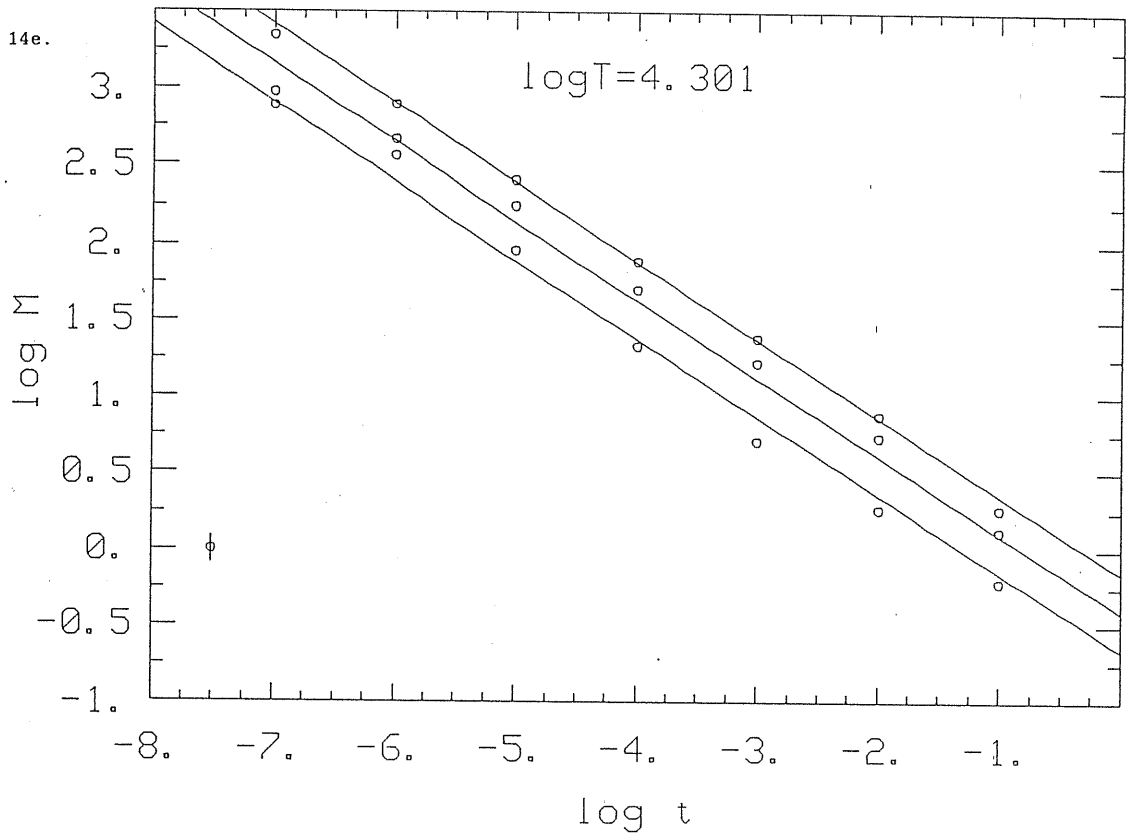

FIGURE 14f.

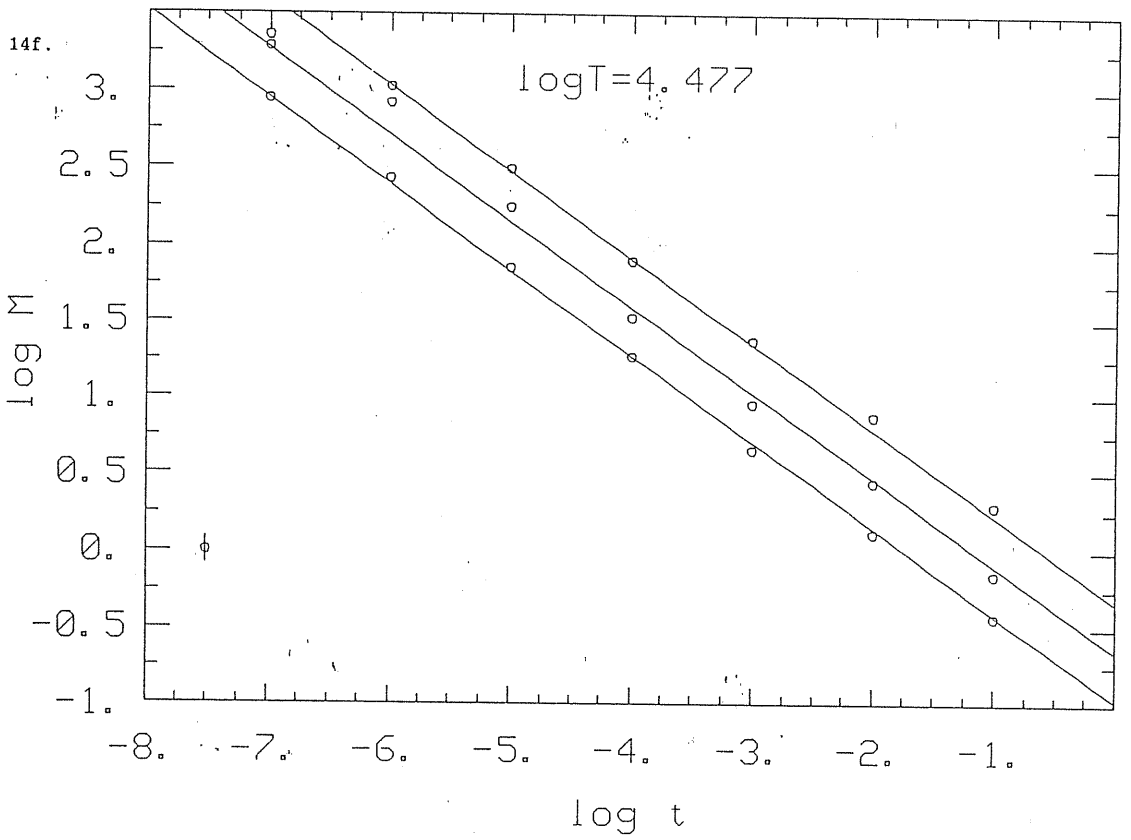

FIGURE 14g.

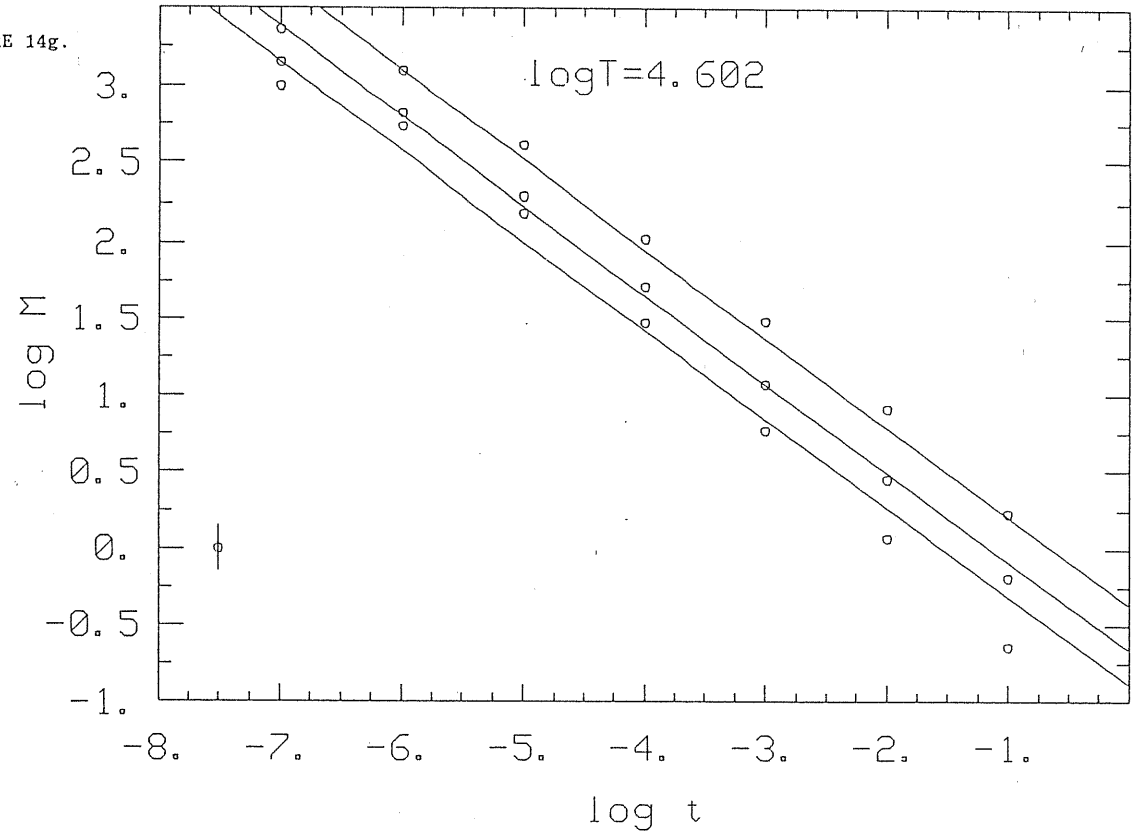

FIGURE 14h.

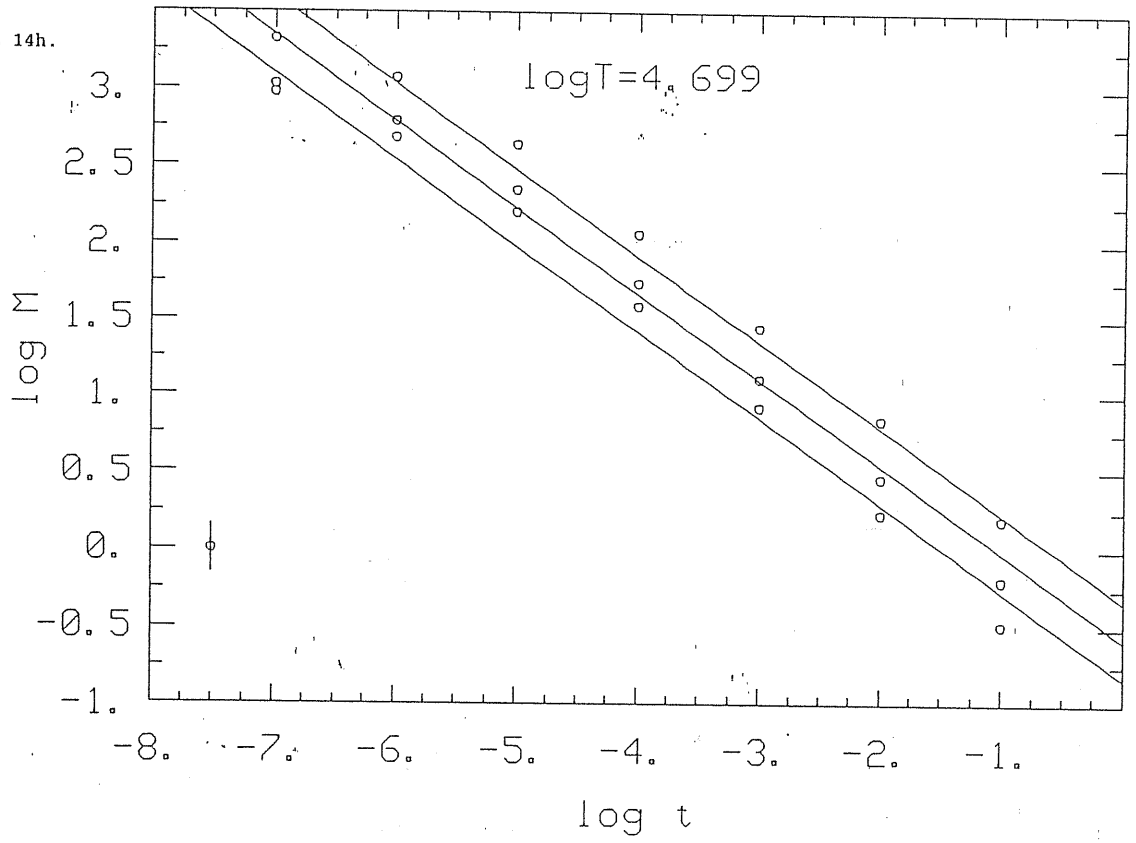

3.3 THE FINITE DISK CORRECTION

The CAK (1975) wind is calculated in the hypotesis of radial streaming of the radiation. This is not the actual case since the photosphere is not a point source but it has a finite angular dimension. So the force multiplier has to be weighted over the angle subtended by the photosphere:

$$M = \frac{\int_0^{\theta_*} M \cos\theta \, d\Omega}{\int_0^{\theta_*} \cos\theta \, d\Omega} \tag{44}$$

Since $\cos\theta_* = [1-(R_*/R)^2]^{1/2} = \mu_*$ and $d\Omega = \text{sen}\theta d\theta d\phi$ we have

$$M = \frac{\int_{\mu_*}^{1} M \, \mu \, d\mu}{\int_{\mu_*}^{1} \mu \, d\mu} = \frac{2}{1-\mu_*^2} \int_{\mu_*}^{1} M \, \mu \, d\mu \tag{45}$$

where

$$M = M(t_\mu) = M(t) \, (t_\mu/t)^{-\alpha} \tag{46}$$

$$t_\mu = t \, \frac{dv/dr}{(1-\mu^2)v/r + \mu^2 dv/dr} \tag{47}$$

Finally, we obtain

$$M = M(t) \cdot K \tag{48}$$

$$K = \frac{1 - [(R_*/r)^2 \, \frac{d\ln r}{d\ln v} + 1 - (R_*/r)^2]^{1+\alpha}}{(1+\alpha) \, (R_*/r)^2 \, (1-\frac{d\ln r}{d\ln v})} \tag{49}$$

3.4 THE EQUATION OF MOTION OF CAK AND M-CAK WINDS: DISCUSSION OF THE SOLUTIONS

The momentum equation is:

$$(50) \qquad v \frac{dv}{dr} = - \frac{1}{\rho} \frac{dP}{dr} - \frac{GM}{r^2} + g_{rad}$$

where:

$$(51) \qquad P = \rho\, a^2 \quad ---> \quad \frac{dP}{\rho} = da^2 + a^2 \frac{d\rho}{\rho}$$

$$\dot{M} = 4\, \pi\, r^2\, \rho\, v \quad ---> \quad 2\frac{dr}{r} + \frac{d\rho}{\rho} + \frac{dv}{v} = 0$$

$$g_{rad} = \frac{\sigma L}{4\pi r^2 c} (1+M)$$

(a is the isothermal sound speed). Therefore, we have:

$$(52) \qquad v \frac{dv}{dr} = - \frac{da^2}{dr} + \frac{2a^2}{r} + \frac{a^2}{v}\frac{dv}{dr} - \frac{GM}{r^2} + \frac{\sigma L}{4\pi r^2 c} (1+M)$$

If we assume:

$$(53) \qquad u = - R_*/r$$

$$w = v^2/V^2$$

$$h(u) = - \frac{GM}{R_*}(1-\Gamma) - \frac{2a^2}{u} - \frac{da^2}{du}$$

we obtain:

$$(54) \qquad (1-\frac{a^2}{V^2 w})\, w' - 2h(u)/V^2 - \frac{\sigma L}{2\pi c V^2 R_*} M = 0$$

1) First, let us study the CAK (1975) wind, in which case the Force Multiplier is simply:

$$(55) \qquad M = k\, t^{-\alpha}$$

where:

$$(56) \qquad t = \sigma \rho v_{th} dr/dv = \sigma \dot{M} v_{th}/(2\pi R_* V^2 w')$$

So, the equation (53) becomes

$$(57) \qquad F(w') = (1-\frac{a^2}{V^2 w})\, w' - 2h(u)/V^2 - C w'^{\alpha} = 0$$

with:

(58) $$C = \frac{L}{c}\, k\, \left(\frac{\sigma}{2\pi R_* V^2}\right)^{1-\alpha} (\dot{M} v_{th})^{-\alpha}$$

Looking for finite positive w' solutions of F(w')=0, in the hypotesis of a constant isothermal sound speed ($da^2/du=0$; ≈isothermal wind) and observing that:

(59) $\alpha<1$

$$F'_{w'} = 1 - \frac{a^2}{V^2 w} - \frac{\alpha\, C}{w'^{1-\alpha}}$$

$$F''_{w'} = \alpha(1-\alpha)\, C\, w'^{1-2\alpha}$$

we obtain the following:

TABLE 7

the sign of:	is the sign of:
$F(0)$	$-2h/V^2$
$F(\infty)$	$1 - \frac{a^2}{V^2 w}$
$F'_{w'}(0)$	$-\alpha C$, always negative
$F'_{w'}(\infty)$	$1 - \frac{a^2}{V^2 w}$
$F''_{w'}$	always positive

There are some cases:

a) $h<0$ (possible only if $\Gamma<1$), that is $u < u_L = -\frac{2\, a^2}{(1-\Gamma)GM/R_*}$ and $1 - \frac{a^2}{V^2 w} < 0$, that is $v < a$;

$F(0)>0$, $F(\infty)<0$: 1 solution (see fig. 15).

b) $h<0$, $v>a$;

$F(0)>0$, $F(\infty)>0$: 2 or no solution.

c) $h\geq 0$, $v<a$;

$F(0)\leq 0$, $F(\infty)<0$: no solution.

d) $h\geq 0$, $v>a$;

$F(0)\leq 0$, $F(\infty)>0$: 1 solution.

If $\Gamma>1$ no transonic flow is possible (unless we have outward increasing temperature) but only supersonic wind (case d). So let us consider the normal case: $\Gamma<1$.

The wind starts at the photosphere ($u=-1$) with subsonic velocity (case a) or eventually at supersonic velocity (case b); the sonic velocity has to be reached before $u=u_L$ otherwise we enter in case c (If $u_L<-1$ we have solution only in case d: the wind starts supersonic and we have no critical point; this is the case of evaporating stars, near the Eddington limit). For $v>a$ and $u<u_L$ we have 2 solutions; for continuity we choose the minor one as we enter in this region since F is a continuous function of w and h, so its shape varies with continuity. However, passing through u_L, we loose this solution and we have a discontinuous passage to the higher one. The only possibility for continuity is that, before this happens, we have a transition from the lower to the higher solution through the case of two coincident solutions (fig. 16), that is, there have to be a point where:

$$(60)\qquad \begin{cases} F=0 \\ F'_{w'}=0 \\ F'_u+F'_{w'}w'=0 \end{cases}$$

where the fist two conditions assure continuity in w' and the last one assures continuity in w".

This is called the critical point u_c.

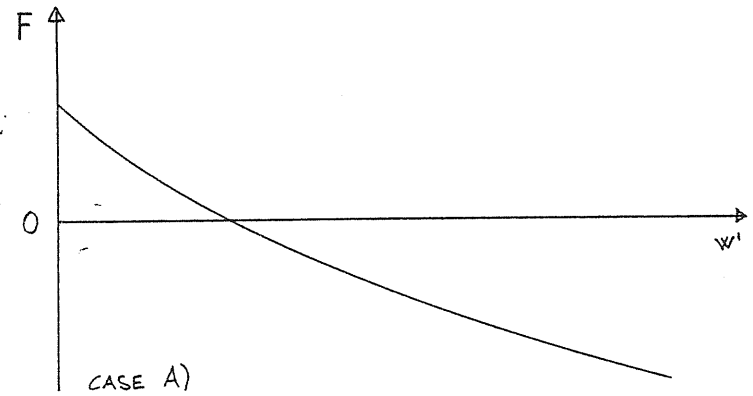

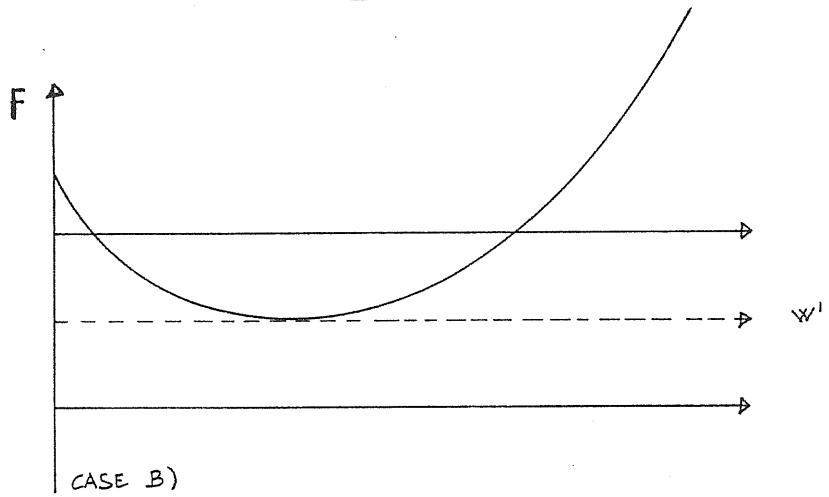

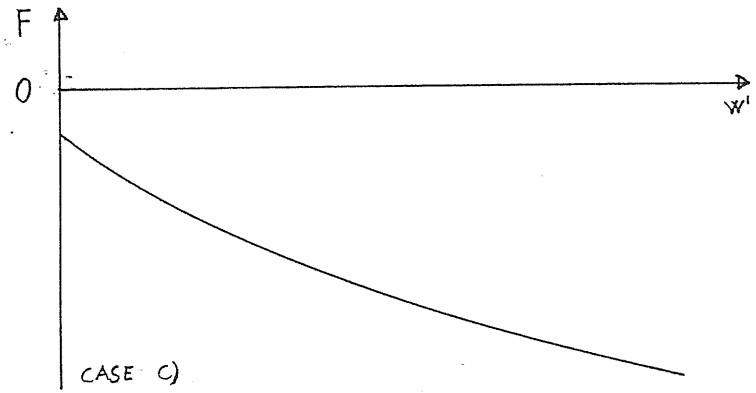

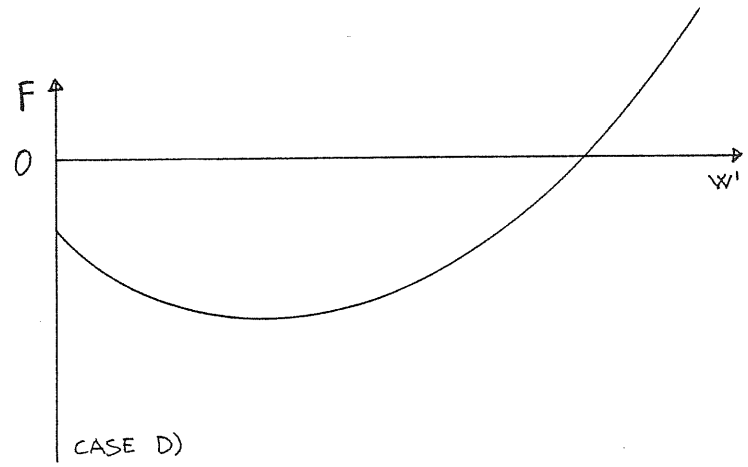

FIGURE 15

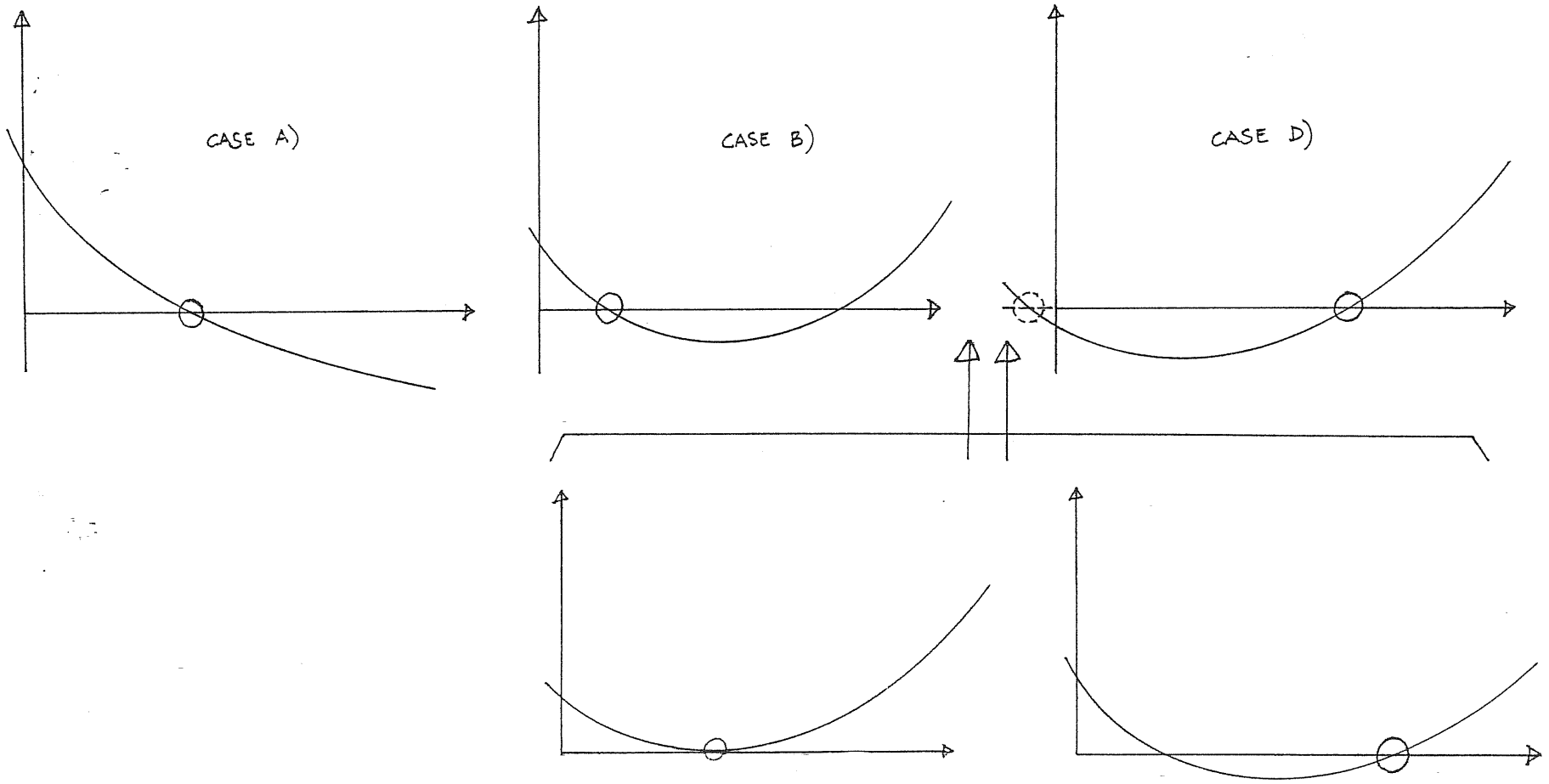

FIGURE 16

2) Let us now consider the Modified-CAK wind, which includes the new Abbott's force multiplier (Abbott, 1982), the finite disk correction factor, as developed by Pauldrach et al. (1986) and Friend & Abbott (1986), and the metallicity dependence. In this case the complete force multiplier is:

(61) $$M = k\, t^{-\alpha}\, (10^{-11} n_e/W)^{\delta} (Z/Z_s)^{1-\alpha} K$$

where K is the finite disk correction factor (49). With the positions (52), we have:

(62) $$(1 - \frac{a^2}{V^2 w})\, w' - 2h(u)/V^2 - Cg(u,w,w') w'^{\alpha} w^{-\delta/2} = 0$$

where:

(63) $$g(u,w,w') = K(u,w,w')\, [u^2/(1-\sqrt{1-u^2})]^{\delta}$$

(64) $$C = C_{CAK}\, \dot{M}^{\delta}\, (2\cdot 10^{11} \pi \mu_e m_H R_*^2 V)^{-\delta}\, (Z/Z_s)^{1-\alpha} =$$

$$= \frac{L}{c}\, k \left[\frac{\sigma_e Z/Z_s}{2\pi R_* V^2}\right]^{1-\alpha} (\dot{M} v_{th})^{-\alpha}\, \dot{M}^{\delta}\, (2\cdot 10^{11} \pi \mu_e m_H R_*^2 V)^{-\delta}$$

The discussion of the solution is identical to the CAK wind: we have a critical point only for $v>a$ and $-1<u<u_L$.

3.5 THE CRITICAL POINT OF M-CAK WIND

Let us assume that $g(u,w,w')$ is given as a function of u, as in the iteratively approach of Pauldrach et al. (1986). We have:

(65) $$F(u,w,w') = (1 - \frac{a^2}{V^2 w})\, w' - \frac{2h(u)}{V^2} - Cg(u) w'^{\alpha} w^{-\delta/2}$$

(66) $$F'_{w'} = 1 - \frac{a^2}{V^2 w} - \frac{\alpha\, C\, g}{w^{\delta/2} w'^{1-\alpha}}$$

(67) $$F'_w = \frac{a^2 w'}{V^2 w^2} - \frac{\delta C g w'^{\alpha}}{2 w^{1+\delta/2}}$$

(68) $$F'_u = -\frac{w'}{V^2 w}\frac{da^2}{du} - \frac{2}{V^2}\frac{dh}{du} - \frac{C\, w'^{\alpha}}{w^{\delta/2}}\frac{dg}{du}$$

(69) $$\frac{dh}{du} = \frac{2a^2}{u^2} - \frac{2}{u}\frac{da^2}{du} - \frac{d^2 a^2}{du^2}$$

The critical point conditions are:

$$(70)\quad \begin{cases} (1 - \dfrac{a^2}{V^2 w})\, w' - \dfrac{2h(u)}{V^2} - Cg(u) w'^{\alpha} w^{-\delta/2} = 0 \\ 1 - \dfrac{a^2}{V^2 w} - \dfrac{\alpha\, C\, g}{w^{\delta/2} w'^{1-\alpha}} = 0 \\ \dfrac{a^2 w'^2}{V^2 w^2} - \dfrac{\delta C g w'^{1+\alpha}}{2w^{1+\delta/2}} - \dfrac{w'}{V^2 w}\dfrac{da^2}{du} - \dfrac{2}{V^2}\dfrac{dh}{du} - \dfrac{C}{w^{\delta/2}} w'^{\alpha}\dfrac{dg}{du} = 0 \\ w=1 \end{cases}$$

that is, with the positions $v(u_c)=V$, $w(u_c)=W$, $w'(u_c)=W'$:

$$(71)\quad \begin{cases} (1-\alpha) C g W'^{\alpha} = -2h/V^2 = \dfrac{1-\alpha}{\alpha}\left(1 - \dfrac{a^2}{V^2}\right) W' \\ a^2 W'^2 - \left[\dfrac{da^2}{du} + \delta h/(1-\alpha)\right] W' + 2\left[-\dfrac{dh}{du} + \dfrac{h}{(1-\alpha) g}\dfrac{dg}{du}\right] = 0 \\ W = 1 \end{cases}$$

We have one positive definite solution W' and

$$(72)\quad V^2 = a^2 - \frac{\alpha}{1-\alpha}\frac{2h}{W'}$$

$$(73)\quad C = -\frac{2h}{(1-\alpha) V^2 g W'^{\alpha}}$$

Consequently

$$(74)\quad \dot{M} = \left[\frac{Lk}{cC}\left\{\frac{\sigma L/L_s}{2\pi R_* V^2}\right\}^{1-\alpha} v_{th}^{-\alpha} (2\cdot 10^{11} \pi \mu_e H R_*^2 V)^{-\delta}\right]^{1/(\alpha-\delta)}$$

Since $F(u,w,w')=0$, it is also:

$$(75)\quad F'_u + F'_w w' + F'_{w'} w'' = 0$$

and, therefore, we have:

$$(76)\quad w'' = -(F'_u + F'_w w')/F'_{w'}$$

In the critical point, (76) is undetermined (see (59)) so we have to apply te rule of de l'Hospital in order to obtain $w''(u_c)=W''$:

$$(77)\quad W'' = -\lim \left[\frac{d}{du}(F'_u + F'_w w')\right] / \frac{d}{du}(F'_{w'})$$

3.6 THE INTEGRATION STRATEGY

First of all, the temperature fixes the values of k, α, δ. The temperature structure is intended to be fixed previously. In our case we assume T=const. throughout the wind. Second, we choose a value for u_c. Then we adopt a g(u) that is the one of the preceding calculated wind model or, if it lacks,

$$(78) \qquad g_0(u) = \frac{1-(1-u^2)^{1+\alpha}}{(1+\alpha)u^2} \left[\frac{u^2}{1-(1-u^2)^{1/2}} \right]^{\delta}$$

obtained suppressing the dependence on w and w'.

We can now proceed to calculate W', V, C, the mass loss rate and W". After, we integrate w, w' and τ from the critical point out to u_{OUT}, which is assumed, in the wind models presented here, equal to -0.001, corresponding to 1000 R_*. We adopt a Runge-Kutta procedure, with

$$(79) \qquad \frac{dw}{du} = w'$$

$$(80) \qquad \frac{dw'}{du} = w'' = - \frac{F'_w w' - F'_u}{F'_{w'}}$$

$$(81) \qquad \frac{d\tau}{du} = - \dot{M} \left(4\pi R_* V \sigma w^{1/2} \right)^{-1}$$

So, we find the optical depth at the critical point. Next we integrate toward the photosphere (the τ=2/3 locus), that we want to find at u_{FOT}=-1. If we have τ=2/3 at u>-1, then

$$(82) \qquad (u_c)_{NEW} = u_c - (u_{\tau=2/3}+1)$$

If at u_{FOT}, τ<2/3 then

$$(83) \qquad (u_c)_{NEW} = u_c - (2/3-\tau_{u=-1}) \left. \frac{du}{d\tau} \right|_{u=-1}$$

However, we control the change of u_c with two sentinels, u_{cMIN} and u_{cMAX}, which at the beginning are u_{FOT} and u_L or u_{OUT}, respectively, and then are updated, if necessary, according to

$\tau_{u=-1}$. If the estimated $(u_c)_{NEW}$ is outside the range u_{cMIN}-u_{cMAX}, we choose the midpoint

(84) $$(u_c)_{NEW} = (u_{cMIN}+u_{cMAX})/2$$

The equations for the critical point are solved again and the integration is repeated (short iteration). When

(85) $$\tau_{u=-1} = 2/3 \pm \Delta\tau$$

we have completed a grand iteration. We update g(u) and estimate the convergence through the comparison of u_c, the mass loss rate, V, v_{FOT}, v_{OUT} with the same quantities in the preceding grand-iteration. It is found that g(u) converges rapidly confirming the validity of the iterative procedure. We assume $\Delta\tau$=0.0005 since $d\tau/du|_{u=-1}$ is of the order of 10^2 and consequently dlogL≃du/u is of the order of 10^{-6}: a high accuracy in $\tau_{u=-1}$=2/3 is not needed to fix precisely the model on the HR diagram. Instead, it is necessary to fix the wind parameters.

4. THE BEHAVIOUR OF THE MODEL IN THE HR DIAGRAM

In order to study the behaviour of the model, I have calculated the wind structure for a certain number of stellar models which belong to three evolutionary tracks (Bertelli, unpublished) of 20, 60 and 100 M_s at the ZAMS, Z=0.02, overshooting parameter λ=1, mass loss rate according to Chiosi & Olson (1983, in Garmany & Conti, 1984; fig. 17).

The summariziong data both of the stellar models and the calculated winds are in tab. 8-10. The figures 18a-g describe the progressive change of the wind structure along the evolutionary track. I have choosed as rapresentative quantities, the velocity, the force multiplier, the density and the optical depth. The curves are labelled with the wind model number and the position of the critical point is evidenced, too.

1) 20 M_s case.

All the models rapresented are in order of decreasing temperature. It is observed that the terminal velocity decreasesw together with the velocity at the critical point which moves outward in passing from a model to the subsequent one. This is connected to the decrease of the force multiplier or, better, with the outward shift of the force multiplier shoulder.

The optical depth of the wind follows the trend of the density. The force multiplier, instead, has a dependence more complicated: it increases with density, but decreases with the optical depth and this one is the dominant factor. This explains the decrease of the force multiplier in models 1 through 8 (the optical depth of the wind increases) and the subsequent increase in passing from model 9 to model 12 in spite of the density fall,

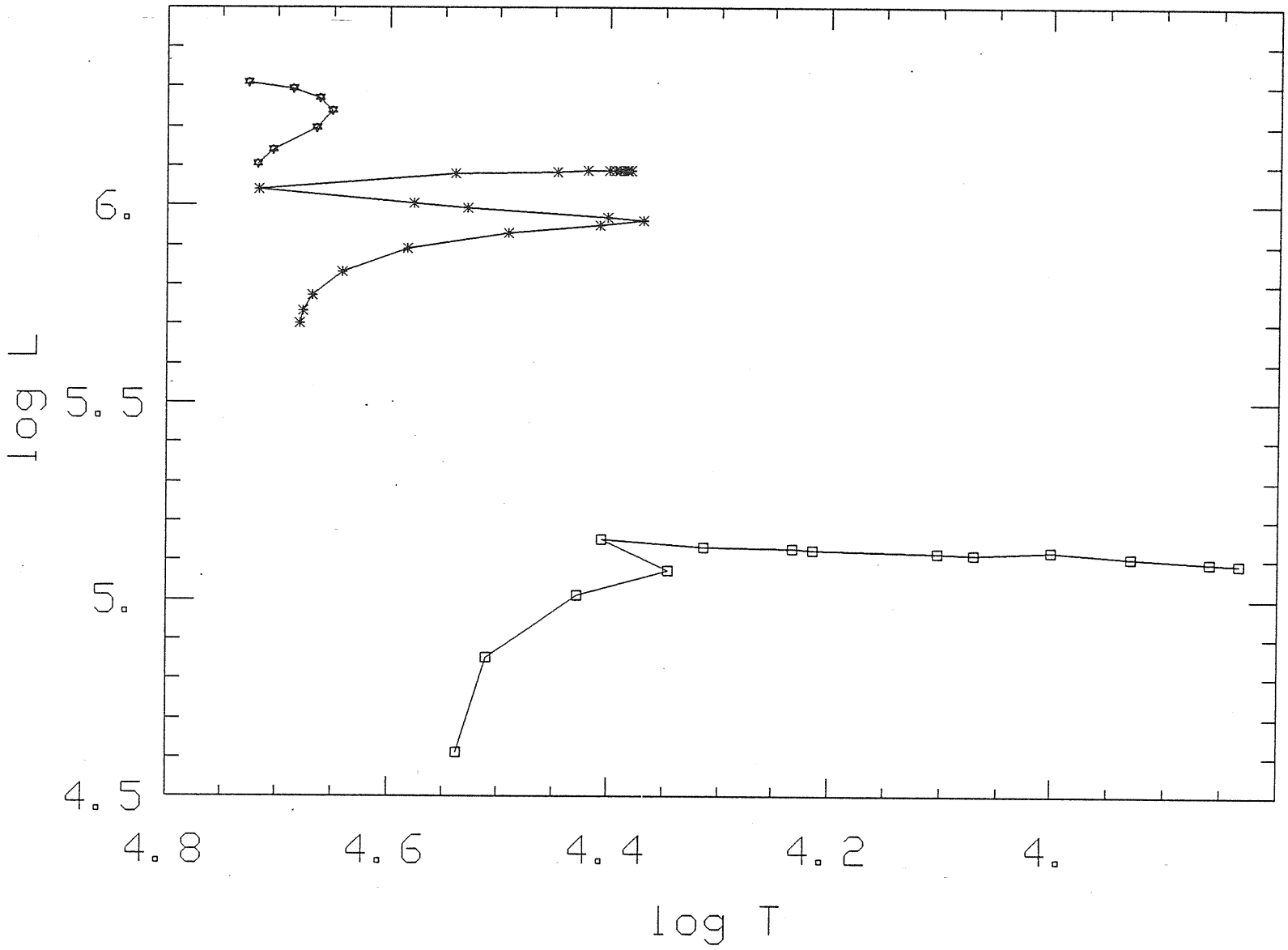

FIGURE 17. Evolutionary tracks (λ=1, Z=0.02; Bertelli, unpublished) and models chosen for wind structure calculation, for 20 (squares), 60 (asterisks) and 100 (stars) initial solar masses.

since the optical depth of the wind has fallen drastically, too.

2) 60 M_s case.

The models 1, 5, 6, 8 and 12, 13, 15, 22 are in order of decreasing temperature. Instead the temperature increases passing from model 8 to 11 to 12. In models 1 through 12 it is observed the same relations as in the 20 M_s case between the velocity curve and the shoulder of the force multiplier, between the force multiplier and the optical depth, between the optical depth and the density. The only exception is that the optical depth decreases from model 8 to 11 in spite of the density increase: this is due to the change of external chemical composition (remember it is electron scattering optical depth).

The most interesting news is that in models 12 through 22 a high photospheric velocity developes, which soon exceeds the sound velocity: interpolating, $v_{FOT}=a\simeq 17.4$ Km/s at logT=4.48, $\log L/L_s=6.08$.

Finally, in models 13 to 22, the optical depth of the wind grows notwithstanding the decrease in wind density. This is due to the fact it is considered a wind extending up to 1000 R_* and the stellar radius is growing rapidly in these stellar phases. This is a point to study: perhaps the wind has to be integrated up to the point where the density falls below the interstellar density; perhaps in the integration it has to be taken into account the evolutionary time path and the time necessary to go through the atmosphere.

3) 100 M_s case.

The same considerations hold as in the preceding cases. $v_{FOT}=a\simeq 21.3$ Km/s at logT=4.69, $\log L/L_s=6.30$. Note that in this

TABLE 8

MODELLO 20 Ms; Z=0.02

n	t 10**7yr	M/Ms	logL/Ls	logT	X	Y	logM. C+O Ms/yr	Rc/R*	logM. Ms/yr	Vfot Km/s	Vc Km/s	Vout Km/s	AKAP	ALF	DEL	TAUc
1	0.	19.990	4.613	4.537	0.700	0.280	-7.939	1.051	-7.513	0.0014	216.14	2332.7	0.202	0.574	0.107	0.0012
2	0.643	19.832	4.852	4.511	0.700	0.280	-7.328	1.059	-7.024	0.0044	180.30	1802.5	0.207	0.569	0.108	0.0030
3	0.910	19.577	5.011	4.428	0.700	0.280	-6.770	1.068	-6.601	0.0103	130.69	1236.3	0.262	0.547	0.098	0.0066
4	0.999	19.340	5.075	4.346	0.700	0.280	-6.427	1.073	-6.267	0.0195	98.67	916.7	0.371	0.522	0.082	0.0121
5	1.0288	19.209	5.151	4.406	0.700	0.280	-6.373	1.076	-6.216	0.0266	112.31	1014.5	0.288	0.541	0.092	0.0147
6	1.0295	19.206	5.132	4.314	0.700	0.280	-6.222	1.082	-6.058	0.0312	89.66	776.8	0.414	0.514	0.082	0.0182
7	1.0297	19.205	5.127	4.232	0.700	0.280	-6.066	1.114	-5.998	0.0299	84.66	558.8	0.478	0.497	0.110	0.0181
8	1.0297	19.204	5.126	4.215	0.700	0.280	-6.032	1.122	-5.992	0.0293	84.00	522.1	0.488	0.494	0.116	0.0178
9	1.0299	19.203	5.117	4.103	0.700	0.280	-5.824	1.139	-5.765	0.0392	66.98	392.7	0.648	0.484	0.110	0.0235
10	1.0299	19.202	5.113	4.070	0.700	0.280	-5.770	1.131	-5.732	0.0389	59.59	379.6	0.672	0.484	0.092	0.0233
11	1.0299	19.201	5.119	4.001	0.700	0.280	-5.620	1.121	-5.942	0.0195	46.48	359.4	0.498	0.490	0.048	0.0118
12		19.200	5.106	3.930	0.700	0.280		1.133	-6.645	0.0031	39.07	331.6	0.202	0.501	0.017	0.0019
13		19.199	5.093	3.860	0.700	0.280		1.211	-7.409	0.0004	39.96	231.5	0.122	0.485	0.059	0.0003
14		19.199	5.088	3.835	0.700	0.280		1.285	-7.774	0.0002	43.01	189.3	0.122	0.472	0.094	0.0001

t, M/M_s, $logL/L_s$, logT, X, Y, logM.(C+O) are from Bertelli's models. The subsequent data are the calculated wind parameters.

TABLE 9

MODELLO 60 Ms; Z=0.02

n	t 10**6yr	M/Ms	logL/Ls	logT	X	Y	logM. C+O	Rc/R*	logM. Ms/yr	Vfot Km/s	Vc Km/s	Vout Km/s	AKAP	ALF	DEL	TAUc
1	0.	59.945	5.703	4.680	0.700	0.280	-6.167	1.039	-5.736	0.0522	223.20	2847.8	0.231	0.565	0.086	0.0331
2	0.56	59.525	5.735	4.676	0.700	0.280	-6.076	1.041	-5.659	0.0647	216.69	2724.3	0.229	0.566	0.086	0.0389
3	1.17	58.894	5.771	4.668	0.700	0.280	-5.959	1.042	-5.570	0.0833	208.42	2562.4	0.226	0.568	0.088	0.0467
4	2.11	57.465	5.833	4.641	0.700	0.280	-5.730	1.047	-5.411	0.1309	191.03	2212.1	0.216	0.573	0.092	0.0631
5	2.90	55.218	5.892	4.583	0.700	0.280	-5.412	1.058	-5.249	0.2041	166.12	1707.6	0.202	0.578	0.101	0.0820
6	3.37	52.363	5.932	4.492	0.700	0.280	-5.067	1.074	-5.079	0.3201	131.80	1153.2	0.214	0.565	0.108	0.1067
7	3.57	49.864	5.952	4.408	0.700	0.280	-4.801	1.080	-4.816	0.7684	99.04	837.0	0.285	0.541	0.093	0.1770
8	3.67	47.737	5.962	4.369	0.700	0.280	-4.638	1.081	-4.630	2.0654	85.31	706.0	0.338	0.529	0.085	0.2654
9	3.73	46.334	5.969	4.402	0.636	0.344	-4.726	1.081	-4.700	1.4629	91.48	757.2	0.293	0.539	0.092	0.2338
10	3.97	42.057	5.995	4.529	0.442	0.538	-4.812	1.074	-4.818	1.0352	116.80	1020.1	0.203	0.573	0.108	0.2061
11	4.02	41.231	6.006	4.577	0.398	0.582	-4.870	1.066	-4.795	1.3412	123.08	1161.0	0.201	0.578	0.102	0.2341
12	4.0489	40.940	6.041	4.717	0.382	0.598	-5.097	1.041	-4.665	20.1399	134.00	1544.8	0.248	0.557	0.080	0.4610
13	4.0519	40.910	6.079	4.540	0.382	0.598	-5.000	1.066	-4.551	11.4593	102.47	895.6	0.201	0.575	0.107	0.4024
14	4.0525	40.885	6.086	4.448	0.382	0.598	-4.409	1.059	-4.419	20.4807	80.54	680.4	0.243	0.553	0.102	0.4658
15		40.866	6.089	4.420	0.382	0.598		1.045	-4.351	29.5468	72.30	641.0	0.271	0.545	0.096	0.5200
16		40.866	6.089	4.400	0.382	0.598		1.034	-4.306	35.4663	66.95	619.0	0.295	0.539	0.091	0.5569
17		40.866	6.089	4.395	0.382	0.598		1.031	-4.295	37.2095	65.55	614.2	0.302	0.537	0.090	0.5666
18		40.866	6.089	4.390	0.382	0.598		1.028	-4.283	38.8307	64.32	609.4	0.308	0.536	0.089	0.5765
19		40.866	6.089	4.387	0.382	0.598		1.026	-4.276	39.8268	63.53	606.6	0.312	0.535	0.088	0.5827
20		40.866	6.089	4.385	0.382	0.598		1.025	-4.271	40.4896	62.95	604.8	0.315	0.534	0.088	0.5869
21	4.0529	40.866	6.089	4.383	0.382	0.598	-4.201	1.024	-4.267	41.0918	62.71	602.9	0.318	0.533	0.087	0.5905
22		40.866	6.089	4.380	0.382	0.598		1.022	-4.260	41.9695	61.54	600.3	0.322	0.533	0.087	0.5973

TABLE 10

MODELLO 100 Ms; Z=0.02

n	t 10**6yr	M/Ms	logL/Ls	logT	X	Y	logM. C+O Ms/yr	Rc/R*	logM. Ms/yr	Vfot Km/s	Vc Km/s	Vout Km/s	AKAP	ALF	DEL	TAUc
1	0.	100.000	6.104	4.718	0.700	0.280	-5.495	1.037	-5.108	0.2093	226.19	2944.4	0.240	0.561	0.083	0.1025
2	0.733	96.920	6.141	4.705	0.700	0.280	-5.357	1.039	-4.991	0.3277	209.32	2656.6	0.240	0.561	0.083	0.1335
3	1.65	90.930	6.194	4.665	0.700	0.280	-5.066	1.046	-4.806	0.7377	182.28	2130.9	0.225	0.569	0.088	0.1951
4	2.27	83.300	6.238	4.651	0.584	0.396	-4.824	1.049	-4.649	1.6328	162.33	1823.2	0.220	0.572	0.090	0.2691
5	2.68	75.960	6.271	4.662	0.440	0.540	-4.699	1.046	-4.522	4.5525	149.01	1688.6	0.224	0.569	0.089	0.3598
6	2.95	70.240	6.294	4.687	0.318	0.662	-4.678	1.039	-4.429	17.7697	140.18	1667.6	0.234	0.564	0.085	0.4586
7	3.12	66.270	6.309	4.727	0.219	0.761	-4.638	1.028	-4.385	44.6942	138.88	1781.2	0.240	0.561	0.083	0.5325

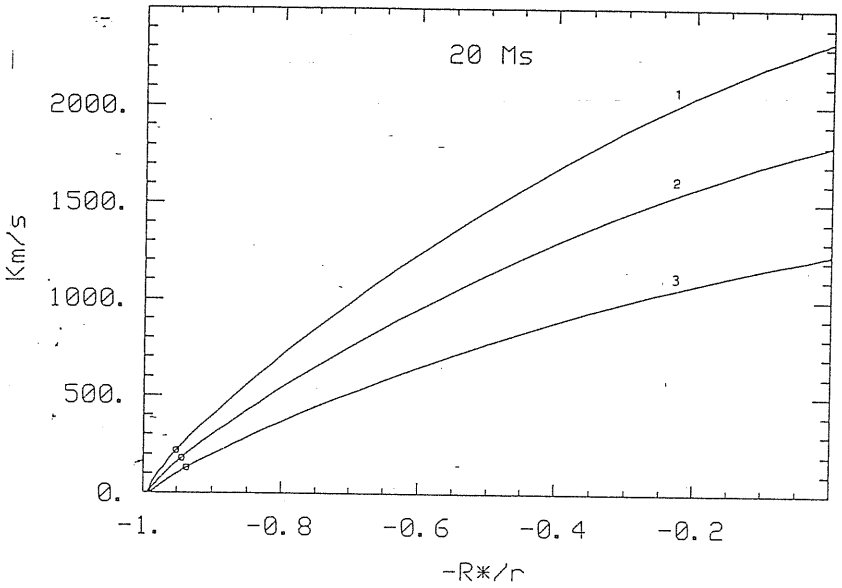
20 Ms
Km/s
2000.
1500.
1000.
500.
0.
-1.
-0.8
-0.6
-0.4
-0.2
-R*/r
1
2
3

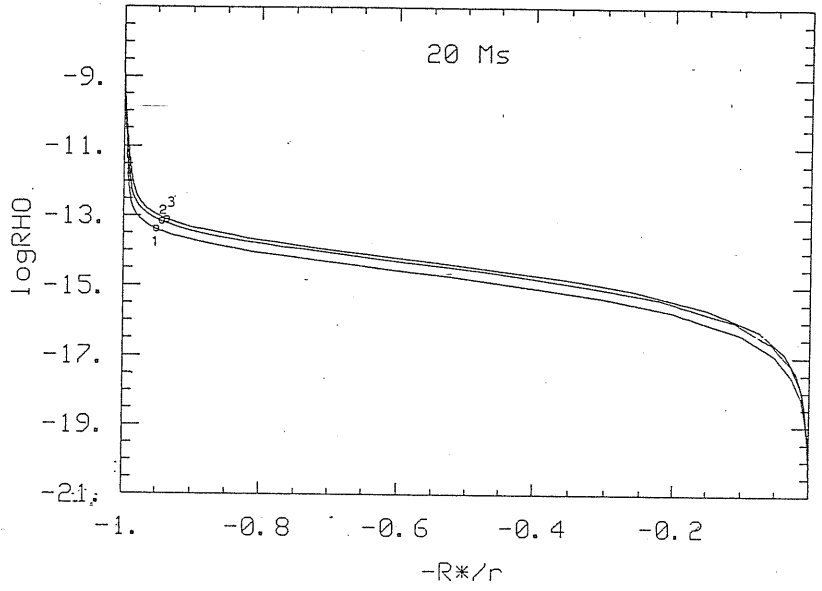
20 Ms
logRHO
-9.
-11.
-13.
-15.
-17.
-19.
-21.
-1.
-0.8
-0.6
-0.4
-0.2
-R*/r
1
2
3

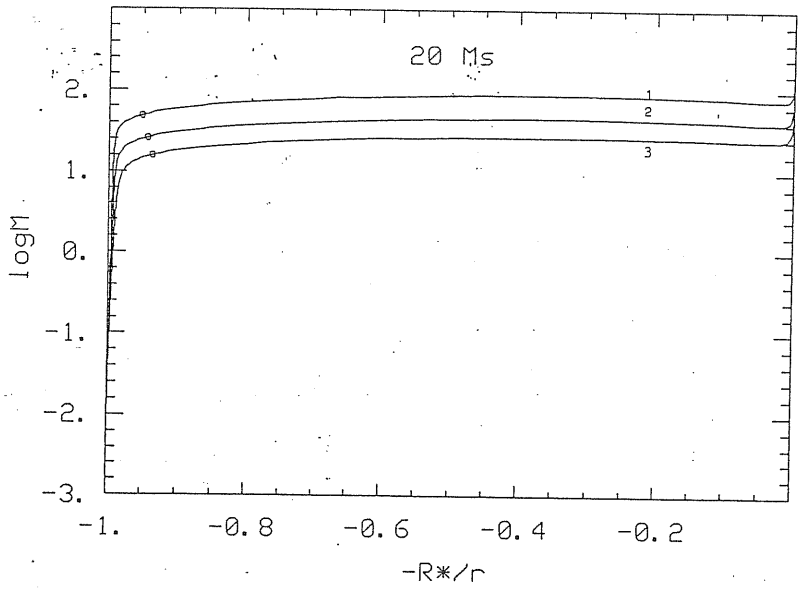
20 Ms
logM
2.
1.
0.
-1.
-2.
-3.
-1.
-0.8
-0.6
-0.4
-0.2
-R*/r
1
2
3

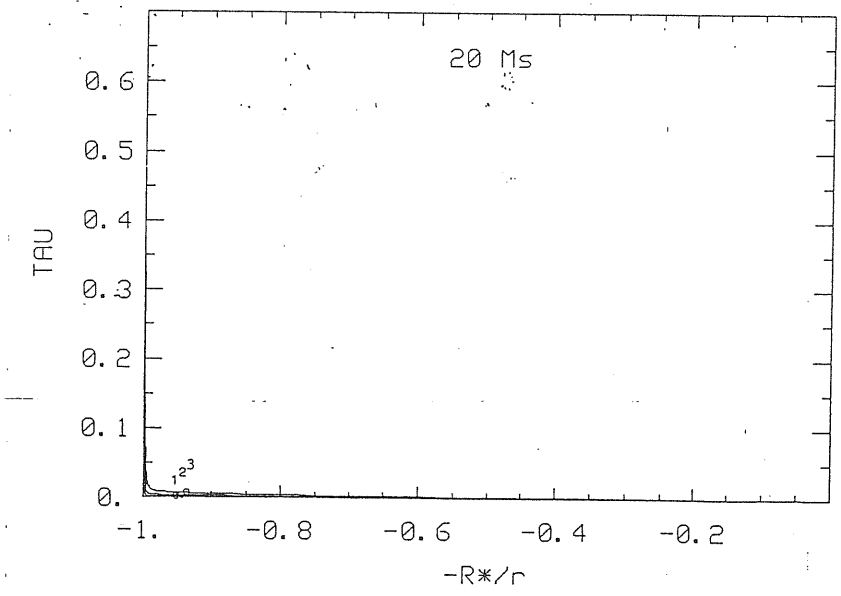
20 Ms
TAU
0.6
0.5
0.4
0.3
0.2
0.1
0.
-1.
-0.8
-0.6
-0.4
-0.2
-R*/r
1
2
3

FIGURE 18a

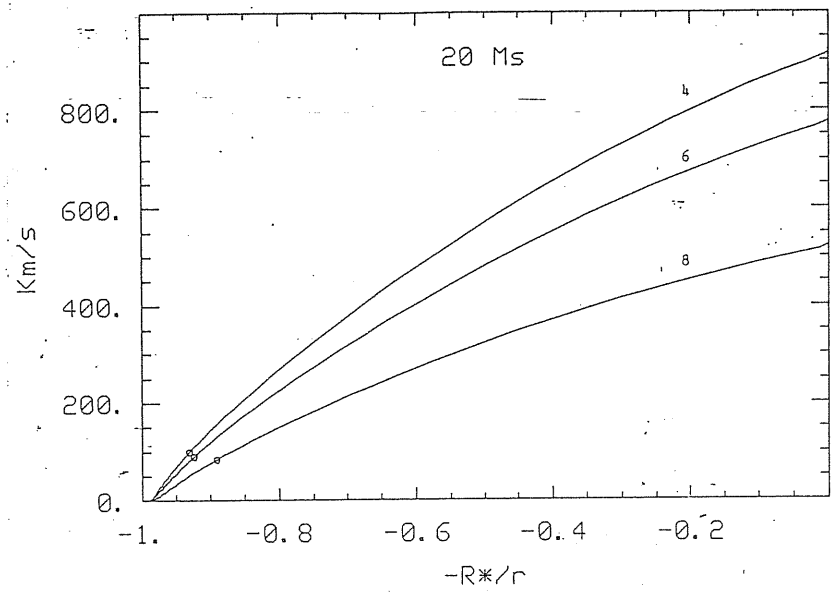
20 Ms
Km/s
800.
600.
400.
200.
0.
-1.
-0.8
-0.6
-0.4
-0.2
-R*/r
4
6
8

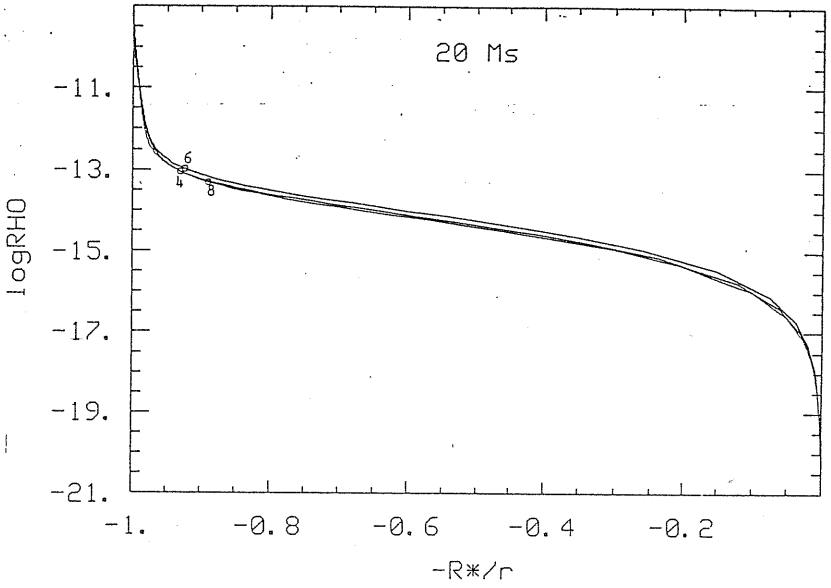
20 Ms
logRHO
-11.
-13.
-15.
-17.
-19.
-21.
-1.
-0.8
-0.6
-0.4
-0.2
-R*/r
4
6
8

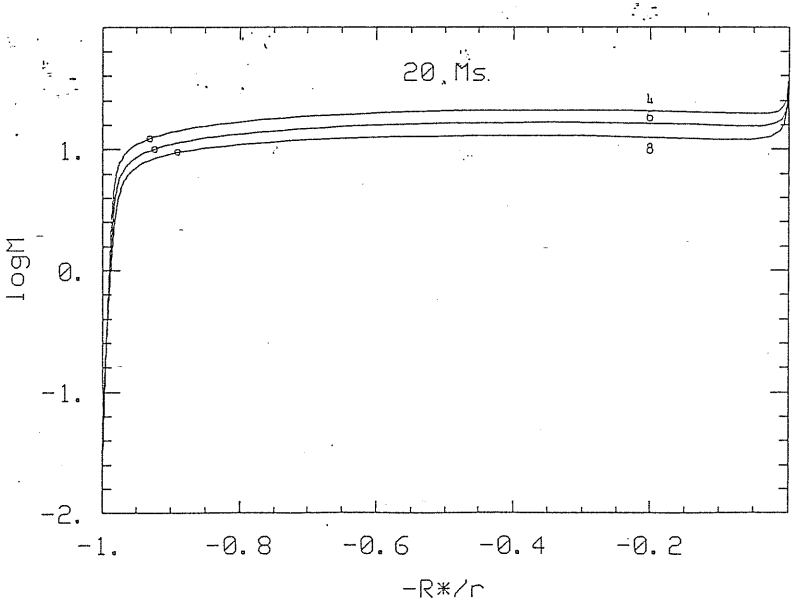
20 Ms.
logM
1.
0.
-1.
-2.
-1.
-0.8
-0.6
-0.4
-0.2
-R*/r
4
6
8

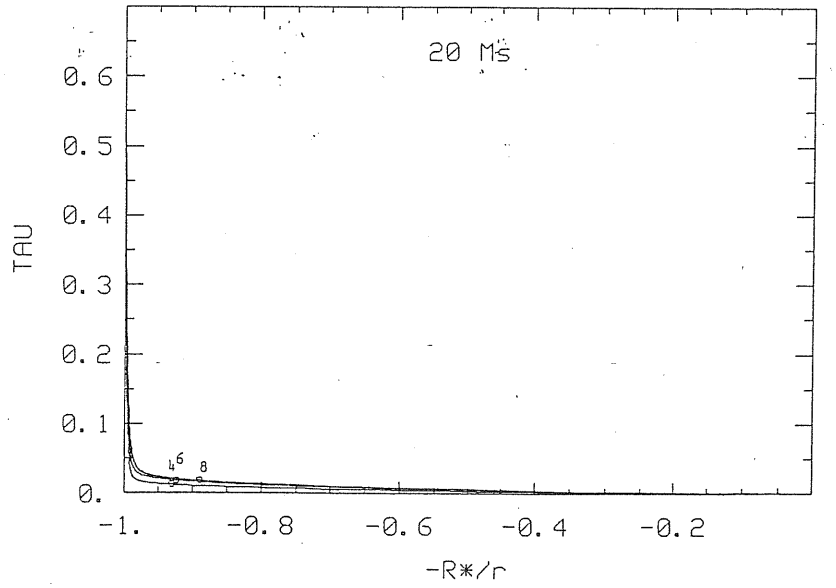
20 Ms
TAU
0.6
0.5
0.4
0.3
0.2
0.1
0.
-1.
-0.8
-0.6
-0.4
-0.2
-R*/r
4
6
8

FIGURE 18b

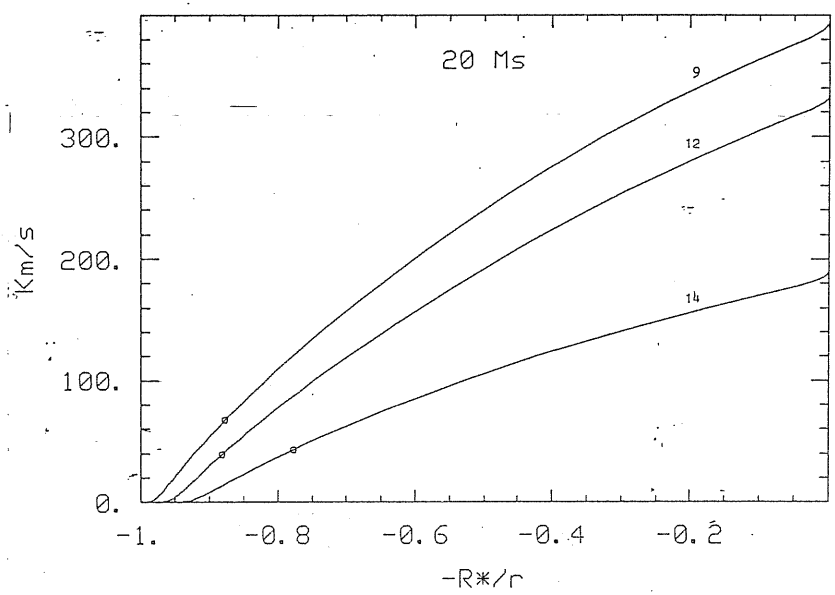
20 Ms
Km/s
300.
200.
100.
0.
9
12
14
-1.
-0.8
-0.6
-0.4
-0.2
-R*/r

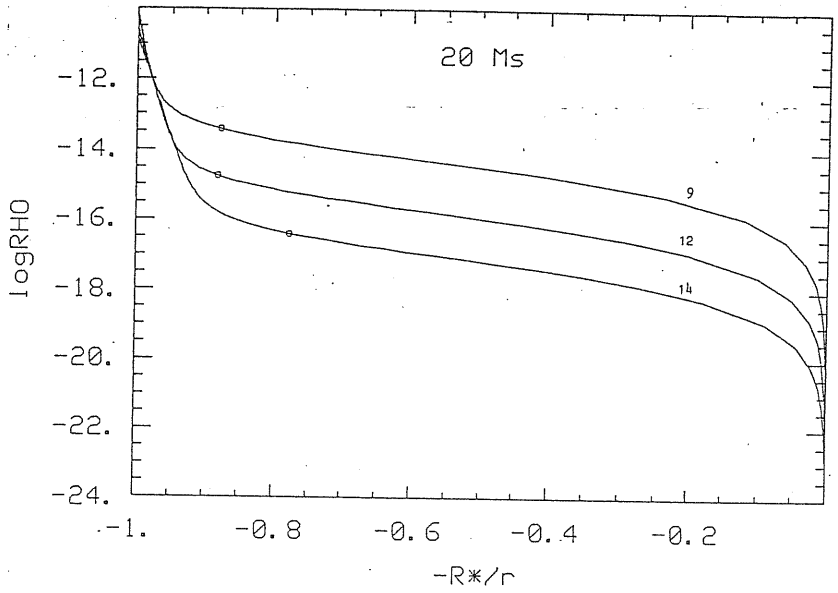
20 Ms
logRHO
-12.
-14.
-16.
-18.
-20.
-22.
-24.
9
12
14
-1.
-0.8
-0.6
-0.4
-0.2
-R*/r

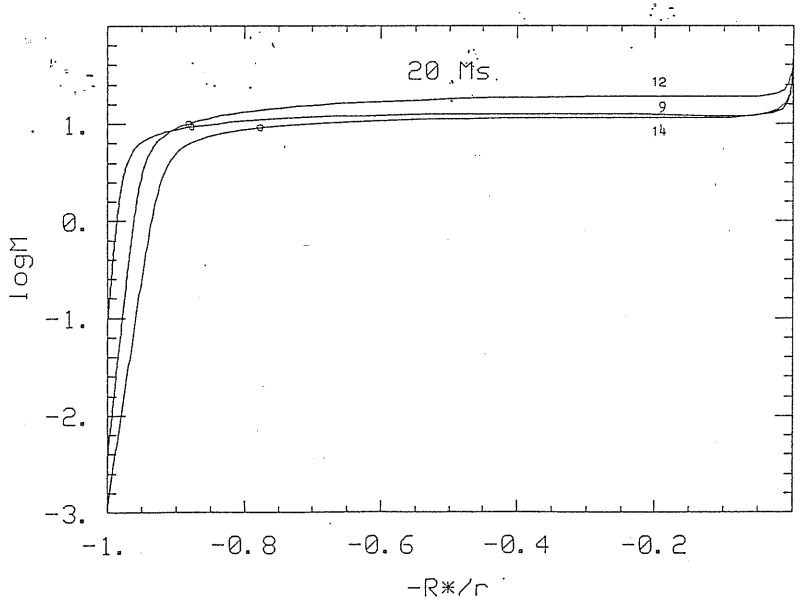
20 Ms
logM
1.
0.
-1.
-2.
-3.
12
9
14
-1.
-0.8
-0.6
-0.4
-0.2
-R*/r

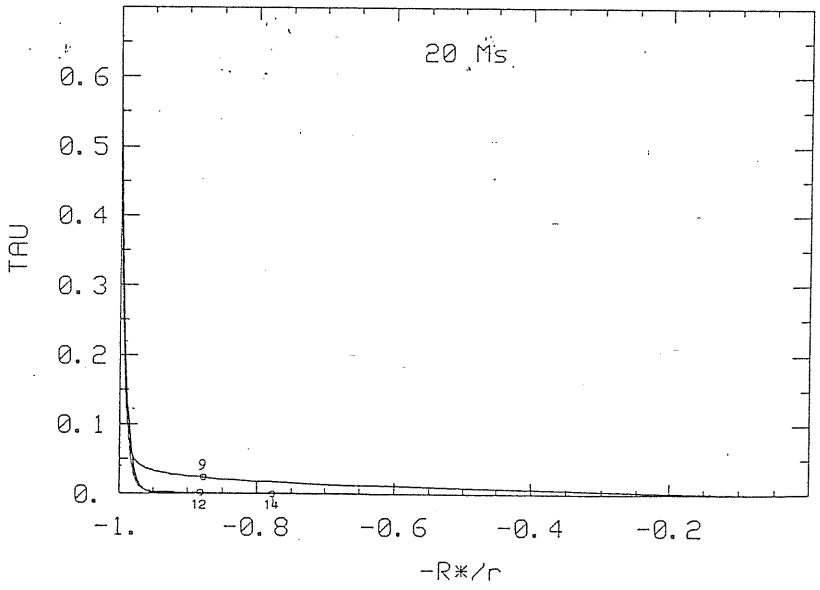
20 Ms
TAU
0.6
0.5
0.4
0.3
0.2
0.1
0.
9
12
14
-1.
-0.8
-0.6
-0.4
-0.2
-R*/r

FIGURE 18c

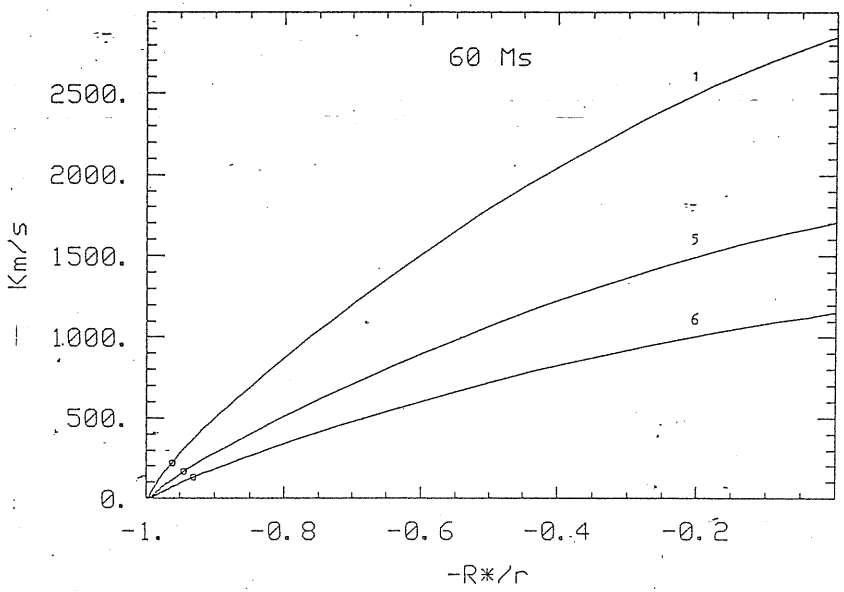
60 Ms
Km/s
2500.
2000.
1500.
1000.
500.
0.
-1.
-0.8
-0.6
-0.4
-0.2
-R*/r
1
5
6

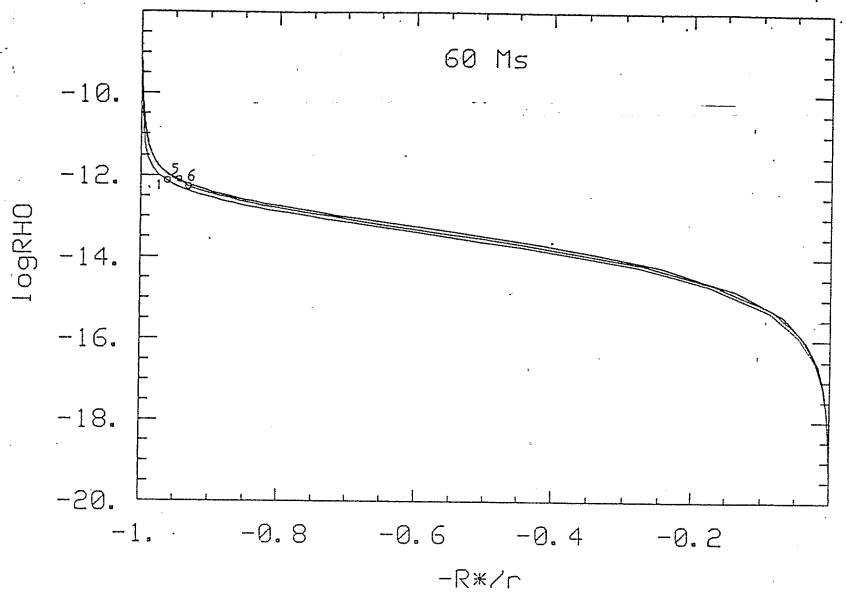
60 Ms
logRHO
-10.
-12.
-14.
-16.
-18.
-20.
-1.
-0.8
-0.6
-0.4
-0.2
-R*/r
1
5
6

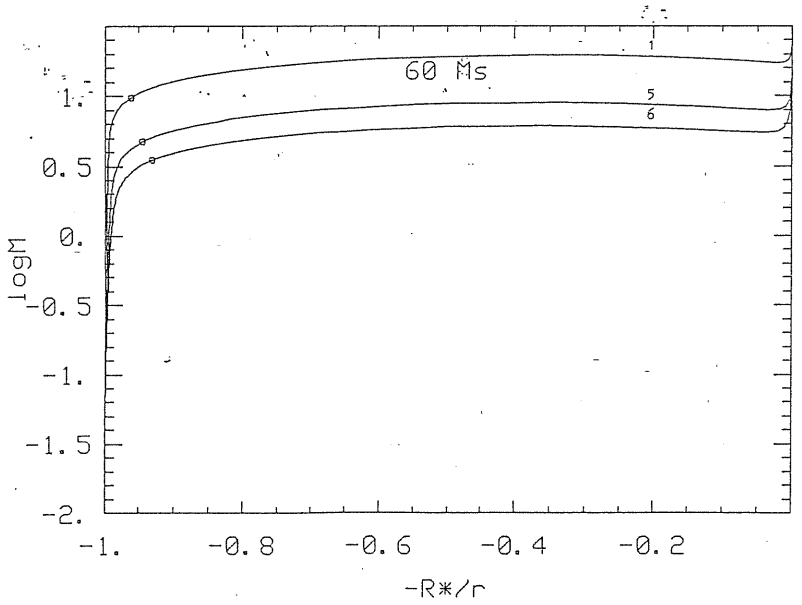
60 Ms
logM
1.
0.5
0.
-0.5
-1.
-1.5
-2.
-1.
-0.8
-0.6
-0.4
-0.2
-R*/r
1
5
6

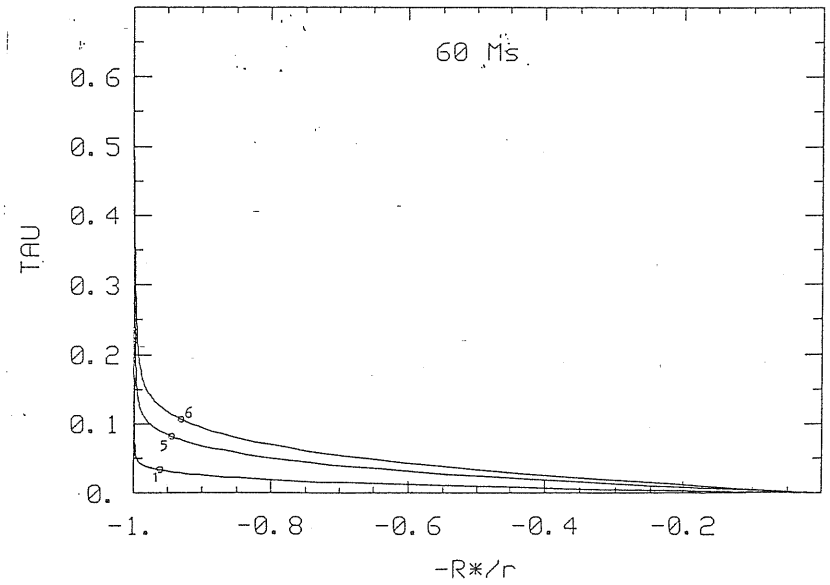
60 Ms
TAU
0.6
0.5
0.4
0.3
0.2
0.1
0.
-1.
-0.8
-0.6
-0.4
-0.2
-R*/r
1
5
6

FIGURE 18d

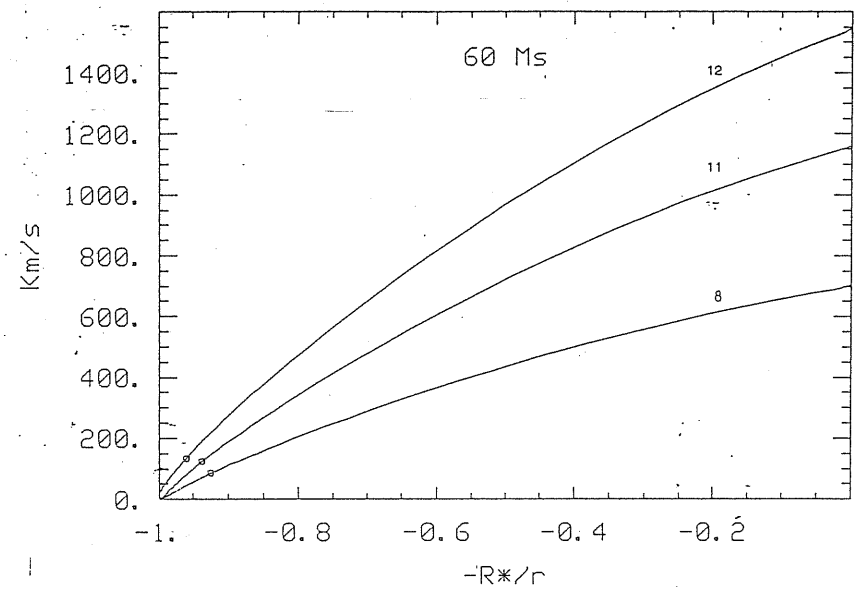
60 Ms
Km/s
1400.
1200.
1000.
800.
600.
400.
200.
0.
-1.
-0.8
-0.6
-0.4
-0.2
-R*/r
12
11
8

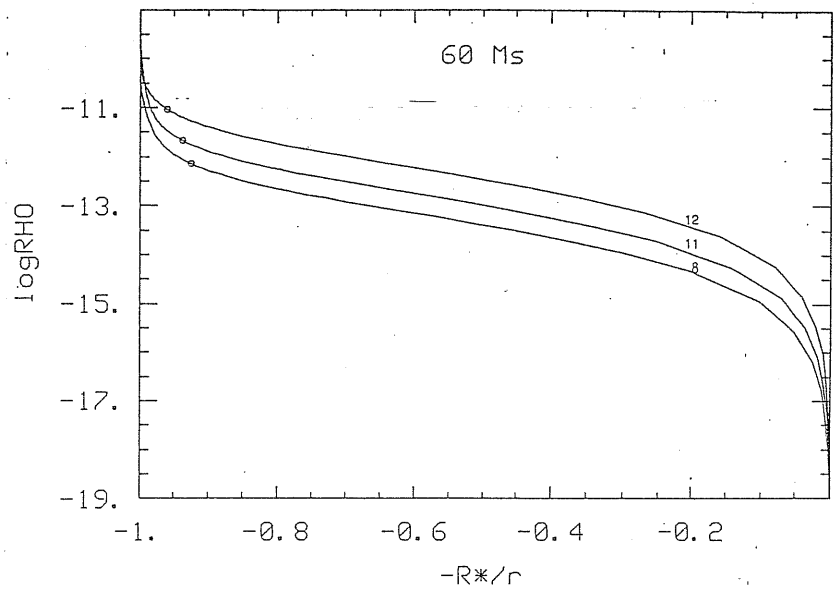
60 Ms
logRHO
-11.
-13.
-15.
-17.
-19.
-1.
-0.8
-0.6
-0.4
-0.2
-R*/r
12
11
8

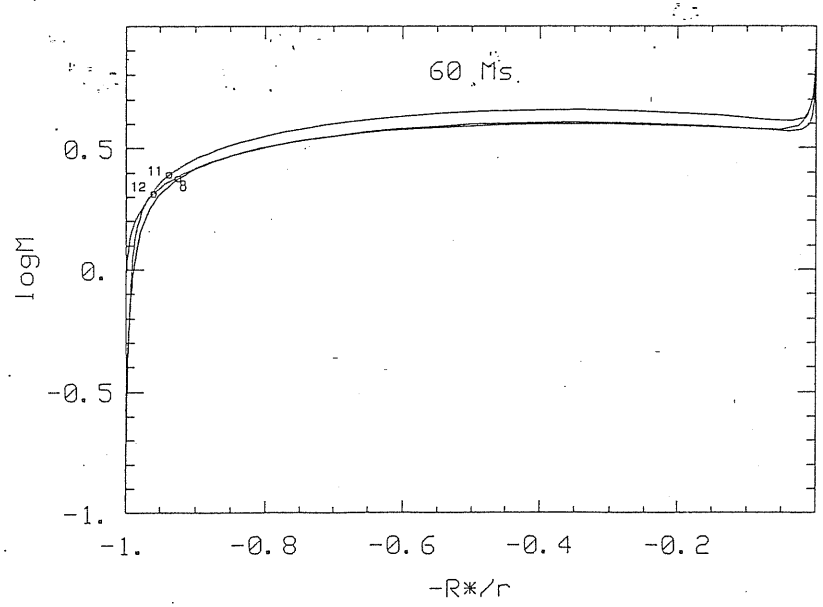
60 Ms
logM
0.5
0.
-0.5
-1.
-1.
-0.8
-0.6
-0.4
-0.2
-R*/r
12
11
8

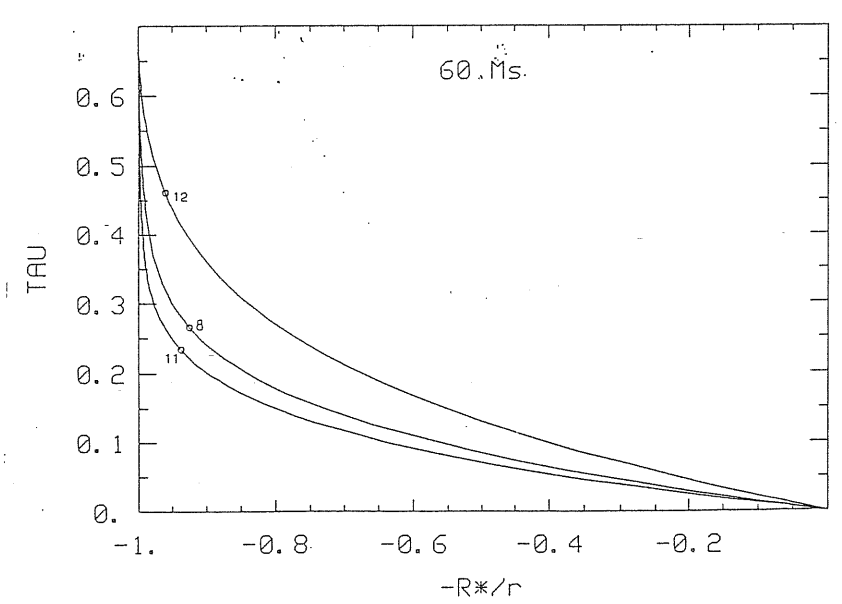
60 Ms
TAU
0.6
0.5
0.4
0.3
0.2
0.1
0.
-1.
-0.8
-0.6
-0.4
-0.2
-R*/r
12
8
11

FIGURE 18e

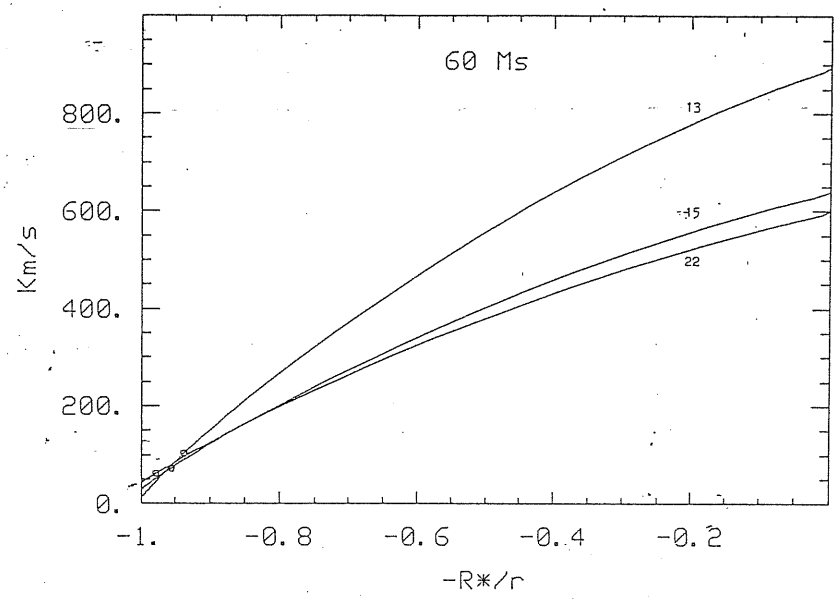
60 Ms
Km/s
800.
600.
400.
200.
0.
-1.
-0.8
-0.6
-0.4
-0.2
-R*/r
13
15
22

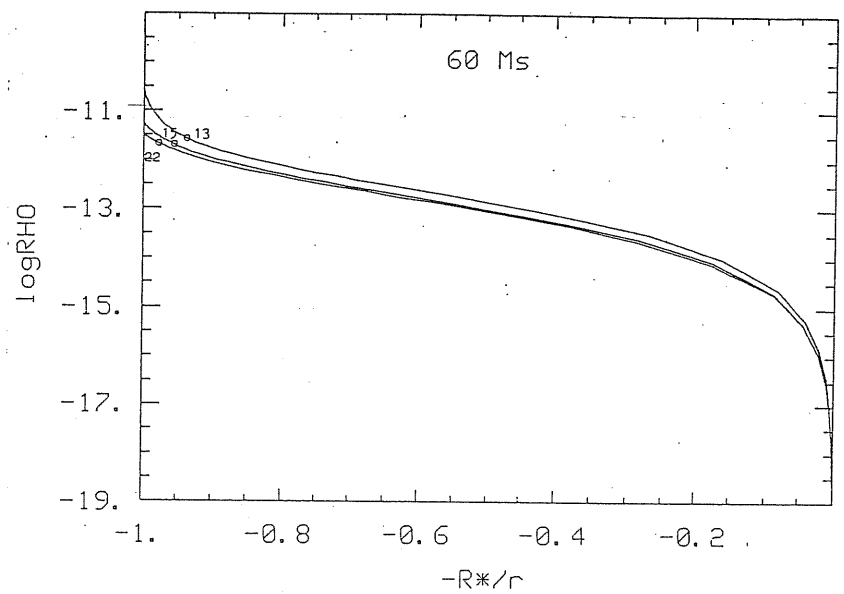
60 Ms
logRHO
-11.
-13.
-15.
-17.
-19.
-1.
-0.8
-0.6
-0.4
-0.2
-R*/r
13
15
22

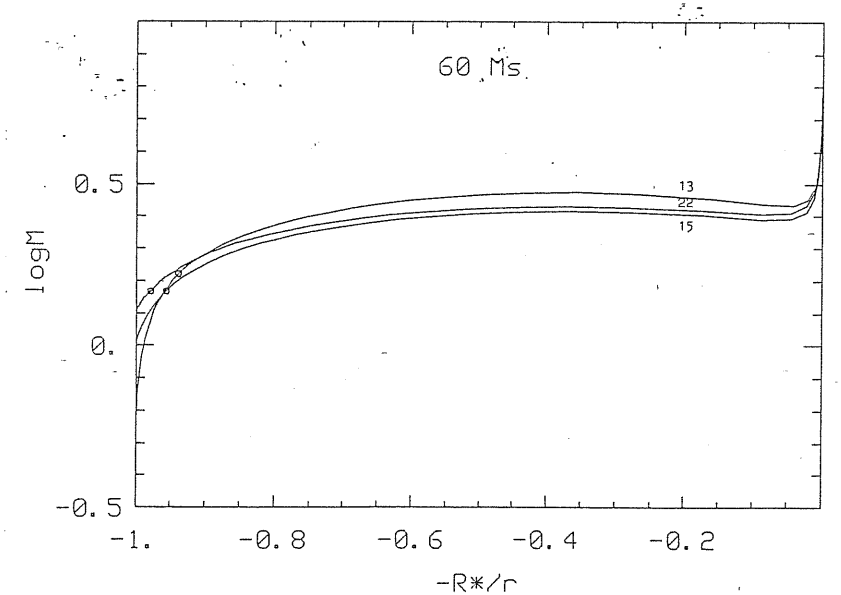
60 Ms
logM
0.5
0.
-0.5
-1.
-0.8
-0.6
-0.4
-0.2
-R*/r
13
22
15

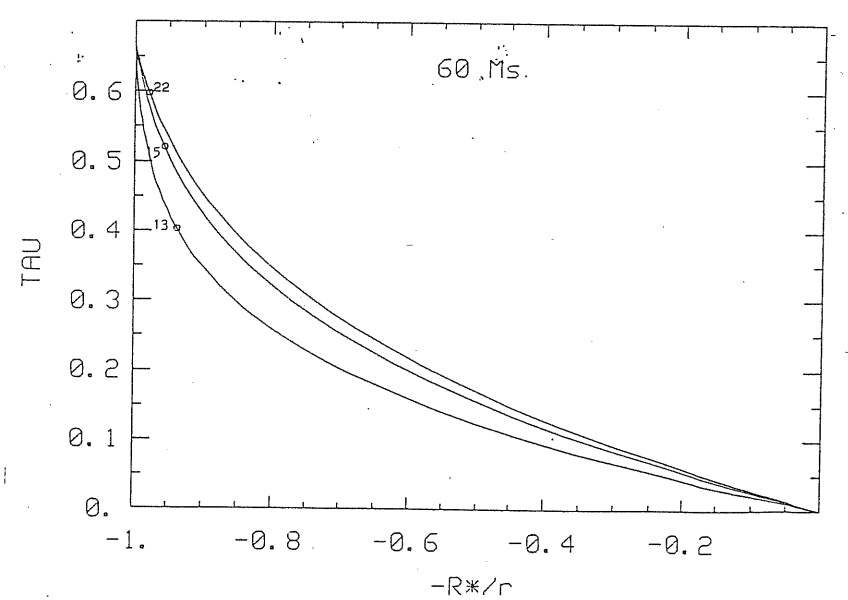
60 Ms
TAU
0.6
0.5
0.4
0.3
0.2
0.1
0.
-1.
-0.8
-0.6
-0.4
-0.2
-R*/r
22
15
13

FIGURE 18f

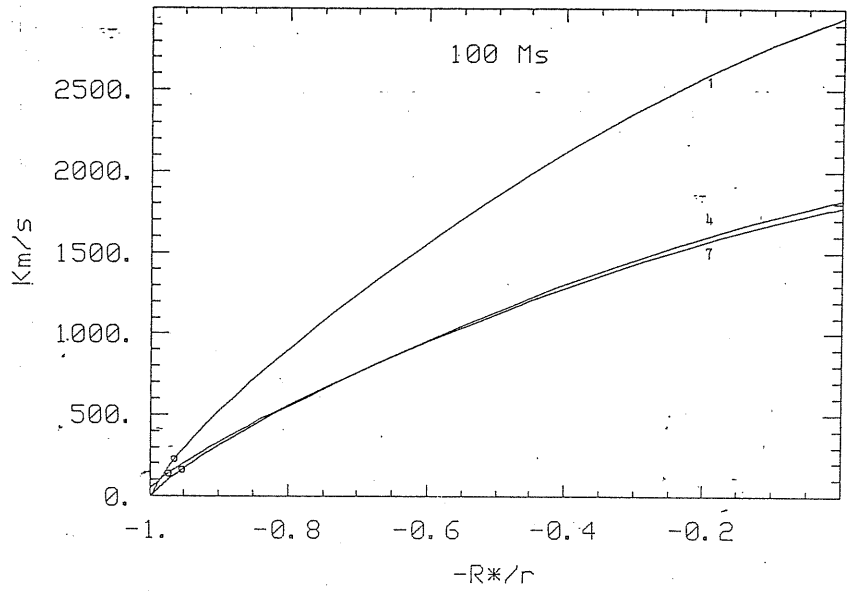
100 Ms
Km/s
2500.
2000.
1500.
1000.
500.
0.
-1.
-0.8
-0.6
-0.4
-0.2
-R*/r
1
4
7

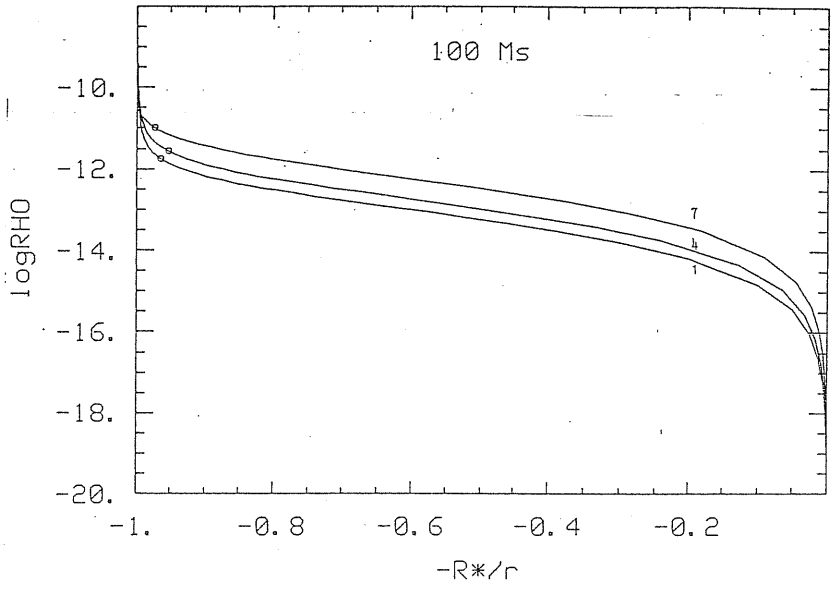
100 Ms
logRHO
-10.
-12.
-14.
-16.
-18.
-20.
-1.
-0.8
-0.6
-0.4
-0.2
-R*/r
7
4
1

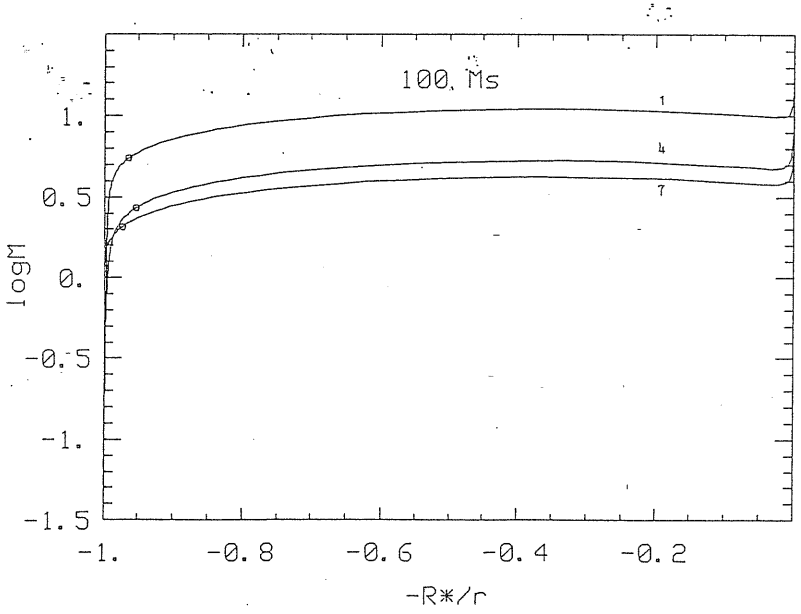
100 Ms
logM
1.
0.5
0.
-0.5
-1.
-1.5
-1.
-0.8
-0.6
-0.4
-0.2
-R*/r
1
4
7

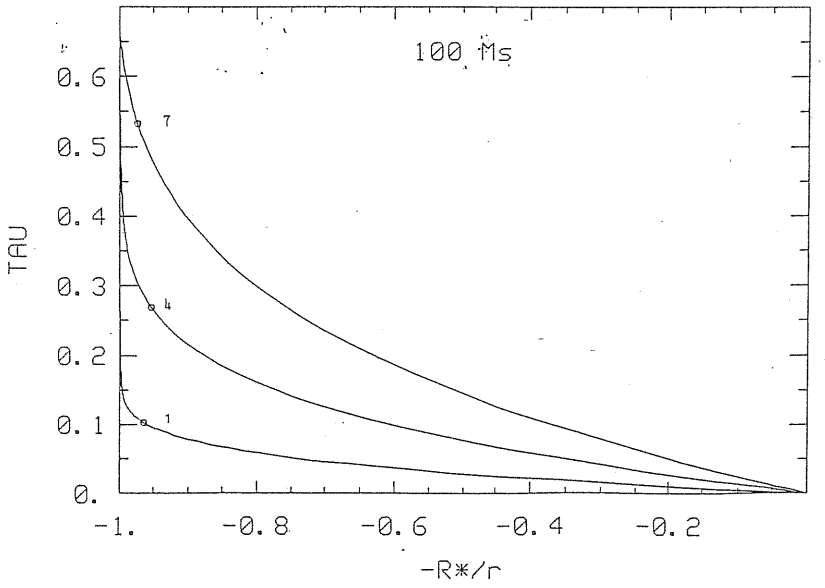
100 Ms
TAU
0.6
0.5
0.4
0.3
0.2
0.1
0.
-1.
-0.8
-0.6
-0.4
-0.2
-R*/r
7
4
1

FIGURE 18g

case v_{FOT} grows with increasing temperature, as it already happened in model 12 of the 60 M_s case.

When high photospheric velocities develope, the photospheric density falls correspondingly.

With the data of tab. 8-10 some important graphs may be constructed:

Figure 19: terminal velocity and temperature relation. A terminal velocity increasing with the temperature is the general trend. But v_{OUT} is higher for lower mass stars and it is higher in main sequence band than in subsequent phases.

Figure 20: mass loss rate and luminosity relation. If we exclude the last two models of the 20 M_s case, which are for logT=3.860 and 3.835, temperatures at which the force multiplier is surely underestimated since molecular lines are not taken into account (see chapter 3.2), we observe a linear relation that is in agreement with the observations. In particular, figure 21 relates the calculated mass loss rates with those of the Chiosi & Olson's parametrization. It is evidenced that in the first stellar phases the mass loss rate in M-CAK wind are higher. When the star leaves the ZAMS, the difference is reduced and then disappeares. However, since the main sequence is a long phase, the evolutionary consequences may be very different. The average logarithmic difference is 0.25.

Very interesting are the relations between the mass loss rate and the photospheric velocity or the optical depth at the critical point, in figure 22 and 23, respectively.

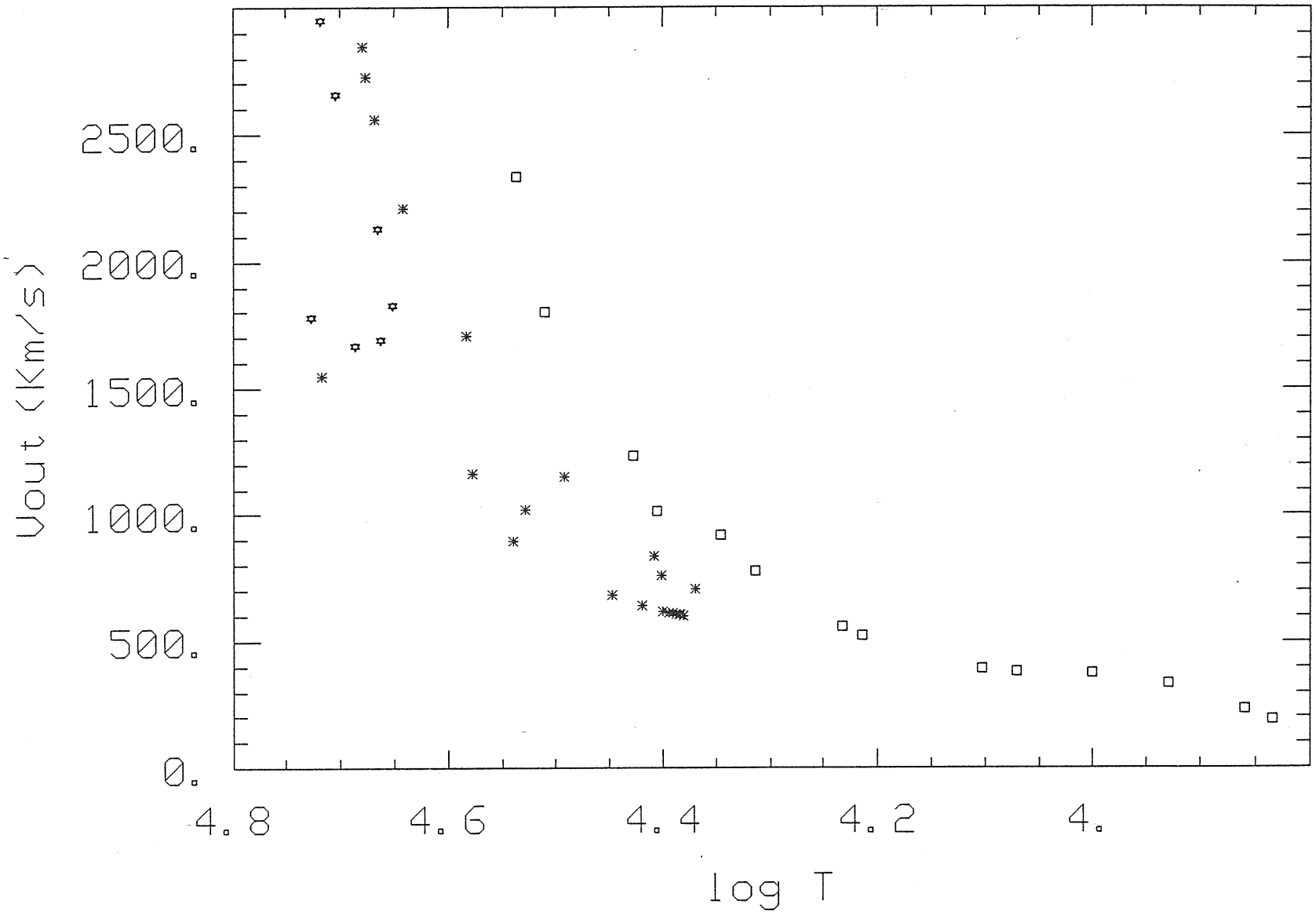

FIGURE 19

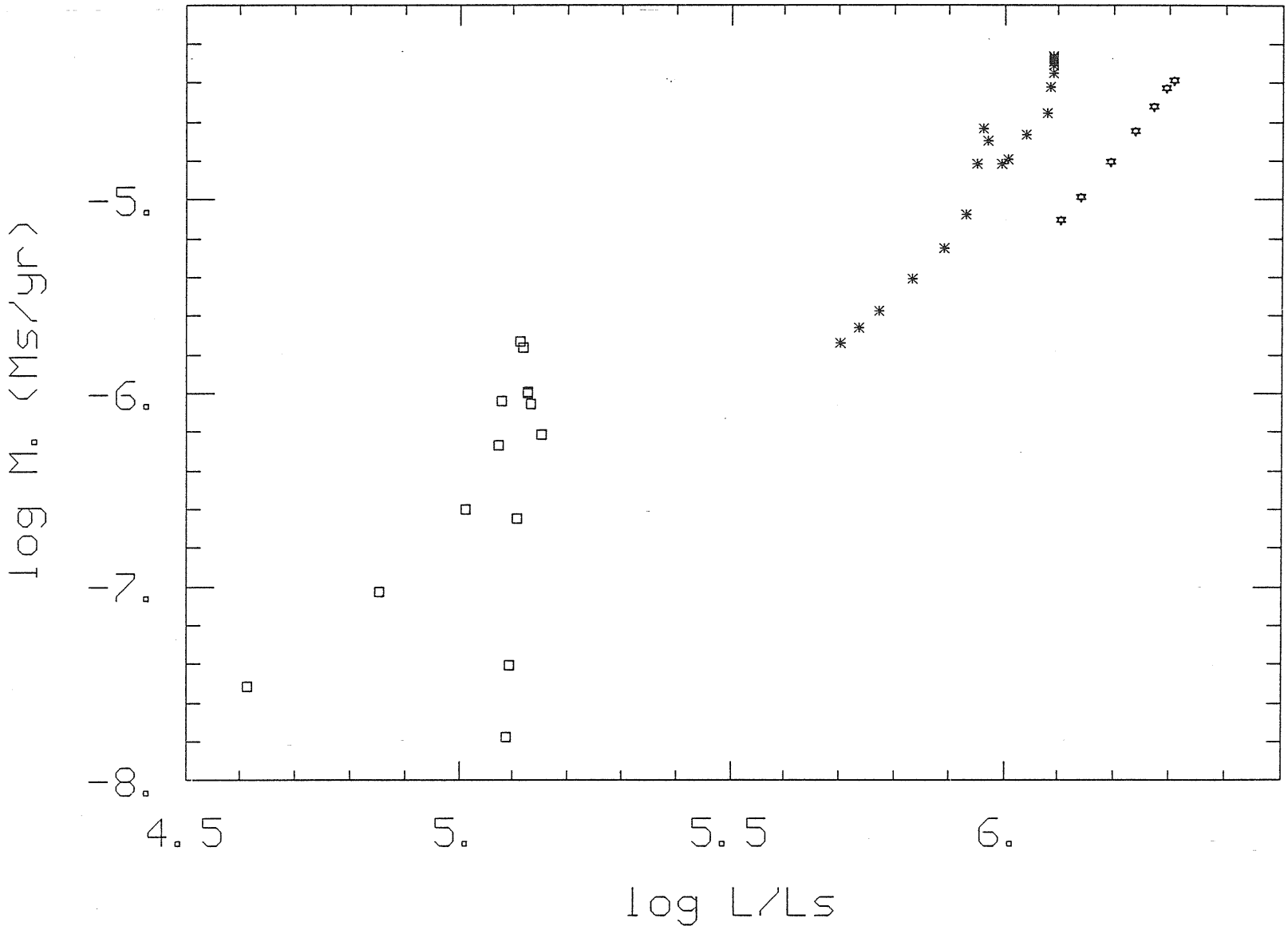

FIGURE 20

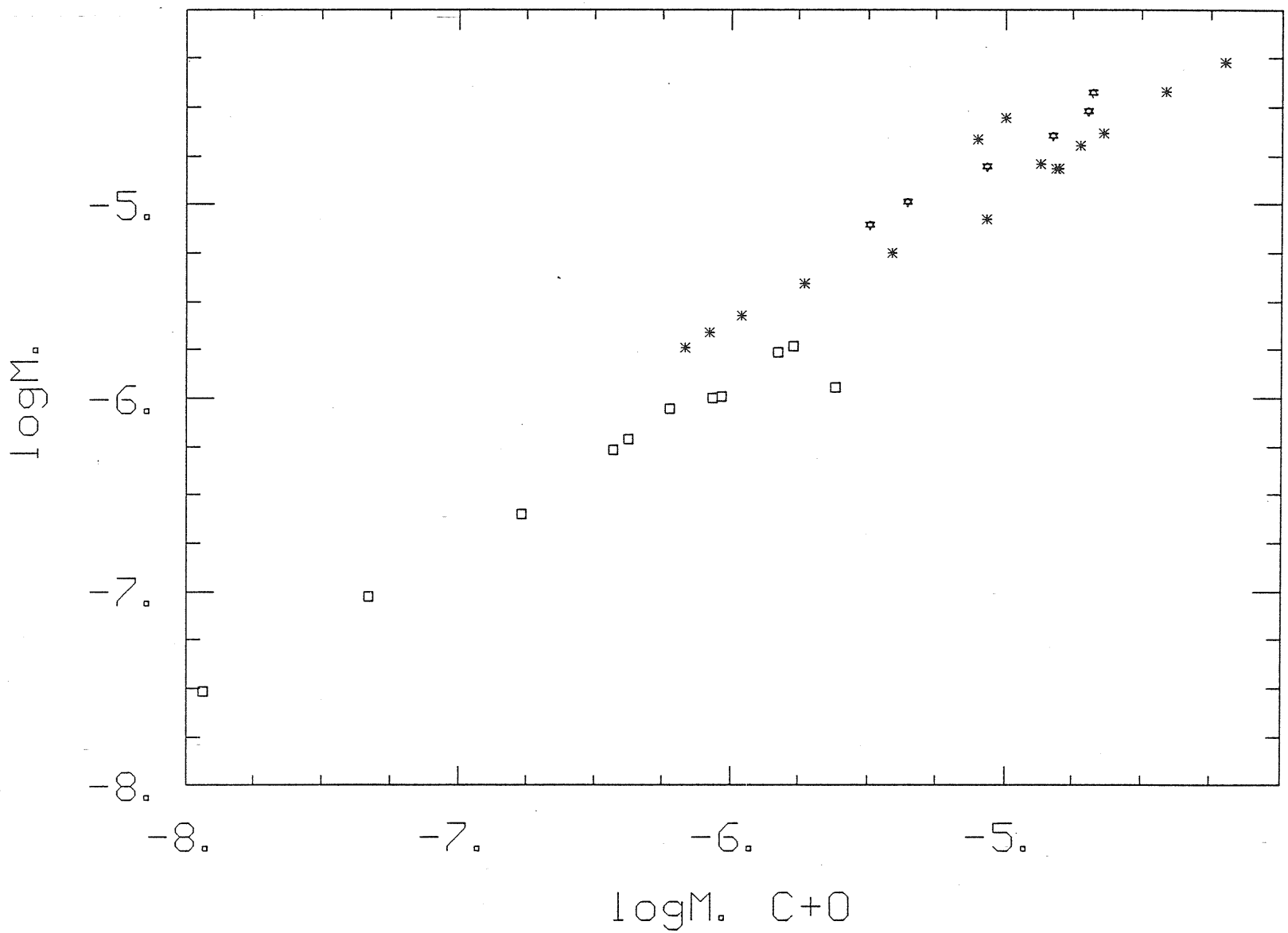

FIGURE 21

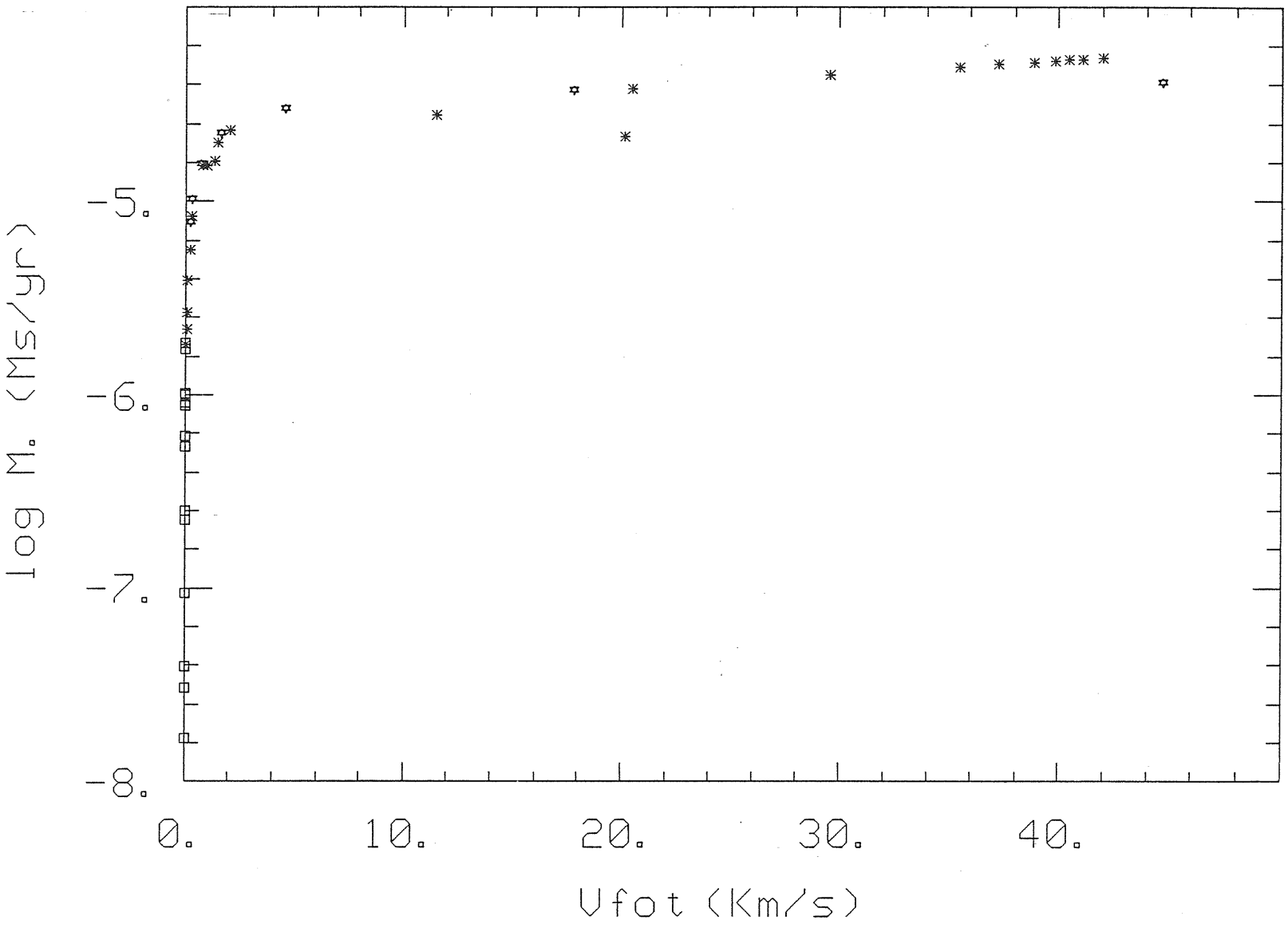

FIGURE 22

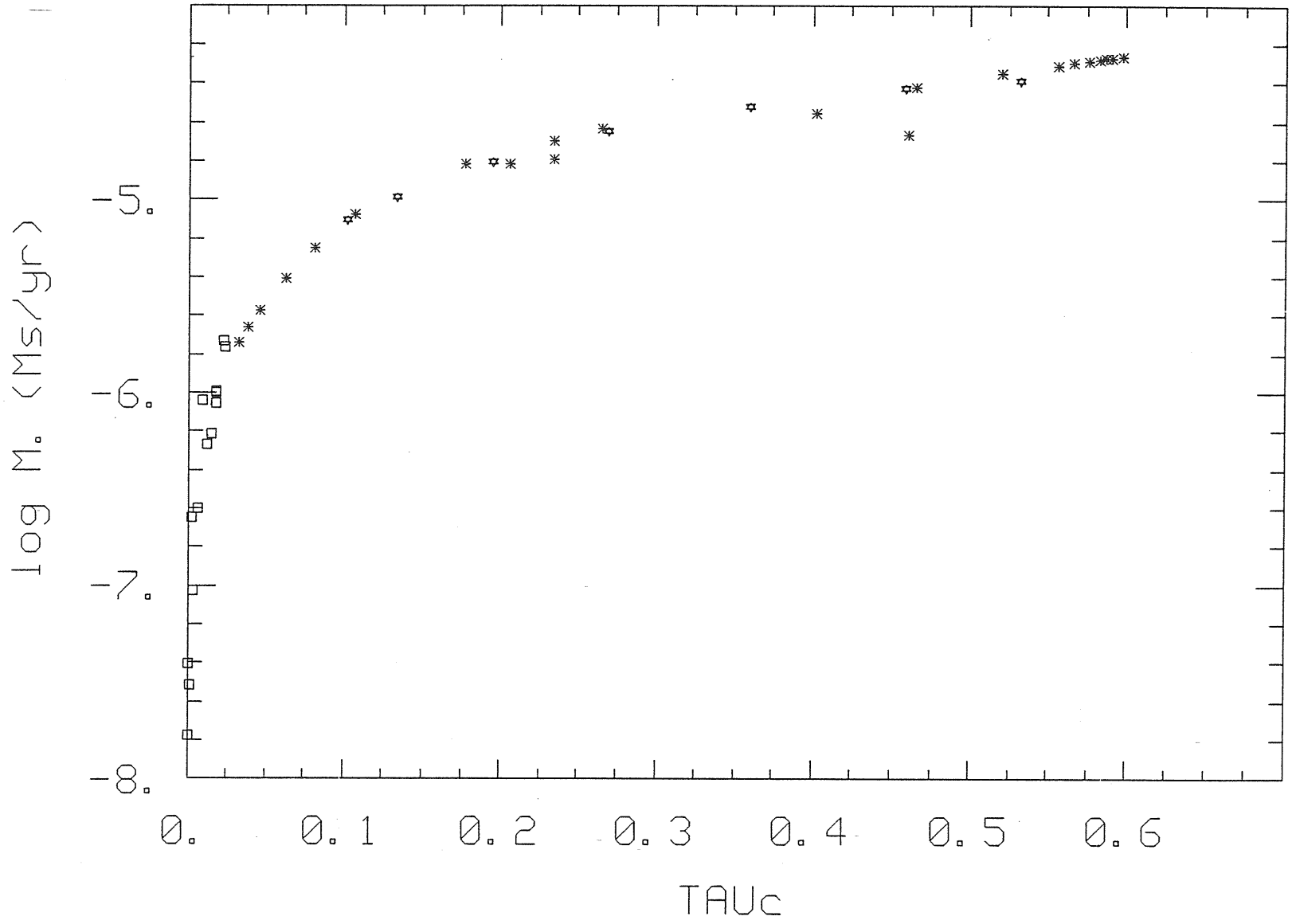

FIGURE 23

The photospheric velocity v_{FOT} is practically zero as long as the mass loss rate is less than 10^{-5} M_s/yr. When the mass loss rate goes from $2 \cdot 10^{-5}$ M_s/yr to $5 \cdot 10^{-5}$ M_s/yr, v_{FOT} goes from 2 Km/s to 40 Km/s, approximately. In this range of mass loss rates the photospheric velocity exceeds the sound velocity. The optical depth at the critical point has a similar behaviour. Extrapolating the data, it is estimated that $TAU_c=2/3$, that is, $u_c=-1$, for a mass loss rate of about $6 \cdot 10^{-5}$ M_s/yr. This, therefore seems to be the maximum mass loss rate possible in the M-CAK wind model theory.

It is very interesting that instabilities and variability in supergiants are observed precisely in stars which are loosing mass at rates between $2 \cdot 10^{-5}$ M_s/yr and $6 \cdot 10^{-5}$ M_s/yr. If this is not only a coincidence, it is argued that these phenomena are connected with the developement of a non hydrostatic subphotospheric structure. So in order to be able to follow this evolutionary phases it is necessary, now, to develop this second step. Since now, it is evident that there will be models with two critical points: one of the M-CAK wind and the other under the photosphere at the isothermal sonic point. These models correspond to stars with supersonic wind velocities at the photosphere and $TAU_c<2/3$. But, soon, the M-CAK point will disappear ($TAU_c>2/3$, that is, $u_c<-1$). In this situation, it is not clear, now, if taking into account the convection, the subphotospheric wind is able to fix the mass loss rate univocally. If we will find that different choiches of the critical point (and mass loss rate) are able to fit the same photospheric luminosity and temperature, we will have the

conditions for thermodynamic fluctuations (see chapter 2.5). Consequently the mass loss rate will be expressed no longer by (74) but by (29) which has a steep dependence on the temperature, perhaps generating a minimum temperature limit of evolutionary tracks because of mass loss.

REFERENCES

Abbott,D.C. 1982, Ap.J. 259, 282

Abbott,D.C., Bieging,J.H., Churchwell,E.B. 1981, Ap.J. 250, 645

Abbott,D.C., Bieging,J.H., Churchwell,E.B., Torres,A.V. 1986, Ap.J. 303, 239

Andriesse,C.D. 1981, in Effects of Mass Loss on Stellar Evolution, eds. C.Chiosi & R.Stalio, p. 213, Dordrecht:Reidel

Appenzeller,I. 1980, in Star Formation, eds. A.Maeder & L.Martinet, p. 3, Geneva:Geneva Obs.

Appenzeller,I. 1986, in Luminous Stars and Associations in Galaxies, eds. W.H.De Loore et al., p. 139, Dordrecht:Reidel

Barlow,M.J. 1979, in Mass Loss and Evolution of O-type Stars, P.S.Conti & C.W.H.De Loore eds., IAU Symp. 83, 119

Barlow,M.J., Cohen,M. 1977, Ap.J. 213, 737

Bertelli,G., Bressan,A., Chiosi,C. 1984, An.Ap. 130, 279

Bressan,A., Bertelli,G., Chiosi,C. 1981, An.Ap. 102,25

Carson,T.R., Huebner,W.F., Magee,N.H.Jr., Mertz,A.L. 1984, Ap.J. 283, 466

Castor,J.I., Abbott,D.C., Klein,R.I. 1975, Ap.J. 195, 157

Chiosi,C. 1981, in Effects of Mass Loss on Stellar Evolution, eds. C.Chiosi & R.Stalio, p. 229, Dordrecht:Reidel

Chiosi,C. 1981b, An.Ap. 93, 163

Chiosi,C., Maeder,A. 1986, Ann.Rev.An.Ap. 24, 329

Chiosi,C., Nasi,E., Sreenivasan,S.R. 1978, An.Ap. 63, 103

de Jager,C. 1980a, in The Brightest Stars, p. 14, Dordrecht:Reidel

de Jager,C. 1980b, in The Brightest Stars, p. 199sgg.

de Jager,C. 1984, An.Ap. 138, 246

de Jager,C., Nieuwenhuijzen,H., van der Hucht,K.A. 1985, in Luminous Stars and Associations in Galaxies, eds. W.H.De Loore et al., Dordrecht:Reidel

De Loore,C. 1984, Phys.Scr. 77, 25

De Loore,C., Hellings,P., Lamers, H.J.G.L.M. 1982, in WR Stars: observations, physics, evolution, eds. C.De Loore & A.J.Willis, p. 53, Dordrecht:Reidel

Doom,C., De Greve,J.P., De Loore,C. 1986, Ap.J. 303, 136

Friend,D.B., Abbott,D.C. 1986, Ap.J. 311, 701

Fusi-Pecci,F., Renzini,A. 1975, An.Ap. 39, 413

Garmany,C.D., Conti,P.S. 1984, Ap.J. 284, 705

Garmany,C.D., Olson,G.L., Conti,P.S., Van Steenberg,M.E. 1981, Ap.J. 250,660

Hartmann,L., Cassinelli,J.P. 1977, Ap.J. 215, 155

Humphreys,R.M. & McElroy,D.B. 1984, Ap.J. 284, 565

Klein,R.I., Castor,J.I. 1978, Ap.J. 220, 902

Kurucz,R.L. 1979, Ap.J.Suppl. 40, 1

Lamers,H.J.G.L.M. 1981, Ap.J. 245, 593

Lamers,H.J.G.L.M. 1986, Luminous Stars and Associations in Galaxies, eds. W.H.De Loore et al., p. 137, Dordrecht:Reidel

Landau,L.D., Lifshitz,E.M. 1969, in Statistical Physics, Pergamon Press, Oxford, p. 372

Maeder,A. 1980, An.Ap. 90, 311

Maeder,A. 1981a, An.Ap. 99, 97

Maeder,A. 1981b, An.Ap. 102, 401

Nasi,E. 1986, in Luminous Stars and Associations in Galaxies,

eds. W.H.De Loore et al., p. 121, Dordrecht:Reidel

Olson,G.L., Ebbets,D. 1981, Ap.J. 248, 1021

Panagia,N., Felli,M. 1975, An.Ap. 39, 1

Parker,E.N. 1958, Ap.J. 128, 664

Pauldrach,A., Puls,J., Kudritzki,R.P. 1986, An.Ap. 164, 86

Prantzos,N., Doom,C., Arnould,M., De Loore,C. 1986, Ap.J. 304, 695

Rebeirot,E., Martin,N., Mianes,P., Prevot,L., Robin,A., Rousseau,J., Peyrin,Y. 1983, An.Ap.Suppl.Ser. 51, 277

Reimers,D. 1975, Mem.Soc.R.Sci.Liege, 6 Ser. 8, 369

Rousseau,J., Martin,N., Prevot,L., Rebeirot,E., Robin,A., Brunet,J.P. 1978, An.Ap.Suppl.Ser. 31, 243

Stasinska,G. & Tylenda,R. 1986, An.Ap. 155, 137

Turolla,R., Nobili,L., Calvani,M. 1986, Ap.J. 303, 573

Veltroni,C. 1984,Le Variabili di Hubble-Sandage, thesis, University of Padova

Waldron,W.L. 1984, in The Origin of Non-radiative Heating/Momentum in Hot Stars, ed. A.B.Underhill, A.G.Michalitsianos, p. 2358, Washington:NASA

Wilson,I.R.G., Dopita,M.A. 1985, An.Ap. 149, 295

Wright,A.E., Barlow,M.J. 1975, M.N.R.A.S. 170, 41

REPORT ON RESEARCH ACTIVITY

During the academic year 1986/87, I have been mainly engaged in two jobs.

First, the distribution of Cepheid Stars in period: the role of convective overshoot and metallicity dispersion. I have calculated the theoretical distribution of Cepheids in period for the evolutionary tracks with convective overshoot of Bertelli et al. (1986, An.Ap.Suppl.Ser. 66,191). It is found that overshooting models are able to account for the position of the peak in the observed distributions, contrary to classical models. A small dispersion in metallicity is needed to account both for the range between the observed minimum and peak periods and for the overall shape of the distribution. In particular, a metallicity $Z=0.0090\pm0.0015$ is estimated for the LMC.

Second, I started a program, currently in progress, which should be the argument of the Ph.D. thesis.

Present theoretical models of massive stars are often unadequate for several reasons:

1) usual atmospheres in structure and evolutionary calculations are thin, hydrostatic, plane parallel and grey. On the contrary, massive stars are loosing mass at high rates and, therefore, have winds, that is, extended atmospheres.

2) Stellar evolution with mass loss is usually calculated through a sequence of hydrostatic models with decreasing mass. The observed mass loss rates, however, require supersonic velocities at the photosphere. Therefore, at least the outer subphotospheric layers of supergiant stars are not in

hydrostatic equilibrium.

3) The mass loss rates adopted in stellar evolution calculations are parametrized on stellar parameters. There are many different parametrizations: which are the right ones? There are several problems: bias, small numbers, crowding of stars in different evolutionary phases. Up to now, no evolutionary track has been calculated with a mass loss rate self-defined.

4) Current models are not able to account the observed HR diagram for supergiant stars.

So, the project is:

1) to replace the thin hydrostatic atmosphere with the wind structure in stellar structure and evolution calculations.

2) To develop a subphotospheric structure which takes into account eventually the non hydrostaticity, and so:

3) to compute completely self-consistent evolutionary tracks and to compare the mass loss rates obtained on the HR diagram with the observations.

The first step is the subject of my thesis for the title of Magister Philosophiae. The second step is currently in progress.

Padova, 12-10-1987

Claudio Veltroni

Claudio Veltroni